UNIVERSITY OF KWAZULU-NATAL

INYUVESI YAKWAZULU-NATALI

OPTIMIZATION OF TURBINE DESIGN FOR DEEP SEA (OCEAN CURRENT) POWER ENERGY TECHNOLOGY

Submitted by

MUTOMBO JIMMY TSHIKAYA,

213567990

Supervisor: PROFESSOR Freddie L. Inambao

2016

OPTIMIZATION OF TURBINE DESIGN FOR DEEP SEA (OCEAN CURRENT) POWER ENERGY TECHNOLOGY

MUTOMBO JIMMY TSHIKAYA

Supervisor: Professor Freddie L. Inambao

Thesis submitted in fulfilment of the requirement for the degree of

MASTER OF SCIENCE IN ENGINEERING

(MECHANICAL ENGINEERING)

School of Engineering, University of KwaZulu-Natal, Durban, South Africa

12th October 2016

As the candidate's supervisor, I have approved this thesis for submission.

Signed……  ……Date…12th October 2016……

Name: Professor Freddie L. Inambao

DECLARATION 1 PLAGIARISM

I, the undersigned, hereby declare that the work contained in this thesis is my own original work and that I have not previously in its entirety or in part submitted it at any other university for a degree.

Signature ….  .... Date 12th October 2016……

DECLARATION 2 PUBLICATION

DETAILS OF CONTRIBUTION TO PUBLICATION that forms part and/or includes research presented in this thesis (include publication in preparation, submitted, in press and published and given details of the contributions of each author to the experimental work and writing of each publication)

Publication: **M. J. Tshikaya** and **F. L. Inambao**: "Deep sea (Ocean Current) power energy technology," Presented at 13th International Conference on Sustainable Energy Technology 25th – 28th August 2014 HES-SO – Geneva – Switzerland (www.hes-so.ch/set2014), 2014

In this paper, I Tshikaya M. J. was the main and corresponding author, whilst Dr Freddie L. Inambao was the co-author and my research supervisor.

Signed

ACKNOWLEDGEMENTS

I would like to express my gratitude to my supervisor, Professor Freddie Inambao, for his support, patience, and encouragement throughout my graduate studies. He has been a supervisor and an advisor and truly speaking, it is not often that one finds an advisor who always finds the time for listening to the little problems that unavoidably crop up in the course of performing research. His technical and editorial advice was essential to the completion of this master's thesis and has taught me innumerable lessons and insights.

I would like to sincerely thank my colleges and members, Taty, Grace, Alain, Andrew, Gloria, Kumarushen, Marc, Emmanuel, Samuel, all of them member of the Green Energy Solution for their valuable comments, advises, suggestions, encouragement, and input to the thesis. I also thank my friends, Dhady, Herve, Omer, Londiwe, Thabede, Khabo, Clive, Mafa, Sipho and others for their presence in my life during the period of this research. Their contribution in the accomplishment of this process was their encouragement that I needed most.

My deepest gratitude goes to my family for their unflagging love and support throughout my life. In the first place to my parents, Mutombo Tshikala and Tshibola Tshikaya for giving me everything in my life. The support, the attention and advises have been in a positive way so that I do not lose my way and stay on the right path. Secondly to my brothers and sisters, Patrick, Nadine, Laetitia, Guelord, Patricia and Tracy for their unparalleled love and care. Finally, I express my gratitude to each and every member in my family, who finds hoy in my every success as much. I am proud to have such a family.

ABSTRACT

The main objective of this thesis is to study renewable energy based on ocean current energy conversion. Different technologies based on ocean energy conversion are described and this research focuses on the design of a horizontal axis turbine running in free stream water under a range of different velocity values. We explain the concept of the design, the source of the power, thrust formulae and use computational tools to analyze the efficiency of the project. For this design, we have considered data collected at different sites where a full scale project could be implemented. The test site was chosen on the basis of statistical analysis of the best velocity profile available. From studies on wind turbine airfoils we chose a profile that seemed to be efficient for the range of Reynold number equivalents required according to the conditions of the chosen site. This profile was adapted to suit an ocean current turbine. Combining the chosen profile data and formulae for optimum pitch angle, we designed different prototypes using Autodesk Inventor Professional. These designs are based on concepts after Betz, Schmitz, Blade Element Momentum and also using a design tool named Turbem which has been developed for design of water turbine blades. We used Autodesk CFD to run simulations and analysis of the turbines. The results provide an average of the change in water pressure on the surface of the blades and average power based on a series of calculations. Results are presented in tables showing the power output of the system in relation with the velocity of water and the radius of the turbine. Studies on material, implantation on site and cost still need to be conducted but we can recommend ocean current energy conversion as an alternative source of electrical energy.

CONTENTS

LIST OF FIGURES

LIST OF TABLES

SYMBOLS AND ABBREVIATIONS

D	Two dimension	OTEC	Ocean Thermal Energy Conversion
3D	Three dimension	P	Power per unit
a	axial induction factor	p	Pressure of the fluid
a’	tangential induction factor	P_{Betz}	Power available on the shaft after Betz
b	ide of the blade	$P_{schmitz}$	Power available on the shaft after Schmitz
B	Number of blades	Q	correction factor
BEMT	Blade Element Momentum Theory	R	Blade radius
C	Length of the chord line	r	Radius of local blade element
C_D	drag coefficient	Re	Reynolds number
CFD	Computational fluid dynamics	Sv	Sverdrup ($1Sv=10^6m^3/s$)
C_L	lift coefficient	T	torque
$C_{L,D}$	Coefficient of lift at the chosen angle of attack	T	Wave period
CO_2	Carbone dioxide	T_e	Wave period
C_P	power coefficient	WSSD	World Summit on Sustainable Development
C_T	Thrust coefficient	α	Angle of attack
dD	drag force on the blade element. ω Relative fluid speed	α_D	Angle of attack for the maximum glide ratio
dL	lift force on the blade element	β	Twist
EDF	Electricité De France	$\beta_{(r)}$	Betz pitch angle of the blade
ESKOM	Electricity Supply Commission (ESCOM)	$\gamma_{(r)}$	Angle of relative fluid to rotor axis
g	Acceleration due to gravity	Δp	Change in pressure
H	Wave crest height	λ	Tip speed ratio
HAHT	Horizontal Axis Hydrokinetic Turbine	λ_r	Local speed ratio
HAMT	Horizontal Axis Marine Turbine	μ	the dynamic viscosity of the fluid
H_S	Wave height	ν	the kinematic viscosity of the fluid
I	moment of inertia of an annulus	ρ	Density of ocean water
kWL	angular moment	σ’	the local solidity
MW	Megawatt	φ	Incoming flow direction angle
N	number of blades	$\varphi_{(r)}$	Angle of relative fluid to rotor plane

Chapter 1 : INTRODUCTION

1.1 BACKGROUND

Global energy demand is currently being met in most countries in the world by an exhaustible resource of fossil fuels (Asif and Muneer 2007). South Africa produces most of its electricity from coal (Menyah and Wolde-Rufael 2010) while the environmental issues are debated by researchers, journalists, industrialists and politicians all over the word in order to fight against global warming and climate change. Coal is the main source of energy used to run the steam turbines producing electricity in South Africa (Dabrowski et al. 2008) for the benefit of consumers, but the burning of coal has a major impact on global warming and climate change in terms of increasing carbon dioxide (CO_2) in the atmosphere. This study is focusing on a form of clean and renewable energy which is based on free-flowing ocean water currents. This project could contribute to the country's electricity production.

The Republic of South Africa is a large country located on the southern tip of the African continent. A total of 2 798 km of its borders are ocean, namely, the Indian Ocean to the southeast and the Atlantic Ocean to the west. According to Statistics South Africa (2011), the country had a population of 50 586 757 people in 2011 and produced sufficient electricity power to meet the demand. Currently, about 72.1% of the country's primary energy needs are provided by steam plant (Dabrowski et al. 2008) which use coal to generate the steam that runs the turbines. Mbuseli (2013), in an overview of the main electrical company Eskom, states that it has an installed capacity (total nominal capacity) of 44 145 MW and its usable capacity (total net maximum capacity) is 41 194 MW. This capacity does not seem to be sufficient for the expected high electricity demand in the coming years. According to Eskom's system status bulletin which is released twice a week in line with its commitment to regular and transparent communication on the power system, the capacity available in April 2013 to meet the evenings' peak demand (from 5pm to 9pm) was low and this situation was maintained until the accident occurred at Majuba power station where a coal storage silo collapsed affecting coal supplies to all six units at the power station and reduced the energy production of the plant from 3 600 MW to 600 MW (Matona 2014). This seriously affected the country and increased the need for more energy production. Eskom's system status is available on their official website "www.eskom.co.za". Thus, the need to produce more

energy in South Africa is urgent and the way to produce it must be clean. The potential that South Africa has to produce electricity using one of the ocean's energy forms is to be considered. The purpose of this study is to elucidate the concept of generating power from the flowing ocean current water and connect it to the grid. Many components in a system using ocean current are analyzed. Data and measurement from different sites where the system can be built have already been completed by Eskom's division of research and development.

Eskom (2013) states in a fact sheet published in January 2013: "In South Africa, coal has dominated the energy supply sector. It's not obvious to see a significant change in the next decade".

As a member of the global community, South Africa has pledged its support for sustainable power generation to be produced by renewable energy sources. Ocean current power energy technology is a potential solution as a suitable alternative energy source (Eskom 2013). This study, is going to focus on the kinetic energy of ocean currents and describe this resource for energy conversion purposes and in this way contribute towards assisting the government in reaching its renewable energy goals.

1.2 MAJOR OCEAN CURRENT SYSTEMS IN THE WORLD

Looking at the position of South Africa on the map in Figure 1-1, two important ocean currents which are the Agulhas and the Benguela Currents have to be taken into consideration. Boundary currents are ocean currents with dynamics determined by the presence of a coastline, and fall into two distinctive categories: the western boundary currents and the eastern boundary currents. This study focuses on the Agulhas Current which is an eastern boundary current. It is a warm, deep, narrow, and fast flowing current that forms on the east side of the ocean basin due to eastern intensification. It carries warm water from the tropics poleward.

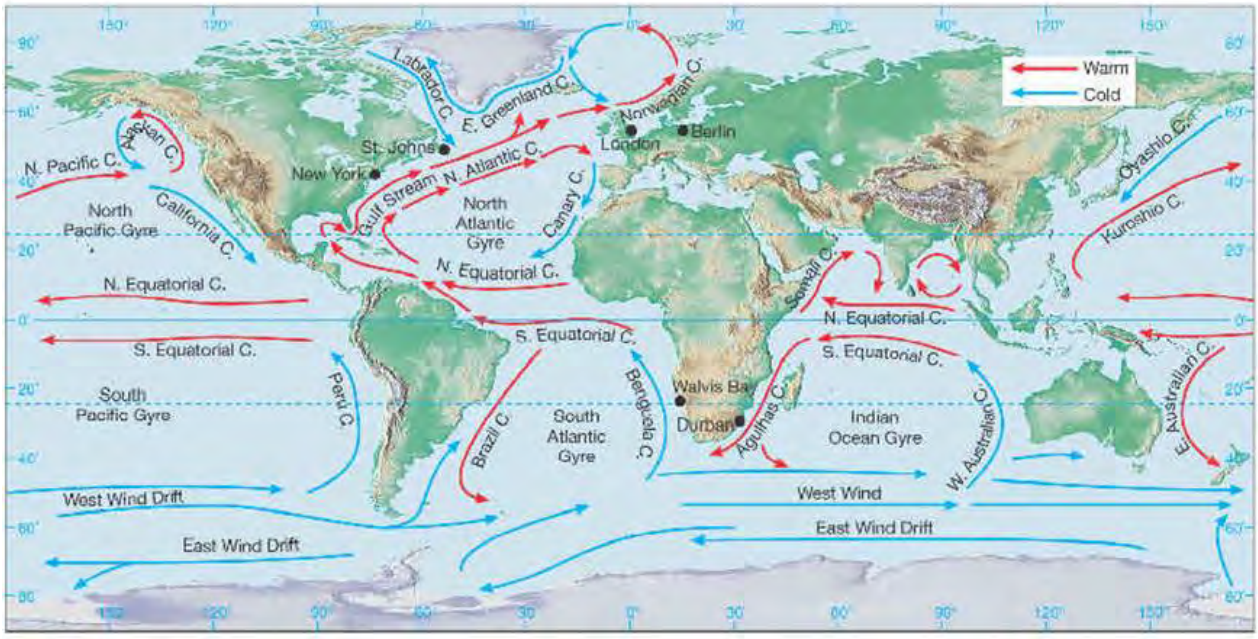

Figure 1-1: Schematic showing the major ocean current systems in the world (Niiler 2001)

Lutjeharms (2006) carried out research of the greater Agulhas Current that covers some aspects of the southern and northern parts of the Agulhas Current. The study shows that the Agulhas Current is 100 km wide and the two parts of this current have distinctly different trajectory behaviors. The northern Agulhas Current is shown to be an eastern boundary current with invariant path. The temperatures of the Agulhas Current can be greater than 22 °C, the speeds 1.3 m/s ± 0.3 m/s and a volume flux estimated at about 72 Sv (1 Sv = 106 m^3/s) over the full depth of the current. The southern Agulhas Current is located downstream of Port Elizabeth. Its surface temperatures are 23 °C to 26 °C and its surface speeds may be in excess of 2 m/s. The Benguela Current is a western boundary current and is relatively shallow, broad and slow-flowing. It is situated on the western coast of the continent. Subtropical western boundary currents flow equatorward, transporting cold water from higher latitudes to lower latitudes. The Benguela Current is a cold, wide current flowing northward along the west coast of Southern Africa. It is 200 km to 300 km wide and has typical surface flow speeds of 0.2 m/s to 0.5 m/s (therefore much slower than the Agulhas Current). That is the reason why this study focuses on the Agulhas Current. Different categories and criteria of ocean energy resources are described in **Error! Reference source not found.**-1.

Table 1-1: Categories and criteria of ocean energy resources in the western Indian Ocean. Temporal variability, predictability, and ranking criteria refer to annual means if not specified otherwise

	Wave power	**OTEC**	**Tidal barrages**	**Tidal current turbines**	**Ocean current power**
Temporal variability	Daily & seasonal	Seasonal	Hourly & weekly	Hourly & weekly	Seasonal
Predictability	Moderate	High	High	High	High
Ranking criteria					
High	≥ 5 kWm^{-1}	≥ 20 ΔT, ≤ 5 km	≥ 5 m mean tidal range	≥ 2 ms^{-1} peak speed	≥ 1.5 ms^{-1} seasonal average speed
Conditional	15-25 kWm^{-1}	≥ 20 ΔT, ≤ 10 km	2.4 - 5 m mean tidal range	≥ 1.5 ms^{-1} peak speed	1 - 1.5 ms^{-1} seasonal average speed

Studies and design of marine current energy conversion have already developed advanced technology for water velocity beyond 2 m/s. The Agulhas Current along South Africa's coastline has a velocity profile that can be predictable and varies in a range that can be used for ocean current energy conversion despite the fact that this velocity profile has a mean value less than 2 m/s. This study focuses on horizontal axis marine turbines designed for an average current water velocity of 1 m/s. The yield from the design of the horizontal axis turbine rotor is expected to be sufficient to drive its own turbine and produce electricity. Different methodologies are considered in terms of offshore and inshore design.

Ocean energy producing a current from tide is a vast energy resource. Tidal power is the use of the rise and fall of tides involving very large volumes of water at low heads to generate electric power (Dictionary.com 2016). This technology was used in France on the estuary of the river Rance for a 240 MW tidal barrage (Électricité de France [EDF] 2012) and is still working today. In the particular case, this study focuses on free flowing ocean water current. This technology does not need a barrage to retain water but needs a strong water current with a velocity profile that can be converted to electricity when turning the rotor of the turbines. Offshore and inshore designs can be developed but in this study a marine current turbine prototype is tested assuming that the plant will be constructed offshore on a site where the Agulhas Current has a surface velocity varying between 1 m/s to 2.5 m/s. This ocean current turbine prototype with a horizontal axis resembles wind energy converters coupled to a gearbox plus a generator. Vertical axis turbines can also be researched in relation to generating electricity from the ocean in South Africa. A comparison between horizontal axis and vertical axis turbines would determine which one has a better yield.

1.3 RESEARCH QUESTIONS

Questions in this research are as follows:

- How can more electrical energy be produce to supply the country?

Eskom Ltd, which is the country's electricity supply utility responsible for generating, transmitting and distributing electricity is presently facing a big challenge to reach the demand (Mbuseli 2013). Most of the electrical energy produced by the company is provided by steam plants. The quantity of CO_2 that is emitted by the use of coal is already debated as dangerous and needs to be reduced. The search to find alternative sources of energy production has become a priority.

- How can electrical energy production avoid the negative effect of CO_2 in the atmosphere which can compromise the safety of our future generations?

South Africa is as dependant on coal as any country in the world, placing the country as the 13th largest CO_2 emitter in the world (Gale et al. 2011). Coal intensity has increased at a time when a commitment was made to reduce coal reliance at the World Summit on Sustainable Development (WSSD) (Steele et al. 2012). Researchers must try by all means to find a way of energy production that avoids the use of coal which increases CO_2 in the atmosphere.

- How can ocean currents surrounding South Africa, such as the Agulhas Current, be capture and convert into electrical energy?

Many different technologies have been developed to convert natural energy into electricity. To solve the problem considering the questions above, ocean current energy conversion is considered, and is one of the ways to contribute to sustainable development and to produce more electricity to supply the country.

Considering the research questions, focusing and analyzing data collected at different potential sites for the implantation of a marine current turbine, some prototype can be designed and analyzed. Designs are based on data from different horizontal axis turbines existing and following different approaches. This can be done by mathematical models and design prototypes using Autodesk Inventor Professional. These prototypes were analyzed using a computational fluid dynamics program with the results showing the best yield leading to design and construction. This study focused on the aim and research questions to find

technical solutions and show the way that ocean energy may be used in South Africa to contribute to energy generation.

1.4 AIM AND OBJECTIVES

The aim of this research is to develop a technology that will utilize the kinetic energy from the ocean current as an alternative source of renewable energy in South-Africa.

The objectives are as follows:

- Demonstrate proof of concept. Ocean currents carry a large amount of kinetic energy in a constant flow. The method to capture and convert this energy in an electrical energy is yet to be developed.
- Modelling a prototype in a laboratory or computer simulation. Using data from a site and building a prototype considering the flow patterns of the ocean current which can be affected by wind, temperature, water salinity, topography of the ocean bed, and rotation of the planet. The prototype or simulation must reflect the state of a real site.

Chapter 2 : LITERATURE REVIEW

2.1 OVERVIEW

The need to produce electricity avoiding the negative effect of the CO_2 could be achieved using nuclear power but following the nuclear power plant accident in 2011 in Japan, many countries have decided to increase projects based on renewable energy from solar, marine, and wind sources.

This work is focused on the production of electricity using ocean current kinetic energy to drive subsea turbines. Ocean current power generation is a method to produce electricity using one of the ocean's energy forms. There are many different forms of ocean energy which can be used to drive turbines and produce electricity. Ocean current power generation in our research concerns generation of electricity from the kinetic energy in freely flowing water where the currents are strong enough to drive turbines.

2.2 REVIEW OF PREVIOUS WORKS

Electricité de France (EDF) (2012) provide an overview of the plant station "La Rance" and its history. From 1943, manufacturers, technicians and engineers developed a thorough research program in the fields of civil engineering and machinery. They paid special attention to the production of electricity by the placement of a plant in the estuary. They developed the "groupe bulbe" which are turbines and alternators combined and mounted together. In 1966 they used these "groupe buble" in La Rance Tidal Power Station which is the world's first tidal power station. Today other projects have been completed using tidal stream and water current power to produce electricity. These powers have the advantage of being stable and predictable.

Wang et al. (2011) studied generation of electricity from the oceans. The authors focused on two of the ocean energy forms, namely, tidal streams or marine currents driven by gravitational effects, and the resources in wind-driven waves, derived ultimately from solar energy. This work provided an overarching analysis of the salient issues related to the conversion of wave and marine current energy resources. It established a step-by-step approach that could be used in technology and project development, depicting important

results derived from experimental and field observations on device fundamentals, modelling approaches, resource assessment, sites and project development.

Grabbe (2008) conducted a study on marine current energy conversion designing a prototype variable speed generator. The construction of this system was based on previous finite element simulations. The experiments showed that the generator was well balanced and there was agreement between measurements and corresponding simulations, both at nominal load and under variable speed operation. It showed that the generator could accommodate fixed tip speed ratio operation with different fixed pitch vertical axis turbines in current velocities in the range 0.5 m/s to 2.5 m/s.

Chong and Lam (2013) undertook studies on renewable ocean energy in Malaysia, particularly the potential of the straits of Malacca. The authors presented the current state and future prospects of renewable energy in Malaysia. They reviewed five types of ocean renewable energy including tidal barrage current energy, wave energy, ocean thermal energy conversion and salinity gradient power. They made comparison of various types of ocean renewable energy in electricity generation technologies and identified tidal current energy as a preferable option particularly in the straits of Malacca. The review renders an important insight into the potentiality of ocean renewable energies in Malaysia.

Grabbe et al. (2009) conducted a review on the conditions for and the potential of the tidal current energy resources in Norway. They examined the oceanography of the Norwegian coastline, and numerical models of tidal currents in Norwegian waters. The extensive coastline with its numerous fjords, islands, sounds, and inlets makes for strong tidal currents with large flux volume. Several numerical models of tidal flow in waters have been reviewed, and a model has been developed at the university to calculate the velocity and volume flux of tidal flow through narrow sounds – the next step to calculate the theoretical tidal energy resource should not be insurmountable. However, a theoretical resource on its own is probably a poor indicator of how much energy from a site can in practice be converted and delivered to the electricity grid.

Yuen et al. (2009) undertook studies on matching a permanent magnet synchronous generator to a fixed pitch vertical axis turbine for marine current energy conversion. This study was about extracting energy from a free-flow marine current using a vertical axis fixed pitch turbine with a generator that can handle varying speeds and loads, since such a turbine gives maximum power capture for a fixed tip speed ratio. A prototype of a generator suitable for

variable speed and load operation was designed and constructed. The comparison of measurements and simulations showed that the measurements were 90% of simulated values. The prototype generator vertical axis matched fixed tip speed ratio operation of several turbines for current speeds between approximately 0.5 m/s and 2.5 m/s.

Akimoto et al. (2013) conducted a conceptual study of floating axis water current turbines for low-cost energy capturing from river, tide and ocean currents. They made a comparison between the cost of utilizing kinetic energy of river stream, ocean current and wind for power generation. They concluded that the water current model was the most costly because of difficulties in construction and maintenance of devices installed in seawater. They proposed the concept of a floating axis water stream turbine. Their configuration is suitable for small low-cost hydro power.

Bahaj and Myers (2004) estimated the energy yield potential from the Alderney Race (Channel Islands) using marine current energy converters. The results indicated the potential of marine current energy converters showing that from the Alderney site alone the analytically predicted energy yield was approximately 2% of the year 2000 United Kingdom requirements.

Nicholls-Lee et al. (2013) analyzed the application of bend-twist coupled blades for horizontal axes. This paper discusses individual analyses and the manner in which the blades are coupled. Several example problems were analyzed using the design tool. The results compared well to the preliminary studies and indicate that a decrease of up to 12% in thrust and an increase of up to 5% in power capture could be achieved through the use of properly designed, bend-twist coupled blades. A tool for the design of passively adaptive, composite horizontal axis tidal turbines blades was developed. A surface panel code was used to predict the pressure loading on an initial horizontal axis tidal turbine blade.

Myers and Bahaj (2012) conducted an experimental investigation simulating flow effects in first generation marine current energy converter arrays. They concluded that the jet between the disks had a greater velocity than the inflow resulting in an increase in available kinetic energy of 22%. Single row array results showed that close lateral separation increased the thrust force acting upon adjacent rotor disks, and optimum lateral separation led to accelerated flow passing between adjacent rotor disks with no negative impacts upon the disks. For the length ratios used in the study a jet was formed with a 22% increase in kinetic energy compared to the inflow to the actuator disks and the spatial extent of this jet varied

depending upon parameters such as: (i) lateral rotor disk separation, (ii) water depth, (iii) turbine rotor disk thrust and (iv) inflow characteristics.

The two row array study showed that: the downstream disk was subject to a greater thrust force than the upstream disks; the downstream disk did not affect the thrust acting upon the upstream disks; the near wake region of the upstream disks was deflected by the presence of the downstream disk; the far wake region of the array had a higher velocity deficit (lower velocity) compared to a single disk due to the combined wake fields proving more difficult to break down; a third row of devices could be installed far downstream but in the short-medium term wider 2-row arrays would offer a more favorable arrangement for a fixed number of devices within an array.

Şen (2012) studied energy generation possibilities from ocean currents in the Bosphorus, Istanbul. The author gathered current speed data measured during different sorties across the Bosphorus. The current power generation in relation to the speed probability distribution of the water was calculated and a simple numerical sample was presented. With a continuous current from the black sea in the north towards the Marmara Sea in the south due to a 30 cm to 40cm level difference between the two seas, current power estimation formulation was developed parametrically by considering the cut-in low current speed as 1.0 m/s.

Wang et al. (2011), conducted an overview of ocean renewable energy in China. Their article presents policy, legislation and the status of development of renewable energy in China. They review resources distribution and technology status of tidal energy, wave energy, marine current energy, ocean thermal energy and salinity gradient energy. They concluded by saying that tidal power generation technology is the most mature ocean energy harnessing technology but it may cause greater possible environmental impact than others. Wave energy and marine current energy development technology is close to maturity and could step into demonstration operating stage in the near future. At the next stage, development of wave energy and marine current energy should focus on building demonstration generation devices rated at hundreds of kW and gain experience for scaled commercial operation in the future.

Jahromi et al. (2013) conducted research on design and evaluation of a tidal in-stream generator power port. The method the authors used to harness part of the vast renewable source of energy was to integrate a large scale tidal in-stream energy converter into a conventional power system. This posed many challenges, particularly in weaker networks. Their investigation provided design details of a hybrid power port solution that establishes an

independent active and reactive power control, enabling it to regulate the point of common coupling voltages, while transferring variable amounts of captured stream power to a nonstiff grid. They concluded by saying that the variable nature of tidal power is a fact and that the output from a tidal generator cluster can be highly unsteady. Then to size a grid-tie hybrid power port, tidal forecasts were used. In this case a small portion of its converter power capacity was dedicated to reactive power control.

VanZwieten et al. (2006a) studied the design of a prototype ocean current turbine. In this first part of their work, they conducted a mathematical modelling and dynamics simulation. They studied a 1/30th scale physical model of a submerged variable depth ocean current turbine named "C-Plane" that is a hydrodynamic platform tethered to the sea floor and uses sustained ocean current to produce electricity. This turbine uses its wingtips and canard to control its depth and orientation so that it can maximize energy production while flying in a temporally and spatially varying current. The mathematical model represents the C-Plane as a rigid body with moveable control surfaces that is moored with three linear elastic cable elements. Gravitational, buoyancy, hydrodynamic, cable, gyroscopic, and inertial forces are included and a PC-based dynamics simulation was created. The simulation demonstrated that the C-Plane is stable at various depths in all expected operating conditions. The design of the C-Plane allows the heights to be reached in both active and null mode for all expected water velocities. The control surfaces allow for the pitch, roll, and depth to be directly controlled so that the C-Plane can be orientated and positioned to produce maximum electricity from the Gulf Stream.

In the second part of their study, VanZwieten et al. (2006b) undertook studies of the design of a prototype ocean current turbine in terms of the flight control system. They presented and compared control strategies for the 1/30th scale C-Plane prototype. The first objective of this study was to develop three control systems that could effectively control the C-Plane system. The second objective was to implement, validate, and compare the controllers using the dynamics simulation. The three models were: the Mixed PID/Bang Bang (MPID), the Mixed LQR/PID/Bang Bang (MLQR), and Mixed LQG/PID/Bang Bang (MLQG).The researchers concluded that the MPID controller was the most capable and best performing controller.

Hammar et al. (2012) conducted a study on the simplified site-screening method for micro tidal current turbines applied in Mozambique. This study proposed a simplified tidal model that is calibrated to site-specific conditions by short-term observations using lightweight

equipment. The site-screening method was tested in Mozambique at five sites where near-shore tidal currents were measured with lightweight current meters. The currents were estimated to exceed 1 m/s and power output was calculated based on technical assumptions for a micro tidal current turbine on three of the sites. The comparisons and evaluations of the usefulness of power output between potential sites were facilitated by the applied method which offers a low-cost option for micro tidal current turbine. Among the investigated sites in Mozambique, Bazaruto Island has tidal currents in which all small scale micro tidal current turbines could provide useful amounts of electricity for predetermined loads.

Nugraha and Rijanto (2010) studied ocean current energy conversion systems in the Wallacea region using a variable speed control approach. They reviewed four types of green energy conversion systems extracted from the ocean and discussed their advantages and disadvantages. The authors concluded that it is appropriate to implement ocean current energy conversion systems using axial flow water turbines in the Wallacea region, and that to maximize energy conversion a variable speed control approach is best together with control of mechanism to move the turbine vertically as well as to rotate the turbine in yaw direction.

Rourke et al. (2010), analyzed the current status and possible future applications in Ireland of a marine current energy device designed by Marine Current Turbines Ltd. This company designed, developed, installed and tested the world's first offshore tidal current-powered experimental turbine named Seaflow in May 2003 in Lynmouth in the Bristol Channel (United Kingdom). The turbine has a rotor of 11 m and is rated at 300 kW. The basic concept on this prototype was the axial flow rotor, marine drive train, surface breaking monopole, structural integrity, low cost intervention and no significant environmental intervention.

Marine Current Turbines Ltd has undertaken many studies on the design and development of marine current generation. Their first tidal current turbine was manufactured in 1994-1995 rated at 15 KW.

In 2007 the company built and installed the Seagen, a commercial demonstrator rated at 1.2 MW installed in Strangford Narrows (Northern Ireland, United Kingdom). This prototype has 2 x 600 KW rotors of 16 m diameter each, installed on a steel pile and work at 25 m water depth. The rotor and nacelles rise above sea level for maintenance. The transformer and electrical connection to the grid accessible and visible in housing on top of the pile.

Muñoz et al. (2014) designed a small low cost horizontal axis hydrokinetic turbine (HAHT). Using a program named Turbem which combines blade element momentum theory (BEMT) and pseudo-gradient root findings for rotor optimal design, and classical solid mechanics for preliminary structural verification. The profile generated by the Turbem is sufficient for the design of a small turbine and the method used is very close to experimentation tests. The authors concluded that a HAHT system can be a technically and economically feasible energy source for off-grid electricity at locations where an adequate stream flow is available.

Li et al. (2014) proposed a mathematical model describing the nonlinear vibration of horizontal axis wind turbine (HAWT) blades. The system consists of a rotating blade and four components of deformation including longitudinal vibration, out-of-plane bend, in-plane/edgewise bend and torsion. It is assumed that the center of mass, shear center and aerodynamic center of a cross section all lie on the chord line, and do not coincide with each other. The structural damping of the blade, which is brought about by materials and fillers is taken into account based on the Kelvin-Voigt theory of composite materials. The equivalent viscosity factor can be determined from empirical data, theoretical computation and experimental test. Examples concerning the static deformation, aeroelastic stability and dynamics of the blade are given. By employing this model, some design and control problems of blades (such as aeroelastic stability, nonlinear dynamics, etc.) can be handled via analytical and numerical techniques.

Lee et al. (2012) studied computational methods for performance analysis of horizontal axis tidal stream turbines. In this study, two computational procedures, based on BEMT and computational fluid dynamics (CFD), were developed for open water performance prediction of horizontal axis tidal stream turbines (HATST). The developed procedures were verified by comparison with other computational results and existing experimental data and then applied to a turbine design process. The results of the open water performance prediction were discussed in terms of the efficiency and accuracy of the design process. For better cavitation inception performance, a raked tip turbine design was proposed and analyzed with the developed procedure. There are mainly two approaches for numerically analyzing the performance of a HATST system. One is BEMT and the other is CFD. BEMT models the rotor as a set of isolated two-dimensional (2D) blade elements, to which one can apply the 2D hydrodynamics theory individually and then perform an integration to find the thrust and torque. BEMT was mainly used for the analysis of HATSTs. Two computational procedures based on BEMT and CFD were developed for efficient and convenient performance

prediction of HATST, and based on the procedures, a new blade design was proposed for cavitation inception delay.

Goundar and Ahmed (2013) studied the design of a horizontal axis tidal current turbine (HATCT). For this study a 10 m diameter, 3-bladed horizontal HATCT was designed. Hydrofoils were designed for different blade locations, named as HF10XX. The hydrodynamic characteristics of the hydrofoils were analyzed. A thick hydrofoil with a maximum thickness of 24% and a maximum camber of 10% was designed for the root region. The maximum thickness of hydrofoils was varied linearly from the root to the tip for easier surface merging. For the tip region, a thinner hydrofoil of maximum thickness 16% and maximum chamber 10% was designed. It was ensured that the designed hydrofoils did not experience cavitation during the expected operating conditions. The characteristics of the HF10XX hydrofoils were compared with other commonly used hydrofoils. The blade chord and twist distributions were optimized using BEM theory. The theoretical power output and the efficiency of the rotor were also obtained. The maximum power at the rated current of 2 m/s was 150 kW and the maximum efficiency was 47.5%. The designed rotor was found to have good efficiency at current speeds of 1 m/s to 3 m/s. This rotor has better performance than some other rotors designed for HATCT.

Chapter 3 : OCEAN ENERGY CONVERSION TECHNOLOGY

Ocean renewable energy systems have different forms, encompassing tides, ocean circulation, surface waves, salinity and thermal gradients (Moreno et al. 2008). These can be classified in three options which are ocean current energy conversion, wave energy conversion and ocean thermal energy conversion (OTEC). The commonality between ocean current energy and tidal energy is the fact that tidal energy is a current that occurs when the tide is moving in or out. These three forms of energy conversion extract energy from the oceans and convert it into clean, green electrical energy. The technology is not the same and for every form we find many different methods of conversion. Aspects such as speed of water, depth of water, strength of waves, difference in temperature between cool deep water and warm shallow water must be taken into account before deciding which technology to use at any particular site for better performance.

3.1 WAVE ENERGY CONVERSION

Wave energy conversion technology has developed rapidly in recent years. It results from conversion of kinetic energy from waves into electricity. The conversion is possible by capturing the vertical oscillation and the linear motion of waves. Many wave energy converters have been designed for oceans but new ideas are now proposed for rivers and seas (Korde and Ertekin 2014). Figure 3-1 (Bedard 2008) and Figure 3-2 (Henderson 2006) show some examples of devices used to convert ocean wave energy into electrical energy.

Figure 3-1: Scottish Power Renewables' machine operating in Orkney (Bedard 2008)

The Pelamis (Figures 3-1 and 3-2) is an offshore wave energy converter that uses the motion of waves to generate electricity. The machine operates in water depths greater than 50 m and is typically installed 2 km to 10 km from the coast. The machine is rated at 750 kW with a target capacity factor of 25% to 40%, depending on the conditions at the chosen project site. On average one machine will provide sufficient power to meet the annual electricity demand of approximately 500 homes.

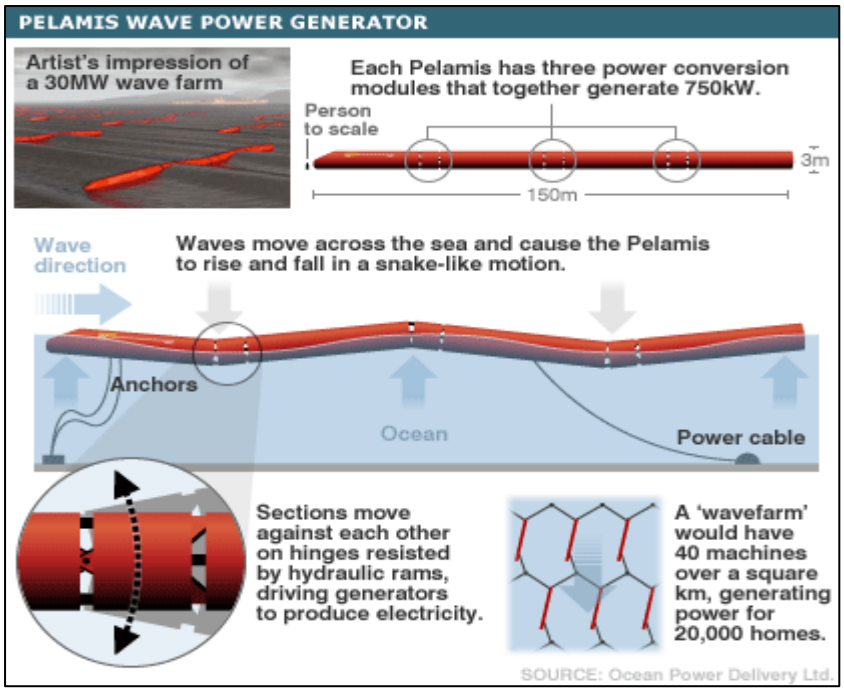

Figure 3-2: Pelamis wave power generation (Henderson 2006)

The Lilypad twin membrane wave energy converter in (Li and Yu 2012) (Figure 3-3) consists of an upper floating flexible membrane following the wave motion, provided on its underside with load distributing flanges taking upward loads to a number of linearly disposed fixation points to which are attached arrays of hose pumps. Hose pumps operate on the principle that as they are elastically elongated from their original large diameter cylindrical shape, they gradually reduce in volume, pressurizing the working fluid within them. At their base, the hose pumps are fixed to load distribution cables which are in turn fixed to the bottom membrane, which is both weighted and valved, so that it will resists upward movement. As it is pulled up by the passing wave, flexible flaps close against a mesh below them. After the wave has passed, the bottom weighted membrane sinks downwards by gravity, the valves open upwards and return to their initial position, ready for the next cycle. The hose pumps extend as the wave passes, expelling working fluid, normally seawater that runs to and along high pressure pipes to a hydraulic generator. Electricity is generated typically at 65% efficiency by a hydraulic turbo-generator. This mode prevails till the hose pump is partially or fully extended by the wave crest.

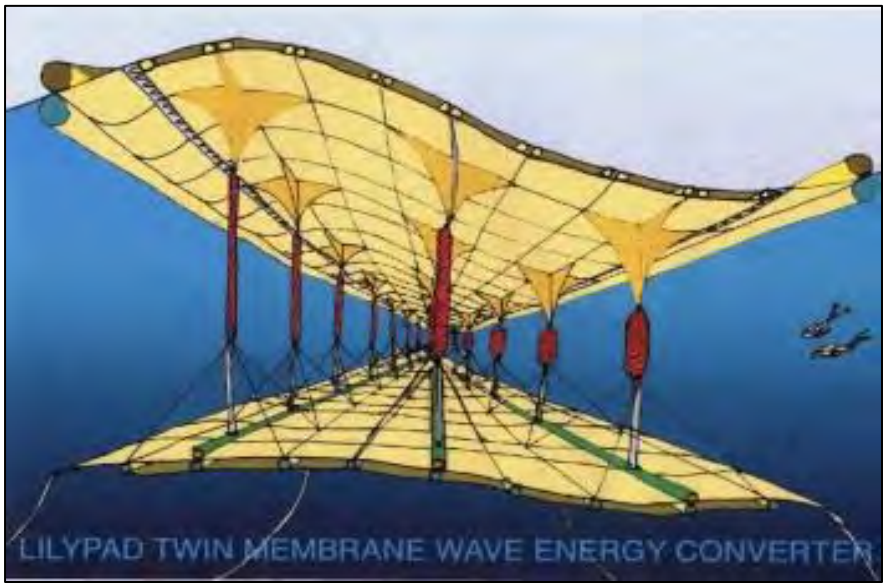

Figure 3-3: Lilypad Twin Membrane Wave Energy Converter (Li and Yu 2012)

As the wave passes, the upper membrane descends, gradually releasing pressure on the hose pump, which elastically returns to its shorter and larger cylindrical shape, drawing in seawater through a one way valve. This allows the lower membrane to descend to its original position, ready for the next upward stroke. The membranes run perpendicularly to prevailing

significant wave direction, the size and length of hose pumps being related to wave length and amplitude spacing of hose pumps and width of marine platform structure.

Deep water ocean waves give large energy fluxes under predictable conditions. The energy E (Wh), per unit wavelength in the direction of the wave, per unit width of wave front is given by:

$$\mathbf{E} = \frac{\rho \mathbf{g}^2}{16\,\pi}(\mathbf{H}^2\mathbf{T}^2) \qquad (3\text{-}1)$$

where:

ρ Density of ocean water (Kg/m^3)

g Acceleration due to gravity (m/s)

H Wave crest height (m)

- T Wave period (s^{-1})

This is the total excess energy in continuous wave motion in deep water (kinetic + potential) in a dynamic ocean (Twiddle and Weir 2006).

The power P per unit width of a wave front is given by:

$$\mathbf{P} = \frac{1}{64}\frac{\rho \mathbf{g}^2}{\pi}(\mathbf{H}_S^2\mathbf{T}_e^2) \qquad (3\text{-}2)$$

Where:

P Power per unit (W/m)

H_S Wave height (m)

T_e Wave period

3.2 OCEAN THERMAL ENERGY CONVERSION (OTEC)

Ocean thermal energy conversion (OTEC) takes advantage of ocean temperature gradients greater than 20 °C. Where such gradients exist between surface waters and waters no more than 1 000 m deep, they can be used to extract thermal energy stored in the ocean, and convert it to electricity (and, often, desalinated water). OTEC uses the natural difference in temperatures between the cool deep water and warm surface water to heat and cool down a

working liquid that is circulating in a closed system passing through a pump and a turbine which will generate electricity.

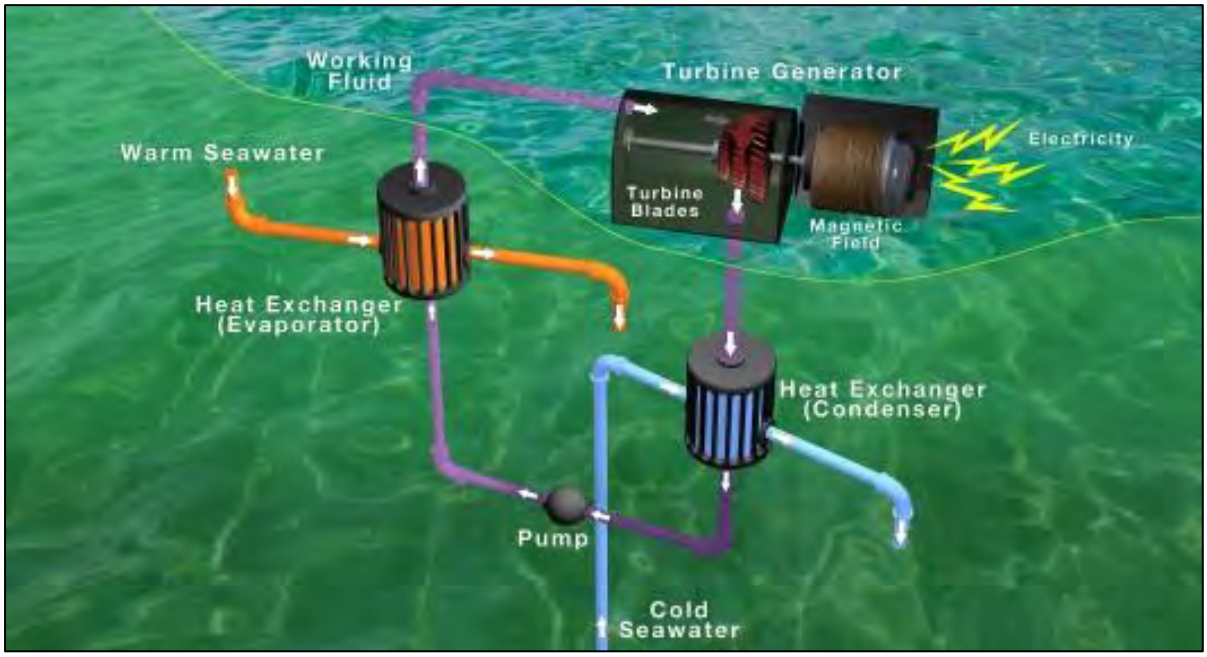

Figure 3-4: Project for a pilot plant of ocean thermal energy conversion. (Xiang et al. 2013)

There are different cycle types of OTEC systems, but the prototype plant on Figure 3-4 of a project for a pilot plant of ocean thermal energy is likely to be a closed-cycle system like the one in Figure 3-5 (Meisen and Loiseau 2009). This sees warm surface seawater pumped through a heat exchanger to vaporize a fluid with a low boiling point, such as ammonia. This expanding vapor is used to drive the turbine that generates electricity. Cold seawater is then used to condense the vapor so it can be recycled through the system. Tropical regions are considered the only viable locations for OTEC plants due to the greater temperature differential between shallow and deep water. Unlike wind and solar power, OTEC can produce electricity around the clock, 365 days a year to supply base load power. OTEC plants also produce cold water as a by-product that can be used for air conditioning and refrigeration at locations near the plant.

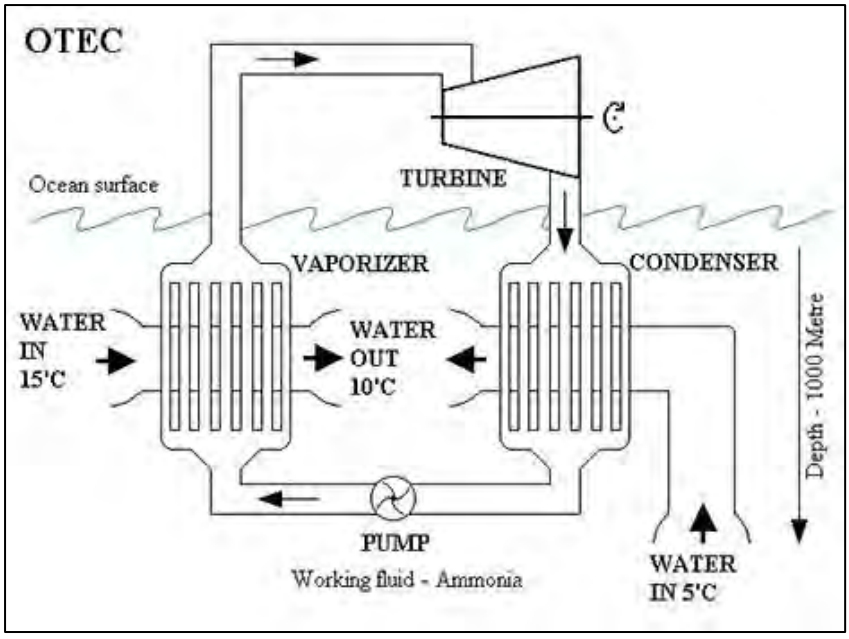

Figure 3-5: Operating principle of an OTEC plant (Meisen and Loiseau 2009)

3.3 OCEAN CURRENT ENERGY CONVERSION

As indicated earlier, ocean currents are classified in terms of kinetic energy. Although this energy is generally diffuse, it is concentrated at a number of sites where sea flows are channelled around or through constraining topographies such as islands and straits. There are many potential sites around the world that could be explored and utilised. The tides which drive such currents are highly predictable, being a consequence of the gravitational effects of the planetary motion of the earth, the moon and the sun (Bahaj 2011).

As the resource is highly predictable albeit variable in intensity, its conversion to useable energy offers an advantage over other renewable energy resources such as wind or wave energy (Bahaj and Myers 2003).

Projects that rely on ocean currents have quantifiable and firmly foreseeable output profiles which can be planned for and managed appropriately within a utility grid. In addition, long term energy yields can be accurately estimated which offer a particular advantage to a project developer in negotiating a better power purchasing agreement with utilities compared to other renewables. Ocean energy which produces a current coming from tide is a vast energy resource. It was used in France on the estuary of the river Rance for a 240 MW tidal barrage (EDF 2012) and is still working. Utilizing ocean currents does not require water-impounding

structures such as dams used in conventional hydropower but some sort of anchoring system within the flow stream.

There are three factors that determine how much power any turbine can produce. The first one is the velocity of the moving water. This factor shows us that the faster the water moves the more energy there is in the water that can be harvested. The second is the size of the turbine rotor. The bigger the turbine rotor the more energy it can harvest from the moving water. Finally looking at the efficiency of the turbine rotor or the ability of the turbine to convert the energy in the moving water into mechanical energy in the form of a rotating shaft with the ability to do useful work – drive a gearbox and generator or pump water etc. In most cases, the fundamental knowledge employed in wind energy conversion is required to predict the conversion of the kinetic energy of a moving fluid to provide useful work. Hence, water energy conversion technology variants are similar or related to those of wind energy conversion although other unique design philosophies are being pursued, as discussed further below.

Chapter 4 : POWER EXTRACTED FROM THE OCEAN CURRENT

Kinetic energy in the ocean current is converted into another source of energy when the water current moves the rotor of the turbine. The pressure change and velocity can be explained using Bernoulli's equation. To make appropriate assumptions and to analyze the velocity profile, we sketch a velocity profile and analyze the variables of velocity and pressure upstream of the rotor, when the interaction happens and downstream of the rotor (Figure 4-1).

The speed of the water current downstream of the rotor of the turbine is v_1 because it is moving freely without any disturbance. Once water interacts with the rotor and runs on the side of the blade element, the speed will reduce to v_3. The pressure downstream of the rotor is p_1 and when the fluid interacts with the rotor, the pressure rises to p^+ and falls suddenly to p_- after passing the rotor. The pressure downstream of the rotor will rise to a pressure p_3 which is equal to p_1. The change in pressure Δp is equal to "$p_+ - p_-$".

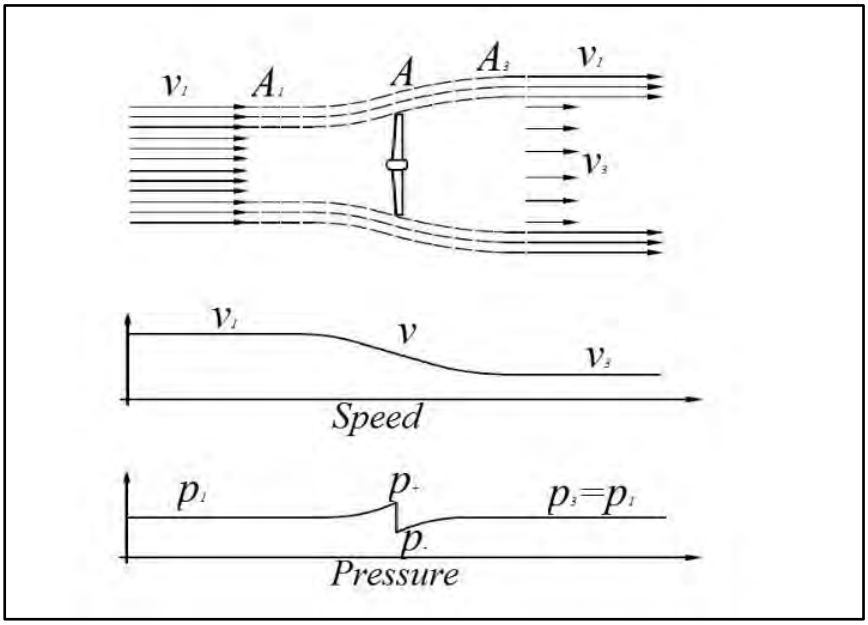

Figure 4-1: Interaction between water current and rotor of the turbine (Lasiecka and Triggiani 1990)

Let's analyze the power in the rotor using Bernoulli's equation. Knowing that the total pressure remains constant (Lasiecka and Triggiani 1990), the relation between the speed and the pressure appears to be inversely proportional by virtue of the fact that the speed of the

flow goes up when the pressure goes down and vice versa (equation 4.1). Assuming that the flow is frictionless and the density of the fluid is constant.

$$\mathbf{\frac{1}{2}\rho v^2 + p = p_{tot}} \quad (4\text{-}1)$$

where ρ denoted water density, υ the velocity and p the pressure.

Applying Bernoulli's equation in the profile from Figure 4-1 above equation 4-1 gives:

$$\mathbf{p_1 + \frac{1}{2}\rho v_1^2 = p_+ + \frac{1}{2}\rho v^2} \quad (4\text{-}2)$$

$$\mathbf{p_+ - \Delta p + \frac{1}{2}\rho v^2 = p_1 + \frac{1}{2}\rho v_3^2} \quad (4\text{-}3)$$

Adding (4.2) to (4.3);

$$\mathbf{p_+ + p_1 - \Delta p + \frac{1}{2}\rho v^2 + \frac{1}{2}\rho v_1^2 = p_1 + p_+ + \frac{1}{2}\rho v_3^2 + \frac{1}{2}\rho v^2}$$

$$\mathbf{\Delta p = \frac{1}{2}\rho(v_1^2 - v_3^2)} \quad (4\text{-}4)$$

These formulas can also be expressed in terms of change of momentum. Our assumptions are in relation to a square meter on a rotor plane where the mass flow is clearly equal to "ρ times υ". Knowing that momentum is the result of mass times velocity and that pressure is equal to force per surface, the differential pressure can be expressed as:

$$\mathbf{\Delta p = \rho v(v_1 - v_3)} \quad (4\text{-}5)$$

Comparing (4-4) and (4-5), it can be seen that they are expressed with quantities υ_1 and υ_3. Figure 4-1 shows υ as the velocity of the fluid when it interacts with the rotor. Extracting it from the two equations above.

$$\frac{1}{2}\rho(v_1^2 - v_3^2) = \rho v(v_1 - v_3)$$

$$\frac{1}{2}\rho(v_1 + v_3)(v_1 - v_3) = \rho v(v_1 - v_3)$$

$$\mathbf{\frac{1}{2}(v_1 + v_3) = v} \quad (4\text{-}6)$$

Equation (4.6) clearly indicates that the speed of the fluid in the rotor is the mean value of the speed upstream and downstream of the rotor.

From formula above, can be deducted the power in the turbine which is the rate of change in kinetic energy in the fluid.

$$\mathbf{P = \frac{1}{2}\rho v\left(v_1^2 - v_3^2\right)A} \qquad (4\text{-}7)$$

where P denotes the power of the fluid in watts "W" and A the surface area swept by the rotor in square meters " m^2".

The axial force on the rotor known as the thrust (in Newton "N") can be calculated as

$$\mathbf{T = \Delta pA} \qquad (4\text{-}8)$$

Knowing the density of water, the initial velocity υ_1 and the final velocity υ_3, Δp can easily be calculated and the value of the power and the thrust will depend on the profile of the blades.

For this study, data have been collected from different sites and the concern is to try to create a system running in existing conditions (Wimpie 2012). Thus velocity υ_1 of the fluid known from site data collection is used in formulas above. The axial interference factor "a" which is a number between 0 and 1 is defined to avoid the use of the velocity "υ" in the rotor and velocity "υ_3" after the rotor in our next formula. Assume:

$$\mathbf{v = (1 - a)v_1} \qquad (4\text{-}9)$$

Using (4-9) in (4-5), (4-6) and (4-7), equations can be expressed as followed:

$\frac{1}{2}(v_1 + v_3) = (1 - a)v_1$

$v_3 = v_1(1 - 2a)$

$$\mathbf{P = 2\rho a(1 - a)^2 v_1^3 A} \qquad (4\text{-}10)$$

$$\mathbf{T = 2\rho a(1 - a)v_1^2 A} \qquad (4\text{-}11)$$

From formulas (4.10) and (4.11) of P and T, define two coefficients, "C_P" for the power production and "C_T" for the axial forces as:

$$\mathbf{C_P = 4a(1 - a)^2} \qquad (4\text{-}12)$$

$$\mathbf{C_T = 4a(1 - a)} \qquad (4\text{-}13)$$

Then (4.10) and (4.11) can be expressed as

$$\mathbf{P = \frac{1}{2}\rho v_1^3 A C_P} \qquad (4\text{-}14)$$

$$\mathbf{T = \frac{1}{2}\rho v_1^2 A C_T} \qquad (4\text{-}15)$$

Curves of the two coefficient C_P and C_T as function of "a" are shown in Figure 4-2.

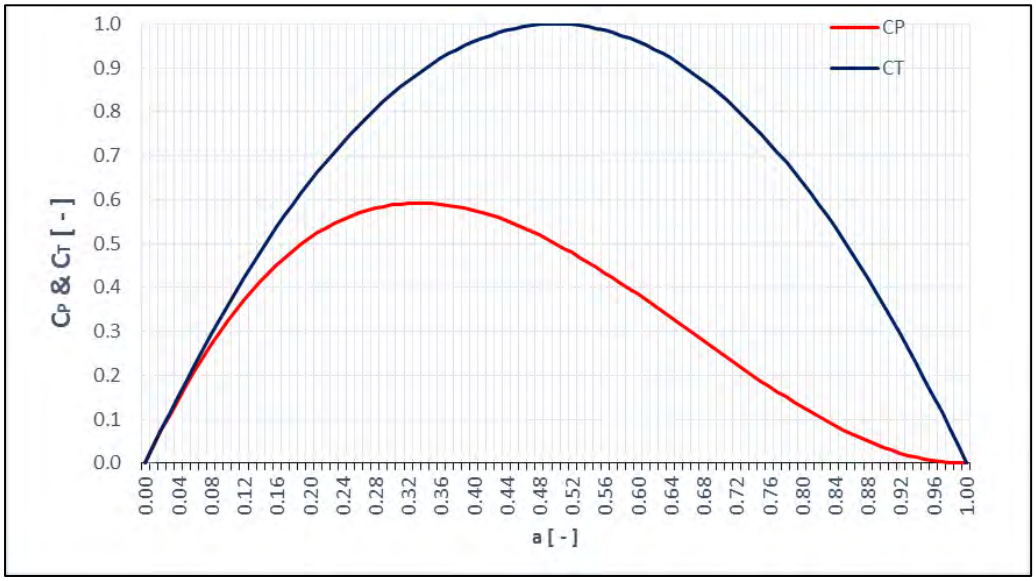

Figure 4-2: Coefficient of power C_P and coefficient of axial force C_T for idealized wind or marine current turbine

The turning points of the curve representative of the coefficient C_P in Figure 4-2 can easily be find by a simple calculation using the derivative of the function C_P regarding the axial interference factor "a" and equalizing it to zero. Values of "a" which give "C_P derivative = 0" are maximum and minimum of the function C_P.

$$C_P = 4a(1 - a)^2$$

$$\frac{dC_P}{da} = 4(1 - a)(1 - 3a)$$

$$\frac{dC_P}{da} = 0 \implies (1 - a) = 0 \; or \; (1 - 3a) = 0$$

$$For \; a = 1 \; \Rightarrow C_P = 4 * 1(1 - 1)^2 = 0$$

$$For\ a = \frac{1}{3} \Rightarrow C_P = 4 * \frac{1}{3}\left(1 - \frac{1}{3}\right)^2 = \frac{16}{27} = 0.5926$$

C_P as a minimum value $C_P = 0$ when a = 1 and an optimum value $C_P = 16/27 \approx 0.5926$ for a = $1/3 \approx 0.33333$. This means that the maximum power can be obtained when the value of C_P is 16/27. Doing the same for C_T lead to the optimum value of $C_T = 1$ for a = 1/2.

The aim of this research is to harvest power from the system and convert it in order to generate electricity. The value of "a" that gives a maximum value of the power supplied to the rotor by the rate of change in kinetic energy of water is 1/3 and a maximum thrust when it has a value of 1/2. In fact, the design of the rotor must have a profile which will favor the value of "a" kept as close as possible to the value 1/3. The turbine will be designed in a way that the mean value of the velocity profile on the site where the turbine will be constructed gives a maximum value of a = 1/3.

The demonstration above brings us to the formula of power according to Betz:

$$\mathbf{P_{Betz} = C_{P,Betz} \frac{1}{2} \rho v_1^3 A} \qquad (4\text{-}16)$$

with $C_{P,\,Betz} = 16/27$

This formula will allow some assumptions and calculations to estimate the power output from the designed system. The moment of inertia of the rotor is also important to be taken in consideration because the thrust must be strong enough to overcome the momentum of inertia. Data collected from different sites was analyzed in order to choose the best site to construct our system.

Chapter 5 : VELOCITY PROFILE OF THE AGULHAS CURRENT

The Acoustic Doppler Current Profile (ADCP) data collected from September 2005 to December 2010 with 51 deployments on the east coast of South Africa provides details of the velocity variation of the Agulhas Current (Wimpie 2012). Data are in tables containing many fields and values which can be arranged using Excel and placed in graphs as shown in the example in Figure 5-1. Each deployment was done for a period of time between 3 to 5 months. Data are given in bins that divide the water column into horizontal sections. In this folder can be found the depth of the center of the bin, the range or distance from the ADCPs transducer to the center of that bin, the direction at which the current flows at that specific time and the current velocity.

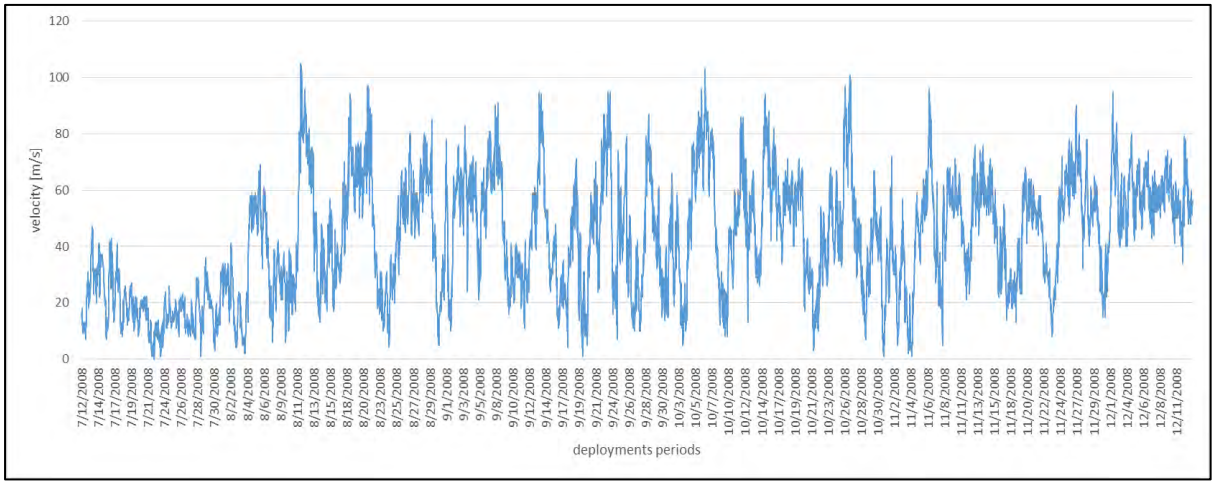

Figure 5-1: Variation of velocity of Agulhas Current from July 12, 2008 to December 13, 2008

The magnitude of the velocity of the Agulhas Current at each site is not the same. The graph in Figure 5-1 is a representative curve of the variation of the velocity magnitude from Cape Morgan which is one of the 51 deployments. This deployment is called CM301 and was measured from July 2008 to December 2008. Formula of the power according to Betz is used and estimation of the power available on the rotor for an ideal marine current turbine. Results of calculations are shown in Figure 5-2.

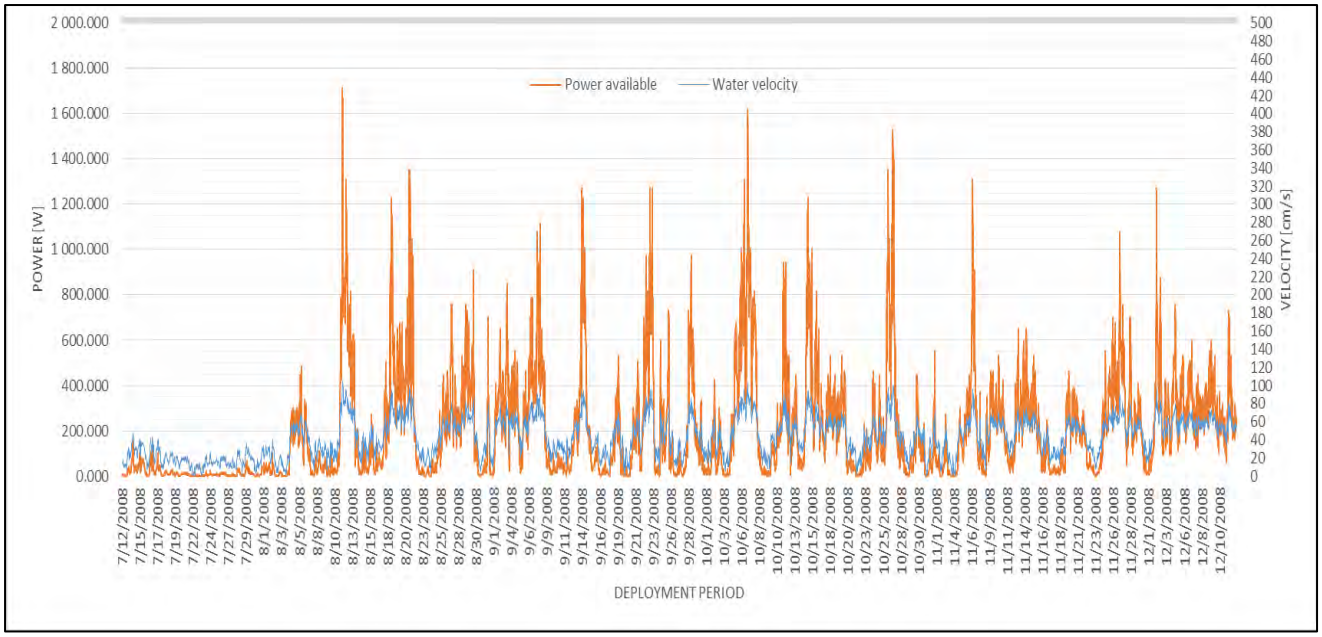

Figure 5-2: estimation after Betz of power available on the rotor.

Due to the weakness of the velocity, the power available is also weak and difficult to harvest with a small scale turbine. It is imperative to design an appropriate turbine which can run for this range of velocity and generate maximum power (Singh et al. 2012). For that, there is a need to start by analyzing the data collected from the deployments and choose the most advantageous site to build the project. Eskom provides some of this data on its website which was enough for the first analysis of the design. For each deployment, statistical analysis of data are conducted in order to evaluate the power available on the rotor of the turbine at each specific site. These values of the power available were taken into consideration for the design that suited the specific site. Analyzing the magnitude of the velocity from the set of data and calculating the mean value, the first percentile, the first quartile, the median, the third quartile, the hundredth percentile and the standard deviation.

Table 5-1: Statistical analysis of data from 9 different sites

	CM301	CM302	CM303	EL303	EL304	EL305	FR301	FR303	FR304	PE301	PE302	PE601
Mean value	42.8	30.0	45.0	44.5	35.2	40.3	34.9	29.5	30.9	32.6	33.5	29.4
First percentile	0	1	0	1	0	0	1	1	0	0	1	0
First quartile	23	14	28	30	22	26	24	17	18	19	21	17
Median	39	23	45	45	35	37	33	28	28	30	35	27
Third quartile	57	40	61	58	48	54	43	39	41	45	46	41
Hundredth percentile	105	107	112	104	91	107	115	103	119	97	70	81
Standard deviation	21.4	18.7	20.9	19.1	17.3	20.7	16.7	16.7	17.3	18.0	15.4	16.3

Define CM – Cape Morgan; EL – East London; FR – Fish River; PE – Port Edward .It can be seen in Table 5-1 that East London 303 and Cape Morgan 303 have the set of data with the highest mean value. The first quartile, the median, the third quartile and the hundredth percentile are also high. The standard deviation gives a high value because the first percentile is very small. Using this sample of data but rearranged in order to have an idea of the spread of magnitude from the first to the hundredth percentile, calculation of the standard deviation is to be done. This is giving us an idea of the consistency of the set of data close to the magnitude of 0.50 m/s. For these reasons, the designed study of the rotor to run with a velocity range between 0.3 m/s and 1.1 m/s is to be done. Remember that this velocity has been calculated at depths of 94 m for East London bin 303 and 83 m for Cape Morgan bin 303. The velocity profile on the surface is high and can reach an average velocity of 2.5 m/s. this velocity profile decreases with the depth. The rotor of our turbine will be centered in a way that the hub is situated where the area swept by the blades gives a maximum power output.

The Reynolds number for a small turbines is also a parameter to take into consideration for the design of the profile in order to harvest the maximum power possible from the power available on the rotor. The Reynolds number is a dimensionless value that measures the ratio of inertial forces to viscous forces and describes the degree of laminar or turbulent flow. Systems that operate at the same Reynolds number will have the same flow characteristics even if the fluid, speed and characteristic lengths vary. In our case the characteristic length used in Reynolds number formula is the mean value of the chord length.

$$\mathbf{R_e} = \frac{\rho v l}{\mu} = \frac{v l}{\upsilon} \qquad (5\text{-}1)$$

where :v Velocity of the fluid

l The characteristics length, the mean chord value of the foil

ρ The density of the fluid

μ The dynamic viscosity of the fluid

ν: The kinematic viscosity of the fluid

For an ideal blade the chord length distribution "c" and the pitch angle "β" are given by the following equations:

$$\mathbf{c} = \frac{8\pi r \cos\beta}{3B\lambda_r} \qquad (5\text{-}2)$$

$$\boldsymbol{\beta} = 90° - \frac{2}{3}\tan^{-1}\left(\frac{1}{\lambda_r}\right) \qquad (5\text{-}3)$$

where: B Number of blade

β Pitch angle of the blade

r Radius of local blade element [m]

λ_r Local tip speed ratio

The mean values of the velocity of the deployments EL303 and CM301 from Table 5-1 are respectively 44.5 m/s and 45.0 m/s. Thus the kinematic viscosity adopted for this calculation is equal to $1.004*10^{-6}$ m^2s^{-1} at 20 °C. The length chord is a characteristic dependent on the radius of the rotor. Betz and Schmitz give us different approaches on the calculation of the chord length, c, and the pitch angle, β.

Formulae after Betz are based on the profile in Figure 5-3 showing a blade element:

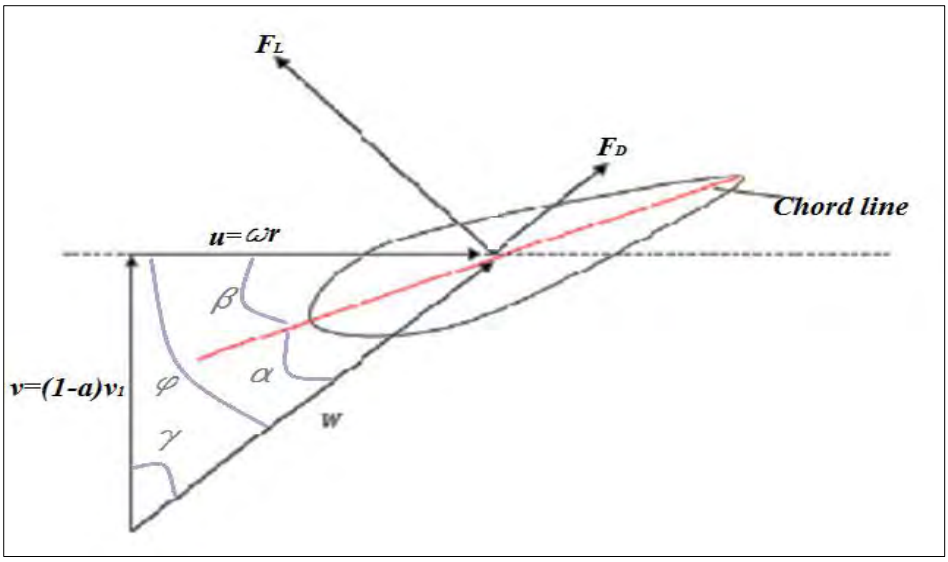

Figure 5-3: Velocities and angles on the blade after Betz. (Gundtoft 2009)

$$\lambda = \frac{v_{tip}}{v_1} = \frac{\omega R}{v_1} \tag{5-4}$$

$$\gamma_{(r)} = \arctan\frac{3r\lambda}{2R} \tag{5-5}$$

$$\varphi_{(r)} = \arctan\frac{2R}{3r\lambda} \tag{5-6}$$

$$\beta_{(r)Betz} = \arctan\frac{2R}{3r\lambda} - \alpha_D \tag{5-7}$$

$$c_{(r)Betz} = \frac{16\pi R}{9BC_{L,D}\lambda\sqrt{\lambda^2(\frac{r}{R})^2+\frac{4}{9}}} \tag{5-8}$$

where: λ Tip speed ratio

$\gamma_{(r)}$ Angle of relative fluid to rotor axis

$\varphi_{(r)}$ Angle of relative fluid to rotor plane

$\beta_{(r)}$ Betz pitch angle of the blade

R Blade radius [m]

r Radius of local blade element [m]

α_D Angle of attack giving the maximum glide ratio

B Number of blades

$C_{L,D}$ Coefficient of lift at the chosen angle of attack

Schmitz has developed a more detailed model of analysis of the flow in the rotor plane (Gundtoft 2009). According to Schmitz, following formulae have to be considered:

$$\beta_{(r)Schmitz} = \frac{2}{3}\arctan\frac{R}{r\lambda} - \alpha_D \quad (5\text{-}9)$$

$$\varphi_1 = \arctan\frac{v_1}{\omega r} = \arctan\frac{R}{r\lambda} \quad (5\text{-}10)$$

$$\varphi_{max} = \frac{2}{3}\varphi_1 \quad (5\text{-}11)$$

$$c_{(r)Schmitz} = \frac{1}{B}\frac{16\pi r}{C_L}\sin^2\left(\frac{1}{3}\arctan\left(\frac{R}{\lambda r}\right)\right) \quad (5\text{-}12)$$

$$C_{P,Schmitz} = \frac{P_{Schmitz}}{\frac{1}{2}\rho v_1^3 A} \quad (5\text{-}13)$$

$$P_{schmitz} = \frac{1}{2}\rho\pi R^2 v_1^3 \int_0^1 4\lambda\left(\frac{r}{R}\right)^2 \frac{\sin^3\left(\frac{2}{3}\varphi_1\right)}{\sin^2(\varphi_1)}\,d\left(\frac{r}{R}\right) \quad (5\text{-}14)$$

Where: C_P Coefficient of power

$P_{schmitz}$ Power of the rotor available on the shaft.

Chapter 6 : ROTOR PROFILE AND EVALUATION OF THE POWER

The design of the rotor depends on the condition in which the turbine is going to operate. The power that a turbine can harness from the ocean current also depends on the rotor design. The characteristics of the flow are the most important values in order to choose the profile of the rotor. Referring to similar studies which are based on marine currents and wind turbines and analyzing those systems in order to develop a system with maximum yield for ocean current in conditions of this study, many airfoil profiles have been analyzed at different Reynolds numbers (Christopher et al. 1997). In this study, a low-speed airfoil profile was firstly adapted and result while using it for ocean current were analyzed. The blade of the rotor is struck in an angle of attack "α" by the water current, creating a force which can be divided into two components that can be described as the lift force "F_L" which is perpendicular to the water direction on the side of the blade and the drag force "F_D" which is parallel (Grogan et al. 2013).

The lift force as shown in Figure 5-3 is calculated as

$$\mathbf{F_L = C_L \frac{1}{2} \rho \omega^2 (bc)} \qquad (6\text{-}1)$$

where: C_L Lift coefficient depending on the angle of attack

ρ Density of the fluid

ω Relative fluid speed

b Wide of the blade

c Length of the chord line.

The drag force also shown in Figure 5-3 is calculated as

$$\mathbf{F_D = C_D \frac{1}{2} \rho \omega^2 (bc)} \qquad (6\text{-}2)$$

where: C_D coefficient of drag depending on the angle of attack

Most blades are designed with an angle of attack of less than 15° in order to avoid the phenomenon called "stall" (Thumthae and Chitsomboon 2009). The different angles in the design of the blade are well described in Figure 5-3 taking as reference the chord line of the

blade (Anyi and Kirke 2011). In addition to the angle of attack, there are also have the angle relative to the rotor axis "$\Upsilon_{(R)}$, the angle of relative wind to the rotor plane "$\phi_{(R)}$, and the pitch angle of the blade "$\beta_{(R)}$. All these angles depend on the given radius (Grogan et al. 2013). Also taking into consideration the glide ratio (GR = C_L/C_D) for marine turbines which, must be as high as possible and can even reach a value of 100 or more. Angles of attack between 5° and 10° are the ones giving a maximum value of the glide ratio.

The wind turbine profile adapted for this analysis is the "Gottingen 417a (M. Fox)" usually called Goe 417a (Christopher et al. 1997; Selig et al. 1995). This particular profile has been chosen because the value of the glide ratio is high for a range of Reynolds for small horizontal axis turbine running in a low-speed water current. Its properties are compared with the "BW-3" designed by Bergey Windpower for use on their small wind turbine systems. The Goe 417a has a wedge-shaped drag polar and a $C_{L,\,max}$ of 1.4 and offers a better performance than the BW-3 according the maximum L/D. Hence the Goe 417a is suitable for low velocity wind turbines or for small Reynolds numbers. The main reason to use this profile in this research is because the Agulhas Current in which need to be build the system has a mean value velocity of less than 1.3 m/s. Figure 6-1 shows the drag polar for different Reynolds numbers of Goe 417a. These curves allow us to find the best value of the glide ratio and to choose the best value for the angle of attack for the design of the blades.

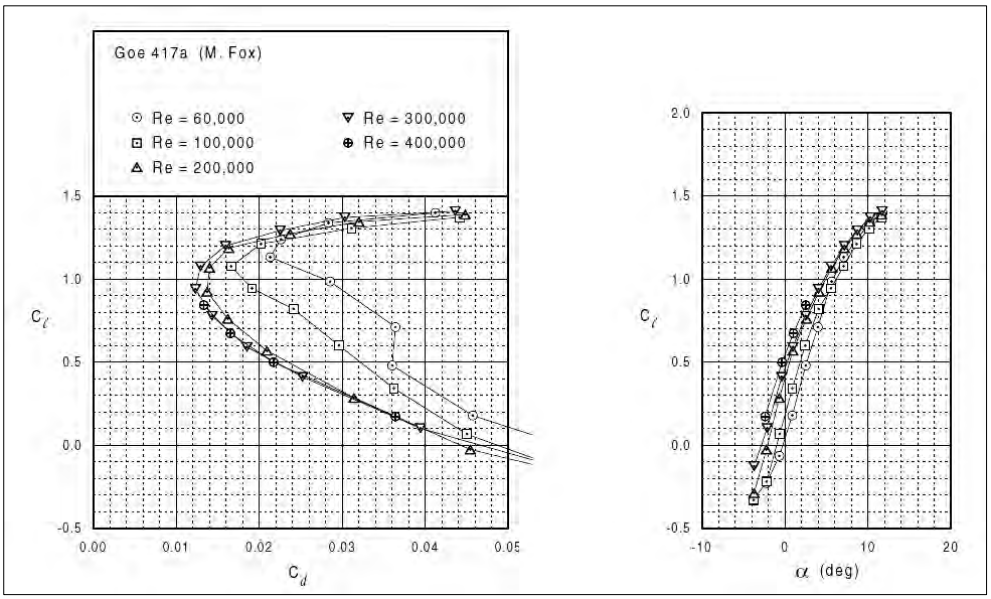

Figure 6-1: Drag polar for Goe 417a and Coefficient of lift as a function of the angle of attack (Selig et al. 1995)

From Figure 6-1Figure 6-1, the highest value of the glide ratio C_L/C_D is calculated and leaded to find the optimum C_L=1.07. This value gave an angle of attack of 6.5°. Choosing a tip speed ratio of 7 to avoid cavitation (Myers and Bahaj 2010). The number of blades is chosen to be 3 and a blade radius of 2 m (Goundar and Ahmed 2014). Then an evaluation of the parameters of the blade after Betz and Schmitz using blade element momentum (BEM) theory and finding the chord length which is important to evaluate the Reynolds number and design the blades.

6.1 : THE BLADE ELEMENT MOMENTUM THEORY

Blade element momentum theory is a theory that combines two methods of examining operations of wind turbines. It is used to calculate the local forces generated by the lift and drag coefficients of an airfoil on a propeller or wind-turbine at many different sections along the blade. Blade element theory is combined with momentum theory which is to use a momentum balance on a rotation annular stream tube passing through a turbine (Ingram 2005). The use of these two methods combined alleviates some of the difficulties in calculating the induced velocities at the rotor by a series of equations that can be solved iteratively. Momentum theory was used to calculate the axial force. Considering the stream tube around the turbine, four stations can be seen as shown in Figure 6-2. We can assume from Figure 4-1that p_1 is equal to p_4 and v_2 is equal to v_3.

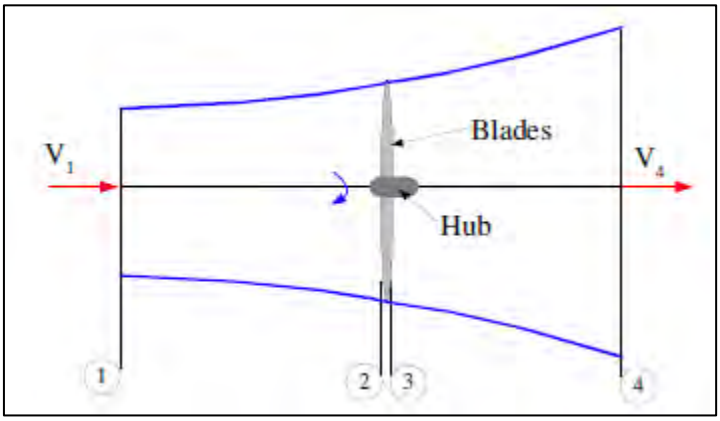

Figure 6-2: Axial stream tube around a wind turbine (Ingram 2005)

Assuming the flow to be frictionless and applying Bernoulli's equation, it gives:

$$p_2 - p_3 = \frac{1}{2}\rho(v_1^2 - v_4^2)$$

$$dF = (p_2 - p_3)dA$$

$$\boldsymbol{dF = \frac{1}{2}\rho\left(v_1^2 - v_4^2\right)dA} \quad (6\text{-}3)$$

Define "a" as the induction factor so:

$v_2 = v_1(1 - a)$

$v_4 = v_1(1 - 2a)$

The axial force can be express as:

$$\boldsymbol{dF = \frac{1}{2}\rho v_1^2[4a(1 - a)]2\pi r dr} \quad (6\text{-}4)$$

6.1.1 MOMENTUM THEORY

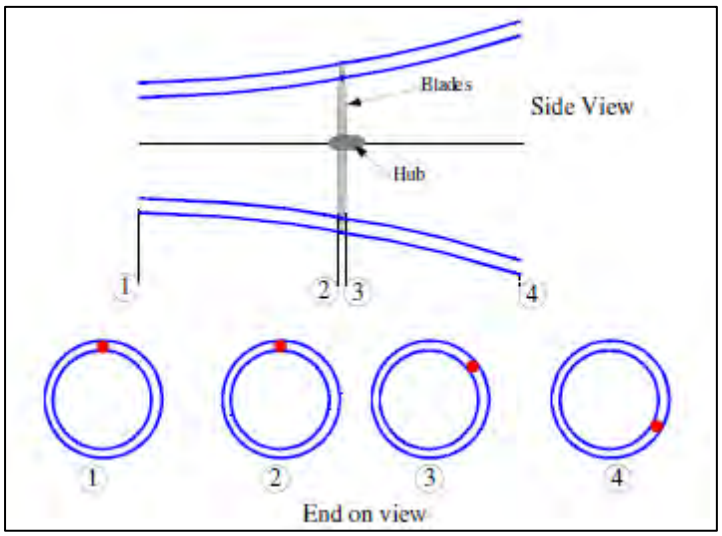

Figure 6-3: Rotating annular stream tube (Ingram 2005)

The rotating annular stream tube shown in Figure 6-3 imparts a rotation onto the blade wake. Assume the blade wake rotating with an angular velocity ω and the blades rotating with an angular velocity of Ω. From these can be calculated the moment of inertia of an annulus I, angular moment L, torque T and the angular induction factor a'.

$I = mr^2$

$L = I\omega$

$T = \frac{dL}{dt}$

$$\mathbf{T = \frac{dI\omega}{dt} = \frac{d(mr^2\omega)}{dt} = \frac{dm}{dt}r^2\omega} \quad (6\text{-}5)$$

For a small element the corresponding torque will be:

$$dT = d\dot{m}\omega r^2$$

And for the rotating annular element

$$d\dot{m} = \rho A v_2$$

$$d\dot{m} = \rho 2\pi r dr v_2$$

$$\mathbf{dT = \rho\omega r^2 2\pi r dr v_2 = \rho v_2 \omega r^2 2\pi r dr} \quad (6\text{-}6)$$

Define angular induction factor a':

$$\mathbf{a' = \frac{\omega}{2\Omega}} \quad (6\text{-}7)$$

Momentum theory has therefore yielded equations for the axial and tangential force on an annular element of fluid.

6.1.2 BLADE ELEMENT THEORY

Dividing a blade into N elements as shown in Figure 6-4Figure 6-4. These elements are different and experience different flow characteristics. The rotational speed (Ωr), the chord length (c) and the whist angle (γ) of each element is different to those of the neighbouring blade. Blade element theory involves the calculation of the flow at each of these elements and performance characteristics are found by numerical integration along the blade span.

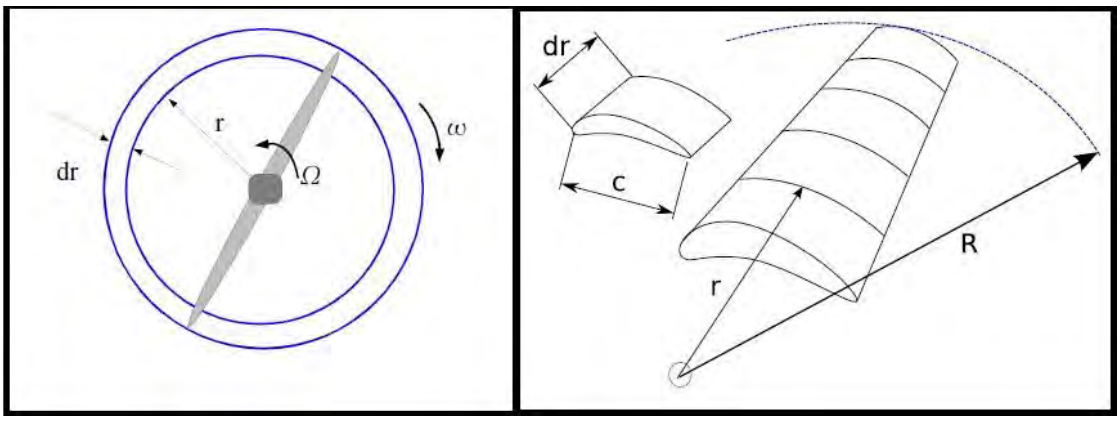

Figure 6-4: Rotating annular stream tube and blade element model (Ingram 2005)

Values of lift and drag coefficient are found from different aerofoils from wind tunnel data (Hansen and Butterfield 1993). Other characteristic values are found from the following figures.

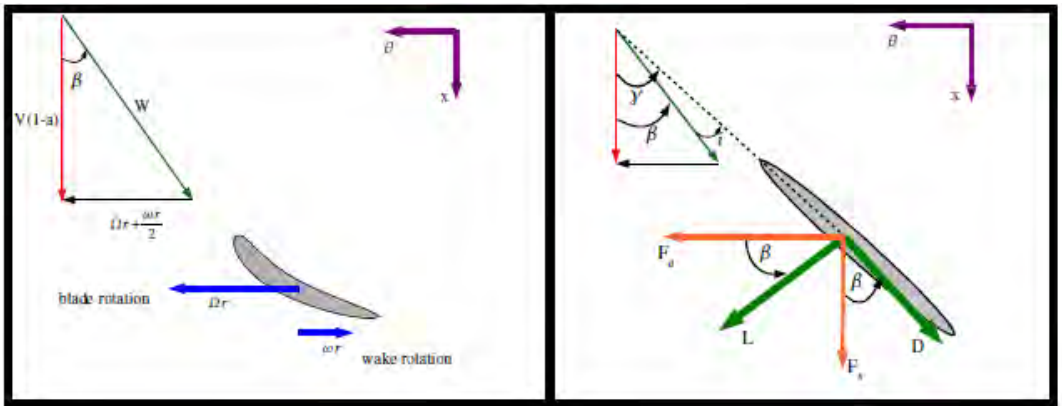

Figure 6-5: Flow on a turbine blade and forces applied on it (Ingram 2005)

The flow around the blades as shown in Figure 6-5starts at station 2 and ends at station 3. This flow is not rotational at the inlet but it has a rotational speed ω at the exit. The average rotational flow is therefore ω/2 while the blade is turning with a speed Ω. The average velocity that the blade experiences is "Ωr+0.5ωr" as shown in Figure 6-5.

- Examining Figure 6-5 the following can be deducted:

$$\Omega r + \frac{\omega r}{2} = \Omega r(1 + a')$$

$$tan\beta = \frac{\Omega r(1+a')}{v(1-a)}$$

"v" is representing the incoming flow velocity "v_1". The value of β is not the same for all blade elements. The local tip speed ratio λ_r is defined as:

$$\lambda_r = \frac{\Omega r}{v}$$

From formulae and figure above, the following can be observed:

$$\mathbf{tan\beta} = \frac{\boldsymbol{\lambda_r(1+a')}}{\mathbf{1-a}} \qquad (6\text{-}8)$$

$$w = \frac{v(1-a)}{cos\beta}$$

Error! Reference source not found. shows forces acting on the blade element as vectors that can be used to calculate the following:

$$dF_\theta = dLcos\beta - dDsin\beta$$

$$dF_x = dLsin\beta + dDcos\beta$$

With: dL: lift force on the blade element

dD: drag force on the blade element.

$$dL = C_L \frac{1}{2}\rho w^2 cdr$$

$$dD = C_D \frac{1}{2}\rho w^2 cdr$$

Knowing that the torque dT is the tangential force multiplied by the radius and simplifying these equations by expressing β and w in terms of induction factors we get to the following:

$$\boldsymbol{dF_x = \sigma'\pi\rho\frac{v^2(1-a)^2}{cos^2\beta}(C_L sin\beta + C_D cos\beta)rdr} \quad (6\text{-}9)$$

$$\boldsymbol{dT = \sigma'\pi\rho\frac{v^2(1-a)^2}{cos^2\beta}(C_L cos\beta - C_D sin\beta)r^2 dr} \quad (6\text{-}10)$$

where σ' is called the local solidity and is defined as:

$$\sigma' = \frac{Bc}{2\pi r}$$

6.1.3 TIP LOSS CORRECTION

Losses at the tip of a turbine blade are unavoidable. A correction factor Q which varies from 0 to 1 is introduced to characterise the reduction in forces along the blade.

$$\boldsymbol{Q = \frac{2}{\pi}cos^{-1}\left\{exp\left[-\frac{\frac{B}{2}\left(1-\frac{r}{R}\right)}{\frac{r}{R}cos\beta}\right]\right\}} \quad (6\text{-}11)$$

Applying the loss correction to the equation of force and torque:

$$\boldsymbol{dF = Q\rho v_1^2[4a(1-a)]\pi r dr} \quad (6\text{-}12)$$

$$\boldsymbol{dT = Q4a'(1-a)\rho v\Omega r^3\pi dr} \quad (6\text{-}13)$$

Having equations describing axial thrust and torques from momentum theory in terms of flow parameters and equations, those derived from consideration of blade forces expressing the axial force and torque in terms of the lift and drag coefficients of aerofoil. From these equations can be extracted the following useful relationships:

$$\frac{a}{1-a} = \frac{\sigma'(C_L sin\beta + C_D cos\beta)}{4Q cos^2\beta} \quad (6\text{-}14)$$

$$\frac{a'}{1-a} = \frac{\sigma'(C_L cos\beta - C_D sin\beta)}{4Q\lambda_r cos^2\beta} \quad (6\text{-}15)$$

6.1.4 POWER OUTPUT

The power output is the total of the power from each annulus

$dP = \Omega dT$

$$\boldsymbol{P = \int_{r_h}^{R} \Omega dT dr} \quad (6\text{-}16)$$

where: r_h Radius of the hub. The power coefficient C_P is given by:

$$\boldsymbol{C_P = \frac{P}{P_{wind}} = \frac{\int_{r_h}^{R} \Omega dT}{\frac{1}{2}\rho\pi R^2 v^3} = \frac{8}{\lambda^2}\int_{\lambda_h}^{\lambda} Q\lambda_r^3 a'(1-a)\left[1 - \frac{C_D}{C_L} tan\beta\right] d\lambda_r} \quad (6\text{-}17)$$

Recall the trapezium rule:

$$\int_{x_0}^{x_n} f(x)dx \approx \frac{x_n - x_0}{2n}[(y_0 + y_n) + 2(y_1 + y_2 + \cdots + y_{n-1})] \quad (6\text{-}18)$$

6.2 DESIGN OF THE ROTOR USING BEM THEORY

The purpose of this research is to design a system generating electricity from the ocean current. Theories and formula as enumerated above are helpful for the design of rotors of horizontal axis ocean current turbines. In this section a 3 blades turbine rotor of 2 m blade radius using the profile of the Goe 417a described above will be design. Water velocity set at 1 m/s and a tip speed ratio of 7 in order to avoid cavitation that can occur for values bigger than 8. We can evaluate the first values that will allow to start iterations until values of "a, a' and β" that will finally be used for the design of the rotor will be obtained. The blade divided into 20 segments and the mean value of ideal chord distribution calculated with equation 5-2. The results are shown in Table 6-1 below and the chord mean value has been evaluated at 0.1088 for the turbine blade. Using the mean chord value to calculate the Reynold number

using equation (5.1) and finding it equal to 103 000. From Figure 6-1 evaluate the right glide ratio on the curve giving a Reynold number of 100 000 and we find the value of C_L at 1.07. This value of C_L gives for the Goe 417a 6.5° as corresponding angle of attack. The following tables was used for our calculations:

Table 6-1: chord length, pitch angle, axial and angular induction factor for ideal blade

$\pi=3.141593;\ v=1\,m/s;\ B=3;\ \lambda=7;\ R=2\,m;\ C_L=1.07;\ C_D=0.0223;\ \alpha=6.5°$							
Station number	Blade element	λr	ideal β [rad]	ideal c [m]	σ'	a guess	a' guess
1	0.1	0.35	0.748049	0.584849	2.792448	0.486029	-0.4852
2	0.2	0.7	0.930749	0.476511	1.137587	0.406273	-0.35006
3	0.3	1.05	1.063454	0.387647	0.61696	0.379298	-0.26662
4	0.4	1.4	1.157297	0.320595	0.382682	0.367325	-0.21729
5	0.5	1.75	1.224699	0.270659	0.25846	0.361094	-0.18742
6	0.6	2.1	1.274517	0.232948	0.185374	0.357481	-0.1685
7	0.7	2.45	1.312447	0.203842	0.139039	0.355214	-0.15597
8	0.8	2.8	1.342114	0.180872	0.10795	0.353703	-0.14732
9	0.9	3.15	1.365865	0.162366	0.086138	0.352649	-0.14113
10	1	3.5	1.385263	0.147183	0.070274	0.351885	-0.13657
11	1.1	3.85	1.40138	0.134526	0.058392	0.351315	-0.13311
12	1.2	4.2	1.414968	0.123828	0.049269	0.350878	-0.13044
13	1.3	4.55	1.426569	0.114675	0.042118	0.350536	-0.12833
14	1.4	4.9	1.436585	0.106761	0.036411	0.350264	-0.12665
15	1.5	5.25	1.445315	0.099854	0.031785	0.350043	-0.12527
16	1.6	5.6	1.45299	0.093776	0.027984	0.349862	-0.12414
17	1.7	5.95	1.459789	0.088387	0.024825	0.349712	-0.12319
18	1.8	6.3	1.465852	0.083578	0.02217	0.349586	-0.1224
19	1.9	6.65	1.471291	0.079261	0.019918	0.349479	-0.12172
20	2	7	1.476198	0.075364	0.017992	0.349387	-0.12115

From the values of pitch angle "β", axial induction factor "a" and angular induction factor "a'" in the Table 6-1 above, evaluation by iterations using equations 7.6, 7.12 and 7.13 to find the appropriate pitch angle, axial and angular induction factors respectively can begin. Results of those iterations are shown in the following tables:

Table 6-2: Iterations 1 to 3 for β, a and a'.

Iteration 1			Iteration 2			Iteration 3		
β	a	a'	β	a	a'	β	a	a'
0.33718	0.21721	1.77033	0.89161	0.59563	1.37389	1.11785	0.77813	1.08203
0.65384	0.22706	0.42332	0.91099	0.39022	0.43247	1.02442	0.49059	0.42620
0.89237	0.24600	0.18884	1.02742	0.34574	0.19889	1.09149	0.40778	0.20184
1.04718	0.26177	0.10796	1.12659	0.33356	0.11339	1.16677	0.37851	0.11559
1.14853	0.27298	0.07008	1.20048	0.32979	0.07316	1.22802	0.36565	0.07456
1.21821	0.28070	0.04918	1.25524	0.32860	0.05108	1.27551	0.35905	0.05201
1.26854	0.28607	0.03641	1.29671	0.32829	0.03767	1.31248	0.35528	0.03831
1.30643	0.28990	0.02803	1.32893	0.32828	0.02892	1.34173	0.35294	0.02939
1.33593	0.29269	0.02223	1.35457	0.32838	0.02290	1.36530	0.35138	0.02325
1.35953	0.29478	0.01806	1.37541	0.32851	0.01858	1.38462	0.35030	0.01885
1.37883	0.29638	0.01496	1.39264	0.32863	0.01537	1.40071	0.34952	0.01559
1.39490	0.29762	0.01259	1.40712	0.32875	0.01293	1.41430	0.34894	0.01311
1.40848	0.29861	0.01075	1.41945	0.32885	0.01102	1.42592	0.34849	0.01117
1.42012	0.29941	0.00928	1.43007	0.32894	0.00951	1.43596	0.34814	0.00964
1.43020	0.30006	0.00809	1.43931	0.32901	0.00829	1.44471	0.34786	0.00840
1.43901	0.30060	0.00712	1.44742	0.32908	0.00729	1.45241	0.34763	0.00738
1.44679	0.30104	0.00631	1.45459	0.32914	0.00646	1.45923	0.34744	0.00654
1.45370	0.30142	0.00563	1.46098	0.32918	0.00576	1.46532	0.34729	0.00584
1.45987	0.30175	0.00505	1.46670	0.32923	0.00517	1.47078	0.34716	0.00524
1.46543	0.30202	0.00456	1.47186	0.32927	0.00467	1.47571	0.34705	0.00473

Table 6-3: Iterations 4 to 6 for β, a and a'.

iteration 4			iteration 5			iteration 6		
β	a	a'	β	a	a'	β	a	a'
1.27525	0.89388	0.77758	1.40186	0.96303	0.46931	1.49902	0.99315	0.20401
1.09898	0.56750	0.41367	1.15876	0.63485	0.39638	1.21328	0.69949	0.37330
1.13202	0.45289	0.20242	1.16188	0.48923	0.20191	1.18622	0.52082	0.20075
1.19208	0.41031	0.11662	1.21008	0.43468	0.11712	1.22394	0.45447	0.11734
1.24545	0.39069	0.07531	1.25766	0.40939	0.07575	1.26679	0.42403	0.07602
1.28842	0.38020	0.05253	1.29740	0.39575	0.05285	1.30402	0.40767	0.05305
1.32258	0.37396	0.03868	1.32958	0.38759	0.03892	1.33468	0.39789	0.03907
1.34996	0.36997	0.02966	1.35565	0.38232	0.02984	1.35978	0.39158	0.02996
1.37222	0.36726	0.02346	1.37699	0.37872	0.02360	1.38045	0.38727	0.02369
1.39058	0.36534	0.01902	1.39469	0.37616	0.01912	1.39765	0.38420	0.01920
1.40594	0.36392	0.01573	1.40955	0.37427	0.01581	1.41214	0.38193	0.01587
1.41896	0.36285	0.01322	1.42218	0.37284	0.01329	1.42448	0.38021	0.01334
1.43012	0.36203	0.01127	1.43302	0.37173	0.01133	1.43510	0.37887	0.01137
1.43979	0.36137	0.00972	1.44243	0.37084	0.00977	1.44432	0.37781	0.00980
1.44823	0.36084	0.00847	1.45066	0.37013	0.00851	1.45239	0.37696	0.00854
1.45567	0.36041	0.00744	1.45791	0.36955	0.00748	1.45951	0.37626	0.00751
1.46226	0.36006	0.00659	1.46435	0.36907	0.00663	1.46584	0.37568	0.00665
1.46815	0.35976	0.00588	1.47011	0.36867	0.00591	1.47150	0.37520	0.00593
1.47344	0.35951	0.00528	1.47528	0.36833	0.00531	1.47659	0.37479	0.00533
1.47822	0.35929	0.00477	1.47995	0.36804	0.00479	1.48119	0.37444	0.00481

After finding the values of β in iteration 6, equation 4-16 is used to find the chord length after Betz's so that the first profile of the blade will be design. Table 6-4 shows the result of calculations using equation 4.16 for Goe 417a.

Table 6-4: values of the chord length after Betz

Station no. (1 root, 20 tip)	Blade element, **r** (meter)	Local tip speed ratio, λ_r	Chord length after Betz **c** (meter)	Twist angle β [rad]	Angle of relative fluid to rotor plan φ=β+α [°]
1	0.1	0.35	0.660	1.49902	92.38774
2	0.2	0.7	0.514	1.21328	76.01563
3	0.3	1.05	0.400	1.18622	74.46534
4	0.4	1.4	0.321	1.22394	76.62674
5	0.5	1.75	0.265	1.26679	79.08197
6	0.6	2.1	0.226	1.30402	81.21459
7	0.7	2.45	0.196	1.33468	82.97168
8	0.8	2.8	0.173	1.35978	84.40942
9	0.9	3.15	0.154	1.38045	85.59368
10	1	3.5	0.140	1.39765	86.57961
11	1.1	3.85	0.127	1.41214	87.40991
12	1.2	4.2	0.117	1.42448	88.11692
13	1.3	4.55	0.108	1.43510	88.72516
14	1.4	4.9	0.101	1.44432	89.25333
15	1.5	5.25	0.094	1.45239	89.71586
16	1.6	5.6	0.088	1.45951	90.12400
17	1.7	5.95	0.083	1.46584	90.48663
18	1.8	6.3	0.078	1.47150	90.81083
19	1.9	6.65	0.074	1.47659	91.10233
20	2	7	0.071	1.48119	91.36576

From values of the chord length in

Table 6-4 and using the aerofoil data file by multiplying its data coordinates by the chord length of each segment. Because the value of the angle near the hub does not really interfere in the power output value, it has been edited in order to give a suitable shape to the blade. This gives00 the profile of each segment and the values are shown in the Table 6-5.

Table 6-5: Coordinates x and y for different segments of the blade design

Goe 417a (Gew-platte) Airfoil data file		c = 0.660		c = 0.514		c = 0.400		c = 0.321	
X	Y	**x**	**y**	**x**	**y**	**x**	**y**	**x**	**y**
0.000	0.000	0.000	0.000	0.000	0.000	0.000	0.000	0.000	0.000
0.013	0.016	0.008	0.010	0.006	0.008	0.005	0.006	0.004	0.005
0.025	0.022	0.017	0.015	0.013	0.011	0.010	0.009	0.008	0.007
0.050	0.033	0.033	0.021	0.026	0.017	0.020	0.013	0.016	0.010
0.075	0.042	0.050	0.027	0.039	0.021	0.030	0.017	0.024	0.013
0.100	0.049	0.066	0.032	0.051	0.025	0.040	0.019	0.032	0.016
0.150	0.057	0.099	0.038	0.077	0.029	0.060	0.023	0.048	0.018
0.200	0.063	0.132	0.042	0.103	0.032	0.080	0.025	0.064	0.020
0.300	0.072	0.198	0.047	0.154	0.037	0.120	0.029	0.096	0.023
0.400	0.074	0.264	0.049	0.206	0.038	0.160	0.029	0.128	0.024
0.500	0.070	0.330	0.046	0.257	0.036	0.200	0.028	0.160	0.022
0.600	0.064	0.396	0.042	0.309	0.033	0.240	0.026	0.192	0.021
0.700	0.055	0.462	0.036	0.360	0.028	0.280	0.022	0.224	0.017
0.800	0.043	0.528	0.028	0.411	0.022	0.320	0.017	0.256	0.014
0.900	0.024	0.594	0.016	0.463	0.012	0.360	0.010	0.289	0.008
1.000	0.000	0.660	0.000	0.514	0.000	0.400	0.000	0.321	0.000
0.900	-0.002	0.594	-0.001	0.463	-0.001	0.360	-0.001	0.289	0.000
0.800	0.014	0.528	0.009	0.411	0.007	0.320	0.005	0.256	0.004
0.700	0.026	0.462	0.017	0.360	0.013	0.280	0.010	0.224	0.008
0.600	0.035	0.396	0.023	0.309	0.018	0.240	0.014	0.192	0.011
0.500	0.041	0.330	0.027	0.257	0.021	0.200	0.016	0.160	0.013
0.400	0.045	0.264	0.029	0.206	0.023	0.160	0.018	0.128	0.014
0.300	0.043	0.198	0.028	0.154	0.022	0.120	0.017	0.096	0.014
0.200	0.034	0.132	0.022	0.103	0.017	0.080	0.014	0.064	0.011
0.150	0.028	0.099	0.018	0.077	0.014	0.060	0.011	0.048	0.009
0.100	0.019	0.066	0.012	0.051	0.010	0.040	0.007	0.032	0.006
0.075	0.011	0.050	0.007	0.039	0.005	0.030	0.004	0.024	0.003
0.050	0.001	0.033	0.001	0.026	0.001	0.020	0.000	0.016	0.000
0.025	-0.010	0.017	-0.007	0.013	-0.005	0.010	-0.004	0.008	-0.003
0.013	-0.014	0.008	-0.009	0.006	-0.007	0.005	-0.006	0.004	-0.004
0.000	0.000	0.000	0.000	0.000	0.000	0.000	0.000	0.000	0.000

6.2.1 ROTOR PROFILE USING AUTODESK INVENTOR PROFESSIONAL

Now that we have the chord length and the pitch angle of each segment, Autodesk Inventor Professional is used to design the 3 blades rotor of the turbine. From Figure 6-6 can be seen step 1 showing 20 different work plans with each profile from the root to the tip. Step 2 shows profiles without work plans. Step 3 is the first blade with the 2D profiles shown after

extruding them. Step 4 shows the blade on its own. Step 5 and 6 show the complete turbine rotor in two different angles of view.

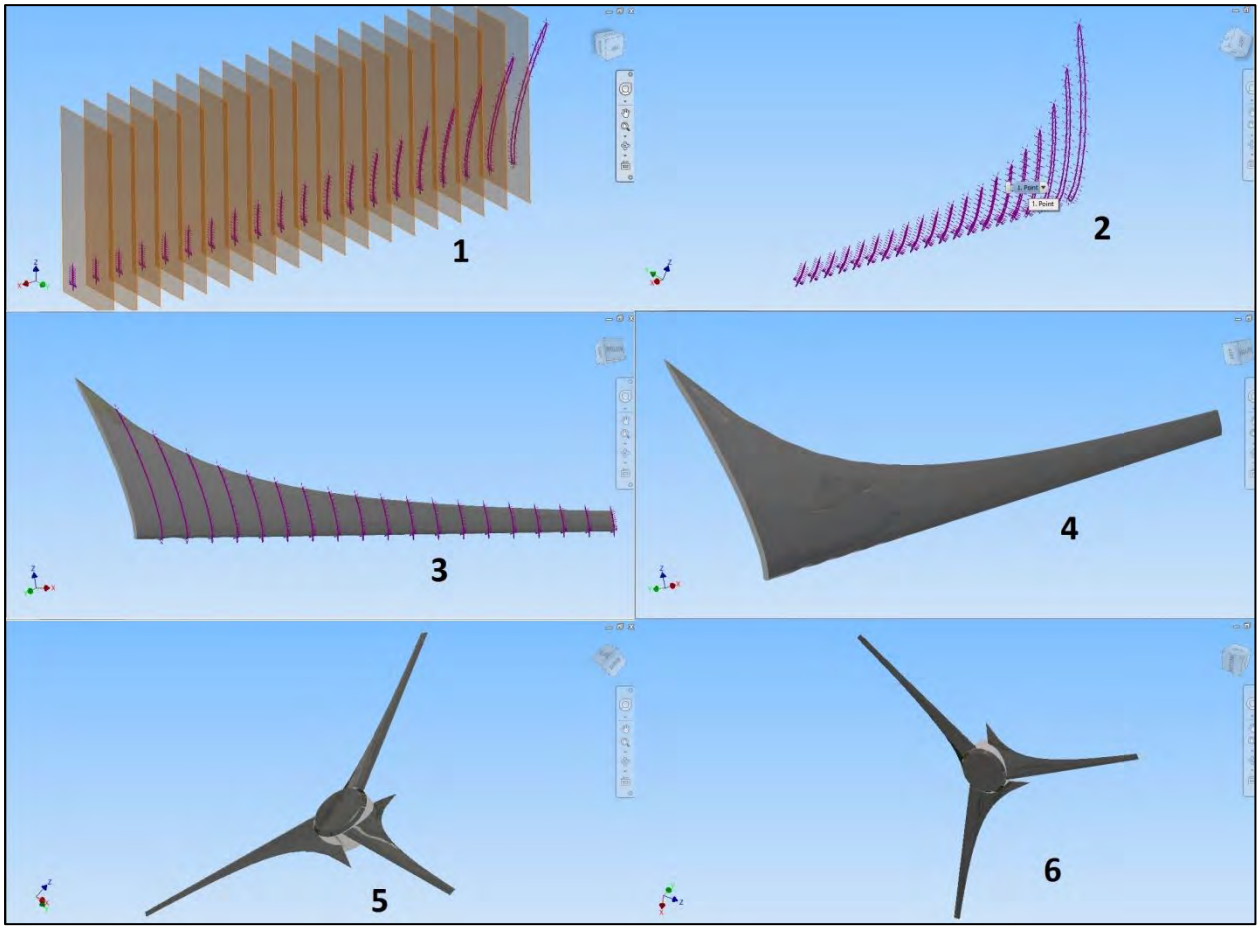

Figure 6-6: Design of the 3 blades turbine after Betz using Autodesk Inventor Professional

The material used for this design is Steel AISI 8640 361 QT which is described as Medium Hardenability Ni-Cr-Mo Steel with 0.40-0.42 carbon content, Quenched & Tempered. It has a Young's Modulus of 2 070E + 11 Pa, Poisson's Ratio of 0.33, Shear Modulus of 7 782E +10 Pa , Density of 7 850E + 03 kg/m³, Yield Strength of 1 306E+09 Pa and Tensile Strength of 1 373E + 09 Pa. For this study it's assumeed that we are using electroplating. This is a process during which the rotor is coated with another metal such tin, chromium or silver to avoid rust. The choice steel as material is just for the undergoing study. The next step of this study will be to find affordable and appropriated materials that will suit all conditions under water. Strength analysis using Autodesk Inventor Professional and simulations using Autodesk CFD were done on this prototype and results are displayed below. The velocity profile of the Agulhas Current on the surface easily reaches 2.5 m/s and decreases with depth.

6.2.2 SIMULATION USING AUTODESK CFD

The CFD model was based on a velocity of 1 m/s as an average velocity. We have data measured at a depth of 80 m under sea level and we know that the Agulhas Current can reach a surface velocity of 2 m/s. Since the profile of the velocity current is not constant, the value of the power output will also vary. We measured the change in pressure by running a simulation. The result of this simulation showed us values that we can measure on a plan that we set across the blade. This plan is cutting the blade element and we pick some point in a straight line starting upstream, passing the blade element and ending downstream of the rotor. From those points we can analyse the change in pressure when water hits the blade. The results shown in curves are just on a very small surface area of the blade. An integration calculation gives a global idea of the total change in pressure. Using the theory of momentum of inertia we were able to evaluate the power output of the whole system.

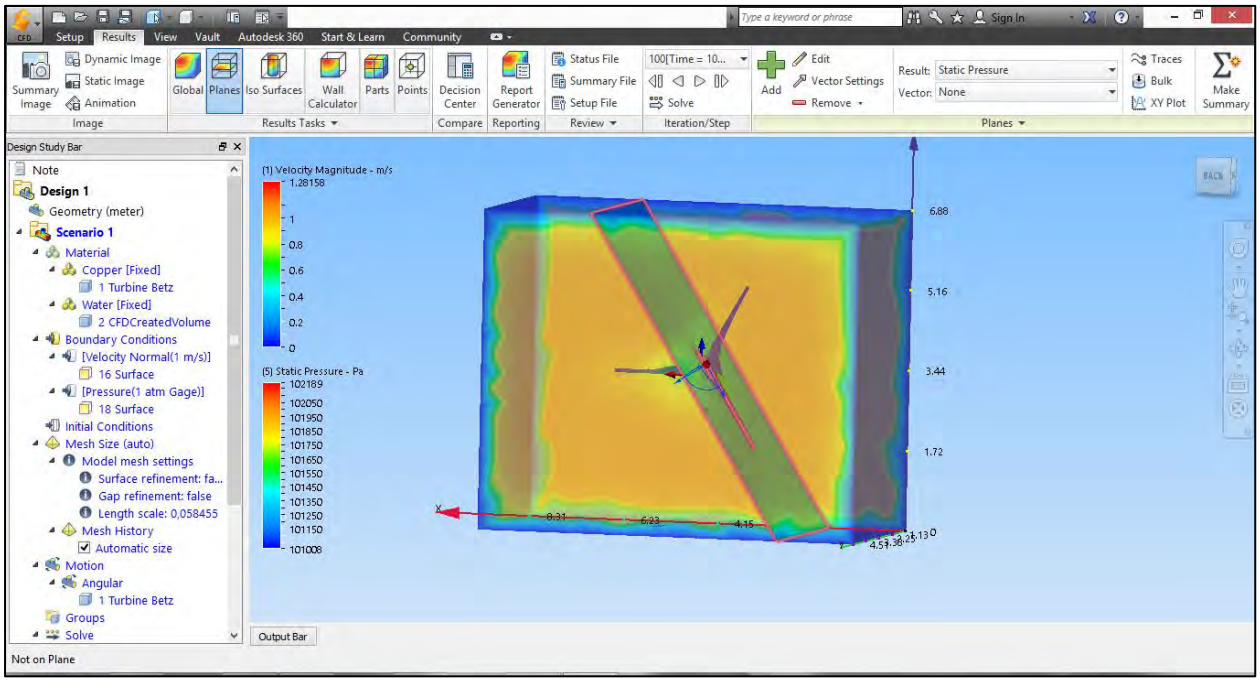

Figure 6-7: Cutting plan cutting turbine blade for pressure change analysis upstream and downstream the blade.

The CFD model in Figure 6-7 represents the turbine surrounded by water and cut on one of its blades by a plan on which measurement of velocity and pressure can be done upstream and downstream the blade. Found the network which is the change in kinetic energy at the surface of the blade where water hits the blade and loses its velocity. The pressure rises then suddenly drops to rise again. This pressure change needs to be analysed for each cut along the

blade to calculate the total pressure change all along the blade. The sum of all forces acting on the blade is the resultant force that can run the turbine.

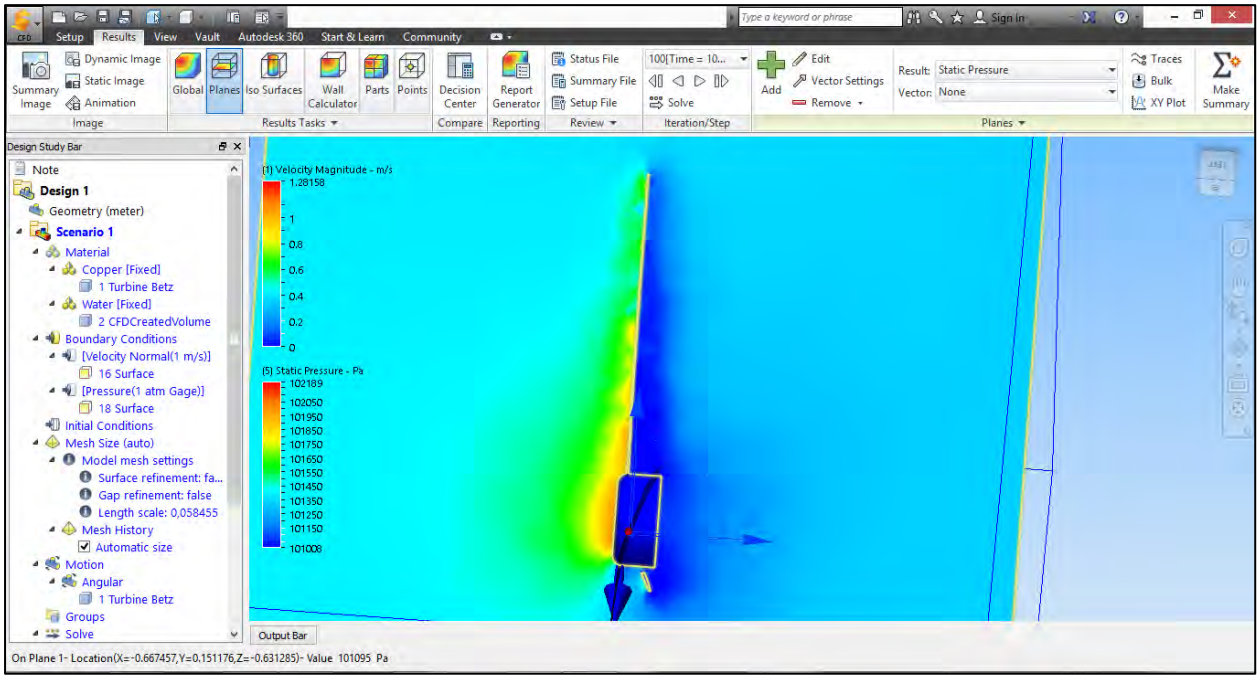

Figure 6-8: Change in pressure along the blade element.

Using Autodesk CFD, we display the result in a plan that is cutting the blade like the one in **Error! Reference source not found.** on this plan we can see the change in pressure of a column of water flowing in the direction of the blade. Figure 6-8 clearly shows an increase in pressure when water is getting closer to the blade and a considerably less pressure just after the blade. This explains the change in pressure that we already studied in chapter 4 as shown in Figure 4-1.

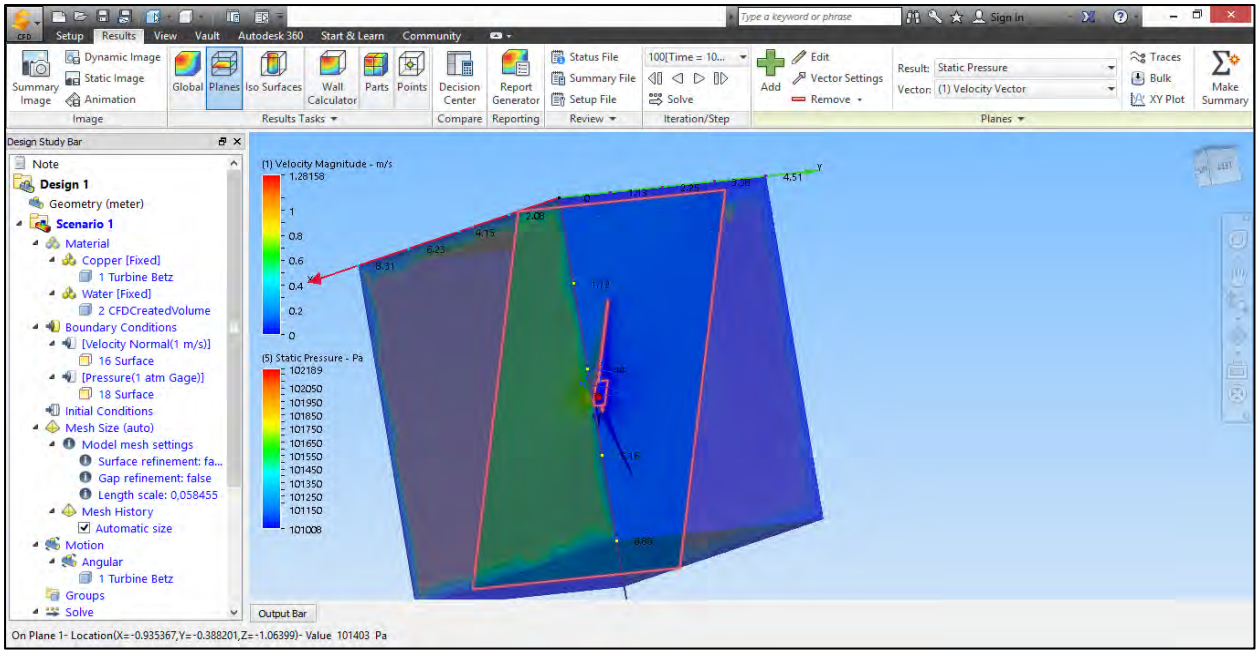

Figure 6-9: Blade cut by a plan with vectors showing the direction of the flow

Figure 6-9 shows the plan and the direction of the flow surrounding the blade. The velocity and pressure in the legend on the left is visible when the picture is taken in bigger scale. This is what the following figures represent. Different points are aligned in one line and analyse the pressure change. The line is shown in red and an XY plot shows the magnitude of the pressure along that line.

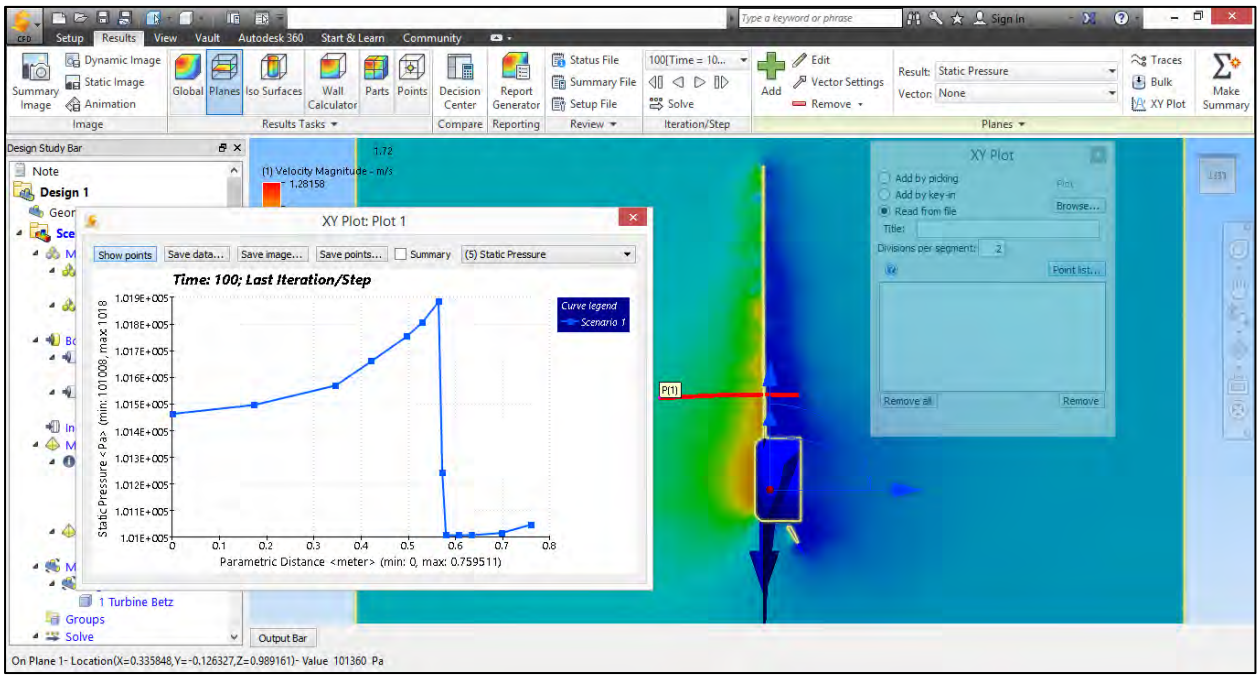

Figure 6-10: Change in pressure near the hub

Figure 6-10 shows the change in pressure measured on a flow line represented by a red line on the figure. The change in pressure at that particular spot multiplied by the area gives the value of the thrust which is the force applied to the blade at that particular point. Now, knowing that force times velocity gives the power available, we can do all the calculations for every single area of the blades but evaluation using software and integration calculations are faster and accurate enough to predict the behaviour and the power output of the system.

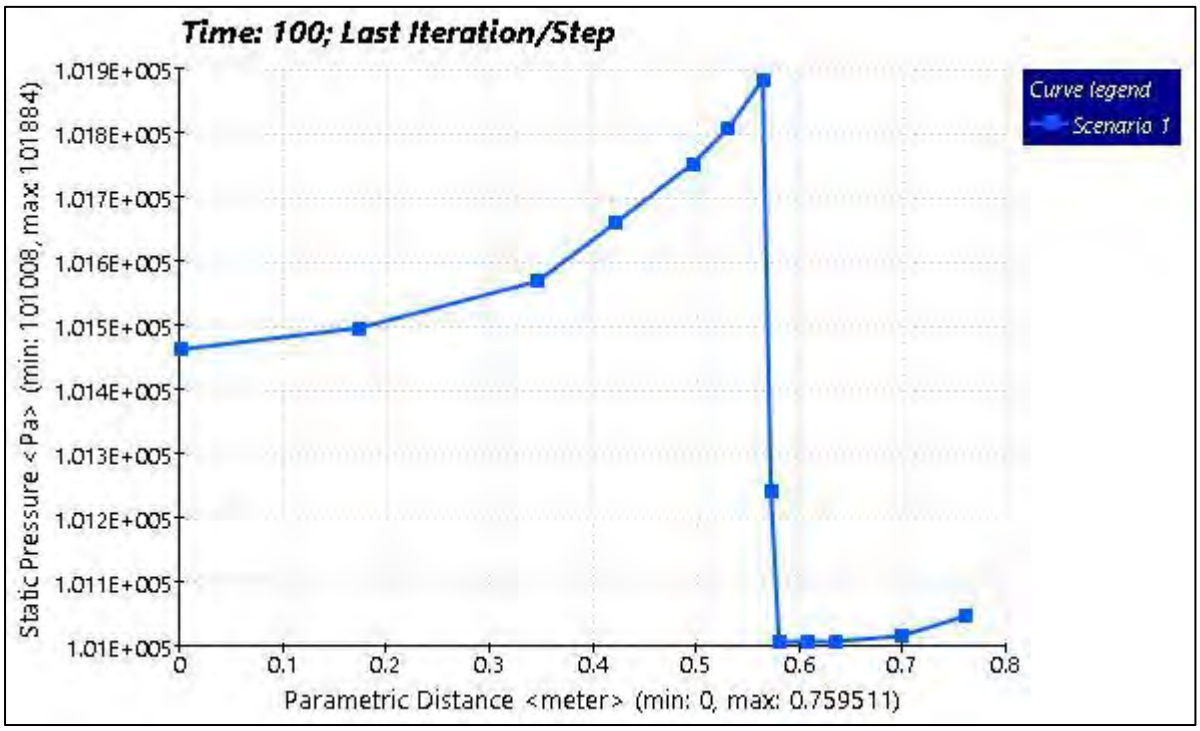

Figure 6-11: Curve of the change in pressure near the hub

Figure 6-11 shows the change in pressure. The curve explains what was understood already from Figure 4-1. The pressure increases when it approaches the blade and reaches a maximum value of 101 884 Pa. suddenly the pressure drops to a minimum value of 100 008 Pa when water is passing the blade. The pressure will start increasing slowly after water has passed the element and reach the normal level of pressure at a certain distance downstream the rotor. The change in pressure at this level is 876 Pa. When multiplying this value by the area on which the change has been applied, the thrust and the power available at that particular point can be obtained.

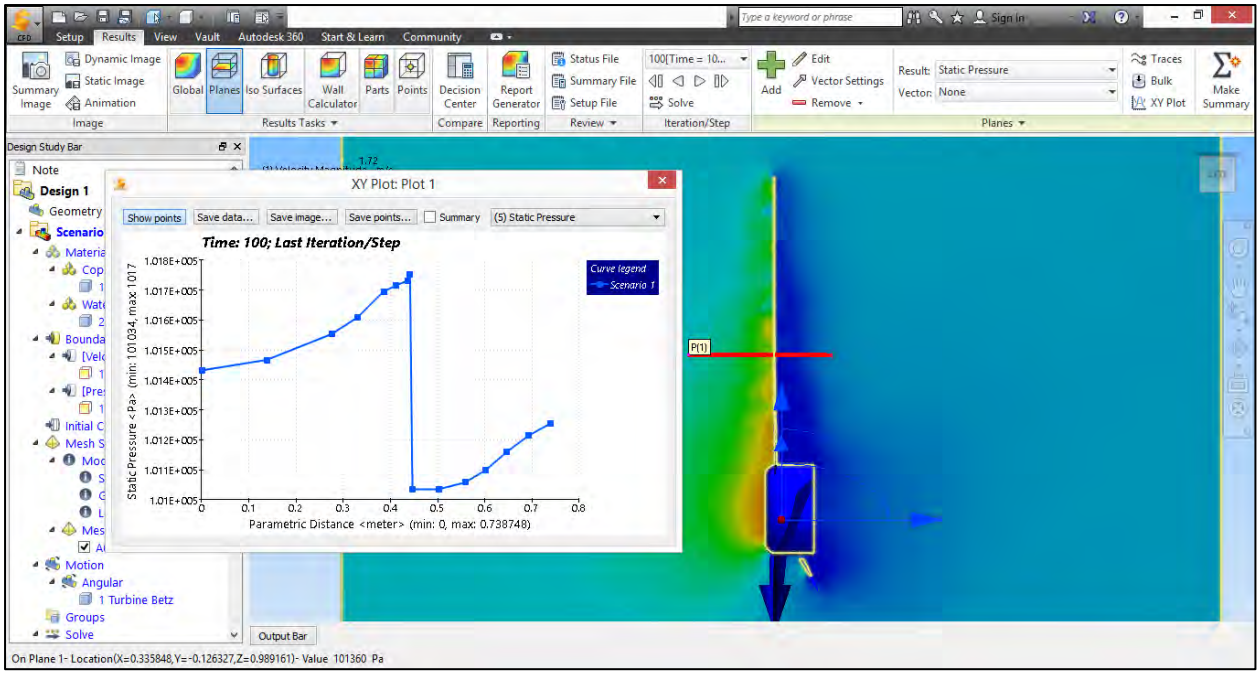

Figure 6-12: Change in pressure near the middle of the blade

Figure 6-12 shows the change in pressure on a streamline which is near the middle of the blade element. Looking at the blade element from the root to the tip and analysing the changes in pressure on a stream line around the middle length from the root.

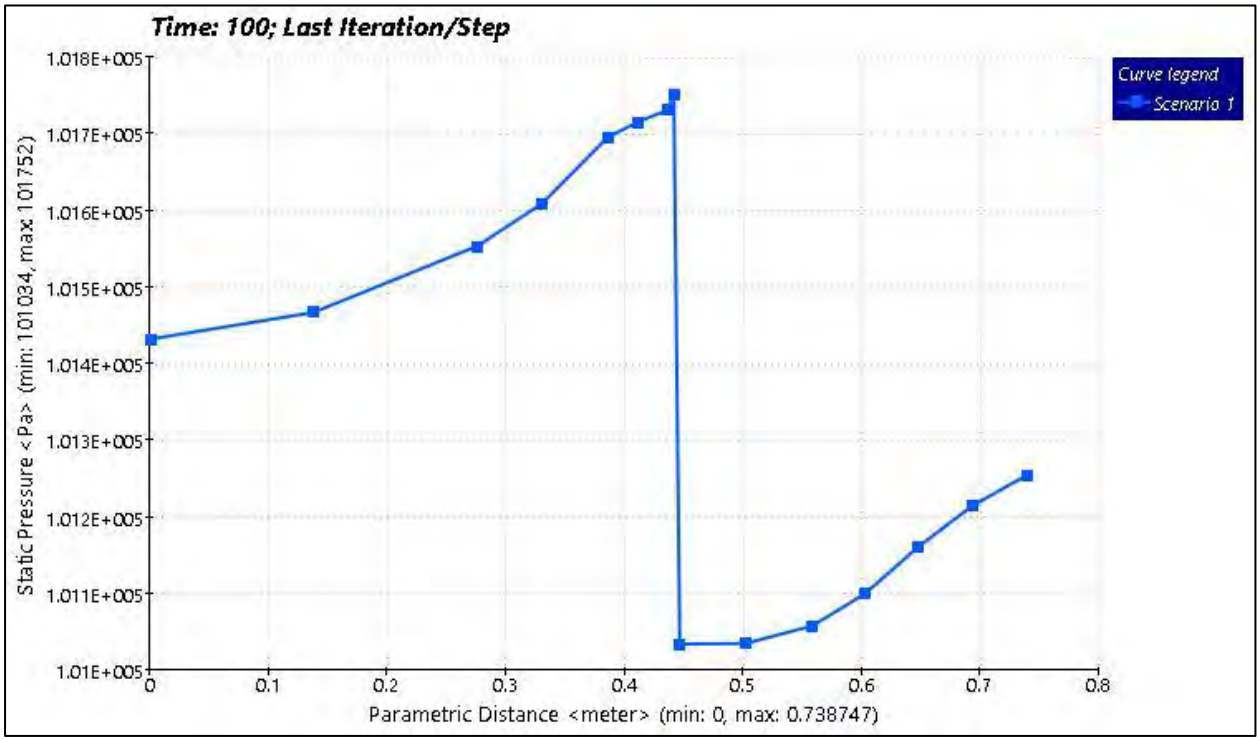

Figure 6-13: Curve of the change in pressure near the middle of the blade element

Figure 6-13 also shows the change in pressure. The pictures in the following figures show the difference between a change near the hub, in the middle and near the tip. It's also known that the momentum of inertia of the rotor will allow the rotor to turn if the location on which the force is applied is far from the hub.

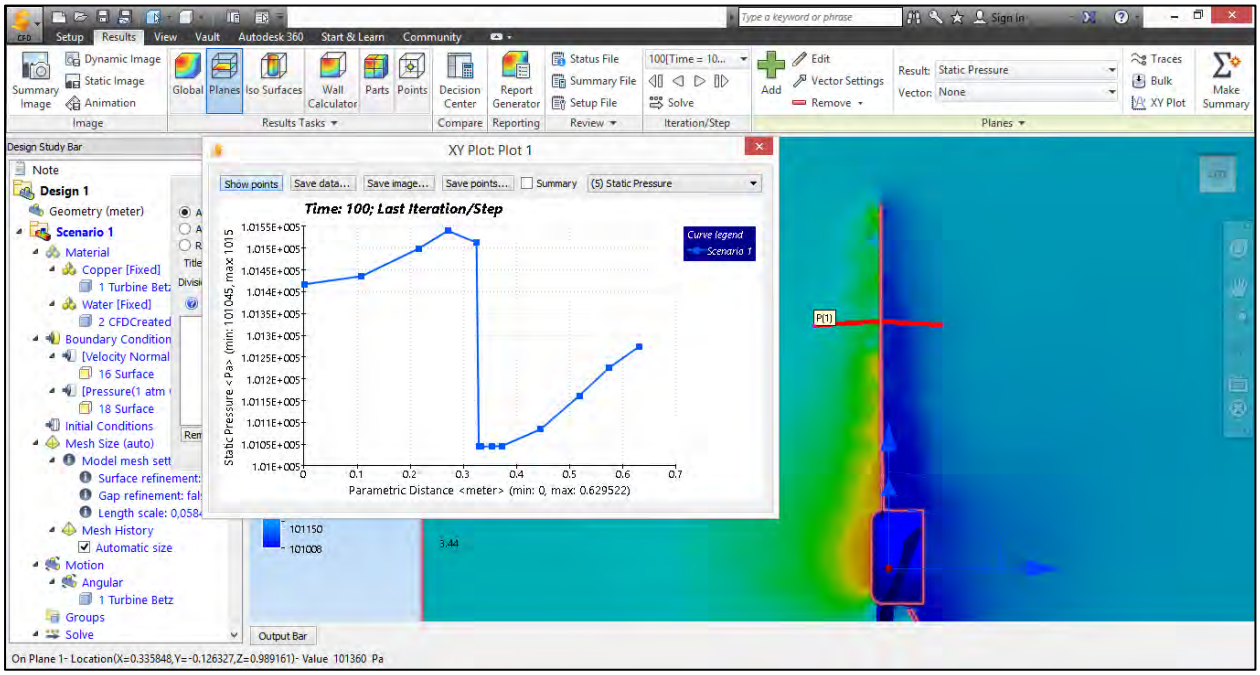

Figure 6-14: Streamline of change in pressure around the radius of gyration

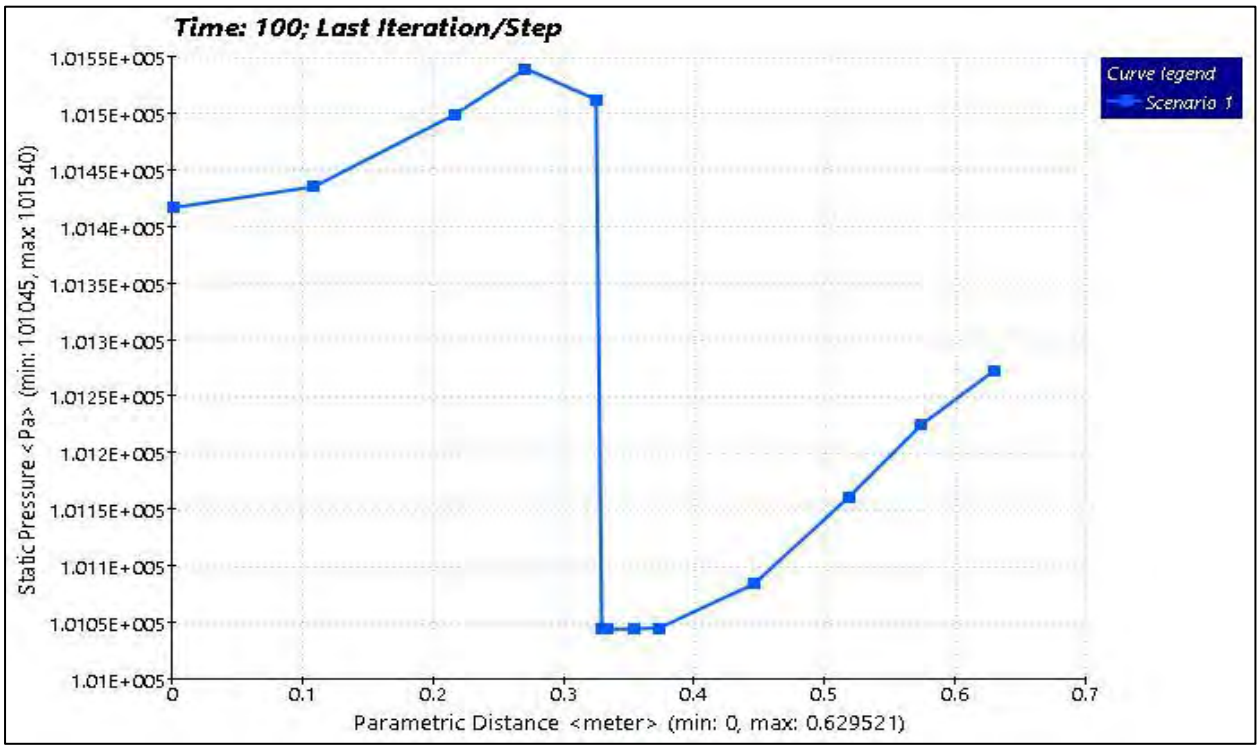

Figure 6-15: Curve of the change in pressure around the radius of gyration

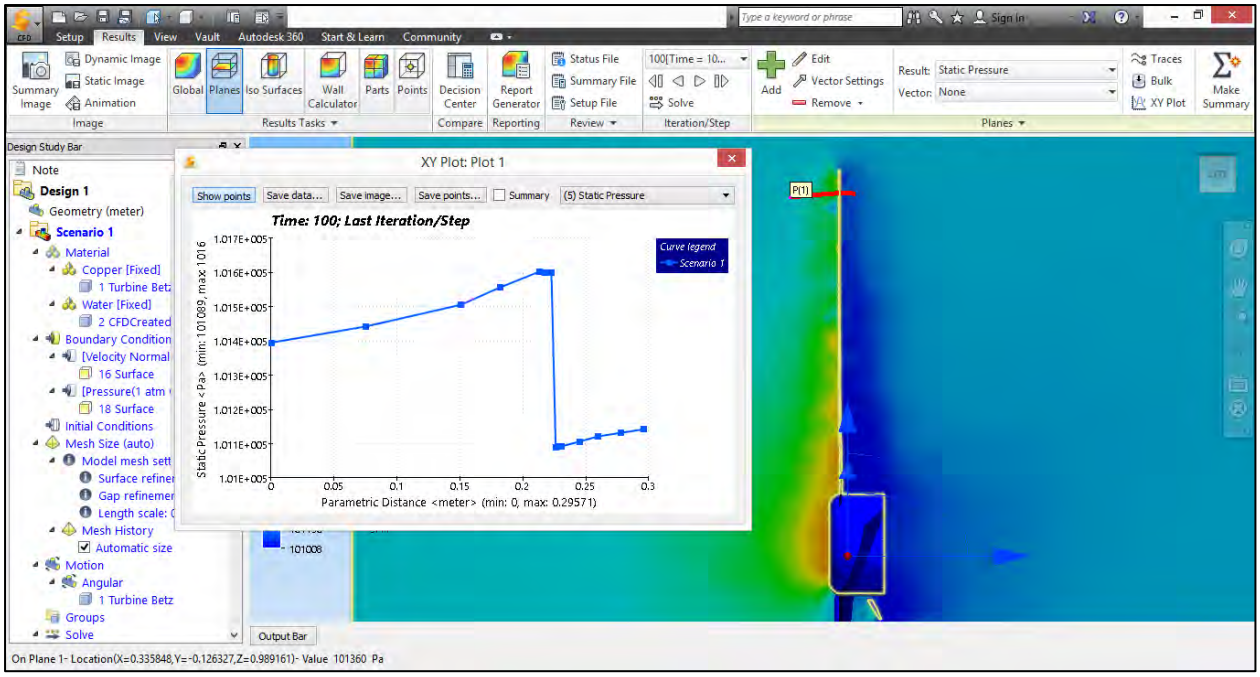

Figure 6-16: Streamline showing the change in pressure near the tip

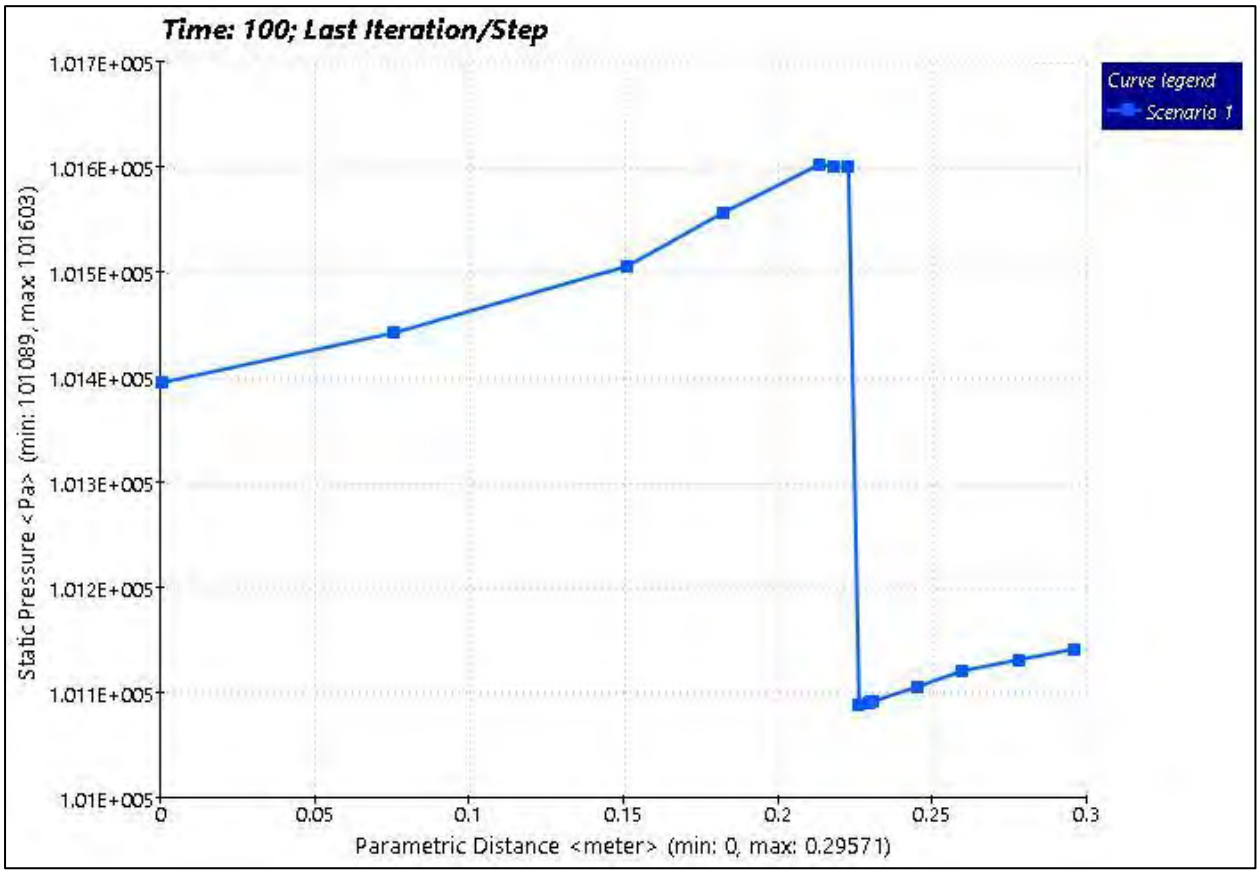

Figure 6-17: Curve showing the change in pressure near the tip

Figure 6-14, Figure 6-15, Figure 6-16and Figure 6-17 show the change in pressure. These figures provide a picture of what is happening when water hits the blade element. The value of the change in pressure shown in any of these figures is taken on a very small surface. Knowing that the pressure is a force applied on a surface, the total change in pressure will be the value of the sum of changes in pressure on the three blades of the rotor. The total change in pressure multiplied by the area swept by the blade and the velocity gives the power available which is the sum of all the changes on all the small surfaces on the three blades. Due to momentum of inertia, the axial force represented by the thrust is going to help bring about a change in pressure with greater force in locations far from the hub rather than closer to the hub. These assumptions have provided the platform to carry on with the design of the turbine.

Using the same pitch angle β from

Table 6-3 and following the same steps as previously to design a rotor turbine after Schmitz (Gundtoft 2009). Using equation 5-12 to evaluate the chord length after Schmitz as shown in Table 6-6 bellow:

Table 6-6: values of the chord length after Schmitz

Station no. (1 root, 20 tip)	Blade element, **r** (meter)	Local tip speed ratio, λ_r	Chord length after Betz **c** (meter)	Twist angle β [rad]	angle of relative fluid to rotor plan $\phi=\beta+\alpha$ [°]
1	0.1	0.35	0.384	1.49902	92.38774
2	0.2	0.7	0.721	1.21328	76.01563
3	0.3	1.05	0.969	1.18622	74.46534
4	0.4	1.4	1.101	1.22394	76.62674
5	0.5	1.75	1.110	1.26679	79.08197
6	0.6	2.1	1.023	1.30402	81.21459
7	0.7	2.45	0.880	1.33468	82.97168
8	0.8	2.8	0.725	1.35978	84.40942
9	0.9	3.15	0.583	1.38045	85.59368
10	1	3.5	0.464	1.39765	86.57961
11	1.1	3.85	0.370	1.41214	87.40991
12	1.2	4.2	0.296	1.42448	88.11692
13	1.3	4.55	0.240	1.43510	88.72516
14	1.4	4.9	0.195	1.44432	89.25333
15	1.5	5.25	0.161	1.45239	89.71586
16	1.6	5.6	0.134	1.45951	90.12400
17	1.7	5.95	0.113	1.46584	90.48663
18	1.8	6.3	0.095	1.47150	90.81083
19	1.9	6.65	0.081	1.47659	91.10233
20	2	7	0.070	1.48119	91.36576

From the chord length and pitch angle can be designed the profiles the same way it was done for Betz (Gundtoft 2009) as shown in Figure 6-18.

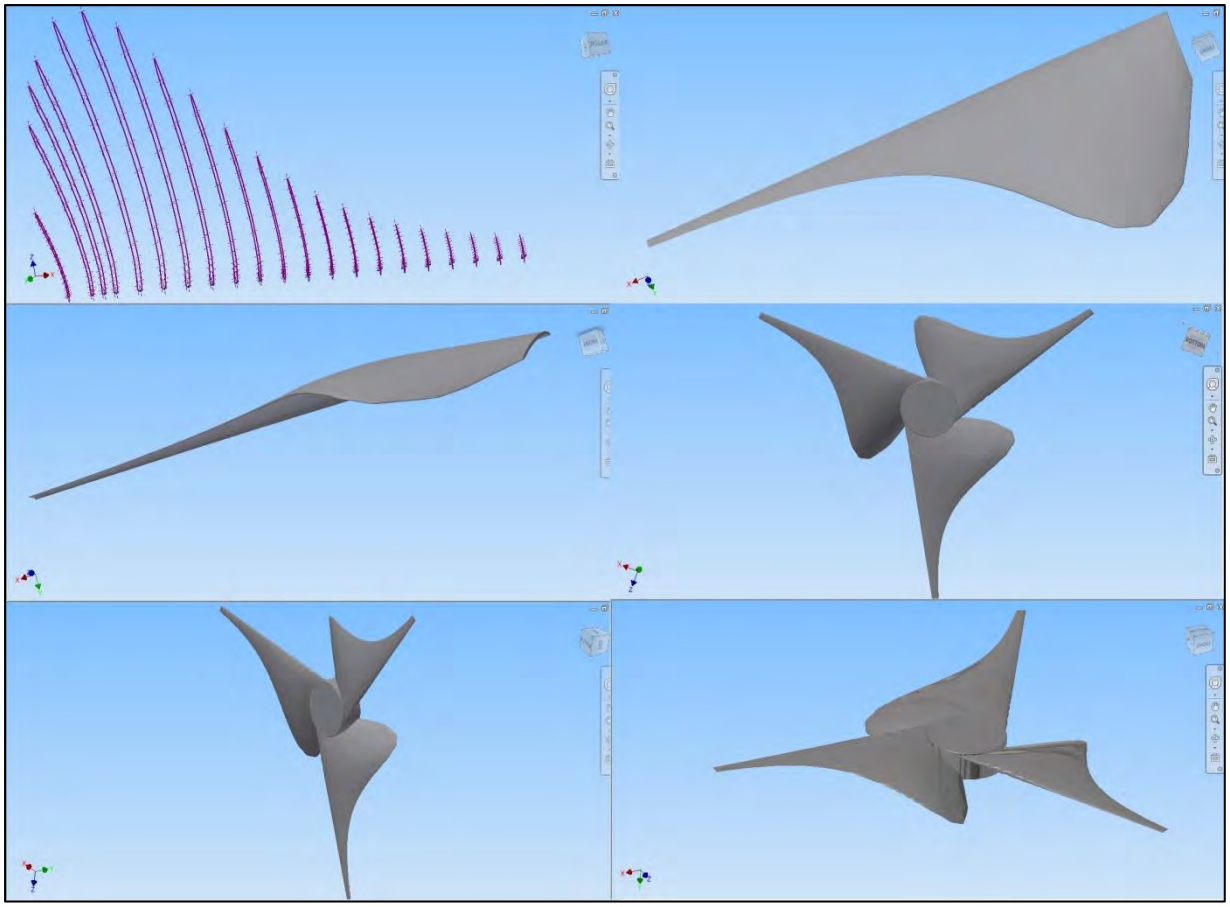

Figure 6-18: Design of the 3 blades turbine after Schmitz using Autodesk Inventor Professional

As for the previous design after Betz (Gundtoft 2009), strength analysis and simulation CFD was done on this prototype and the results are also satisfactory. The next step in this study will be to build a prototype from these two designs and do experiments to compare results.

6.2.3 POWER OUTPUT

We use equation 6-17 to evaluate the power coefficient C_P and the power output from a site. The values in the following table are found recalling the trapezium rule as shown in equation 6-18.

Table 6-7: Evaluation of the power coefficient C_P.

Station number	Λr	a	a'	$f_{(x)}$	$\frac{\lambda_0 - \lambda_n}{2}$	$\int f_{(x)}$
1	0.35	0.993145	0.204009	5.9958E-05	0.175	0.006744141
2	0.7	0.699491	0.373302	0.038477991	0.175	0.026221704
3	1.05	0.52082	0.200754	0.111360315	0.175	0.05022688
4	1.4	0.454472	0.117341	0.175650427	0.175	0.071802946
5	1.75	0.424032	0.076017	0.234652122	0.175	0.091995115
6	2.1	0.407673	0.053055	0.291034252	0.175	0.111480004
7	2.45	0.397889	0.039075	0.345994344	0.175	0.130567913
8	2.8	0.391577	0.029957	0.400108018	0.175	0.149412827
9	3.15	0.387268	0.023689	0.453679563	0.175	0.168098531
10	3.5	0.384196	0.019198	0.506883472	0.175	0.186674267
11	3.85	0.381929	0.015872	0.559826623	0.175	0.205170819
12	4.2	0.380209	0.01334	0.612578059	0.175	0.223608422
13	4.55	0.378871	0.011369	0.665184354	0.175	0.242000925
14	4.9	0.377812	0.009804	0.717678072	0.175	0.260358131
15	5.25	0.376958	0.008542	0.770082678	0.175	0.278687183
16	5.6	0.37626	0.007508	0.822415511	0.175	0.296993406
17	5.95	0.375681	0.006651	0.874689667	0.175	0.315280856
18	6.3	0.375197	0.005933	0.926915226	0.175	0.333552678
19	6.65	0.374787	0.005325	0.979100076	0.175	0.351811347
20	7	0.374437	0.004806	1.031250477	-	-
Sum of $\int f_{(x)}$						3.500688096
C_P						0.571540914

The power coefficient C_P is satisfactory because it is close enough to the optimum value of 16/27 or 0.5926 obtained when the induction factor is equal to 1/3 or 0.3333. From this C_P can be evaluate the power output for different velocities (0.4 m/s to 2 m/s) and different blade radius (0.25 m to 5 m). Values in the following table are the power output in watts [W] expected to be harvested on the shaft of the rotor.

Table 6-8: Evaluation of the power output [watts] from the system at different velocity v and blade radius R

R \ V	0.4 m/s	0.6 m/s	0.8 m/s	1 m/s	1.2 m/s	1.4 m/s	1.6 m/s	1.8 m/s	2 m/s
0.25 m	3.59	12.12	28.73	56.11	96.96	153.97	229.83	327.24	448.89
0.50 m	14.36	48.48	114.92	224.44	387.84	615.87	919.32	1308.96	1795.55
0.75 m	32.32	109.08	258.56	505.00	872.64	1385.71	2068.47	2945.15	4039.98
1.00 m	57.46	193.92	459.66	897.77	1551.35	2463.49	3677.28	5235.82	7182.19
1.50 m	129.28	436.32	1034.24	2019.99	3490.55	5542.86	8273.89	11780.60	16159.94
2.00 m	229.83	775.68	1838.64	3591.10	6205.42	9853.97	14709.14	20943.28	28728.78
2.50 m	359.11	1212.00	2872.88	5611.09	9695.96	15396.83	22983.02	32723.88	44888.72
3.00 m	517.12	1745.27	4136.94	8079.97	13962.19	22171.44	33095.55	47122.38	64639.75
3.50 m	703.86	2375.51	5630.84	10997.74	19004.09	30177.79	45046.73	64138.80	87981.89
4.00 m	919.32	3102.71	7354.57	14364.39	24821.67	39415.89	58836.54	83773.12	114915.12
4.50 m	1163.52	3926.87	9308.12	18179.93	31414.92	49885.73	74465.00	106025.36	145439.45
5.00 m	1436.44	4847.98	11491.51	22444.36	38783.85	61587.32	91932.10	130895.50	179554.87

Looking at the velocity profile of Agulhas Current, a turbine of 5 m radius will generate enough power for a velocity profile higher than 0.6 m/s. The velocity profile used in this research is taken from a depth of about 80 m under the ocean surface. The velocity increases near the surface and the rotor should be placed at a point where the velocity will be high enough for a better generation of power. A turbine having blades of radius 5 m under 1.6 m/s for water current will be able to generate a power of around 92 000 kW. This is the kind of power expected from this research.

6.3 DESIGN OF THE ROTOR USING TURBEM

Muñoz et al. (2014) published a work on design tool and fabrication guidelines for small low cost horizontal axis hydrokinetic turbines. This study showed how they designed their turbine, fabricated it and tested it. In the article there is a link to a video of the first field test (available at: https://www.youtube.com/watch?v=OLQCsgTfSB4). This turbine was designed using software named "Turbem" which means "Turbine Blade Element Momentum" and is easily found as open-source software (available at: http://www.mecatronix.cl/?page_id=2277). Turbem is written in the C# (C sharp) programming language and helps to obtain an optimal horizontal axis hydrokinetic turbine design and to accurately predict its performance under different operating conditions. Turbem software is based on blade element momentum theory which is the most useful theory to design blades (Tangler 2004) and uses pseudo-gradient methods to solve BEM theory.

The software input interface has only 5 inputs as shown on Figure 6-19.

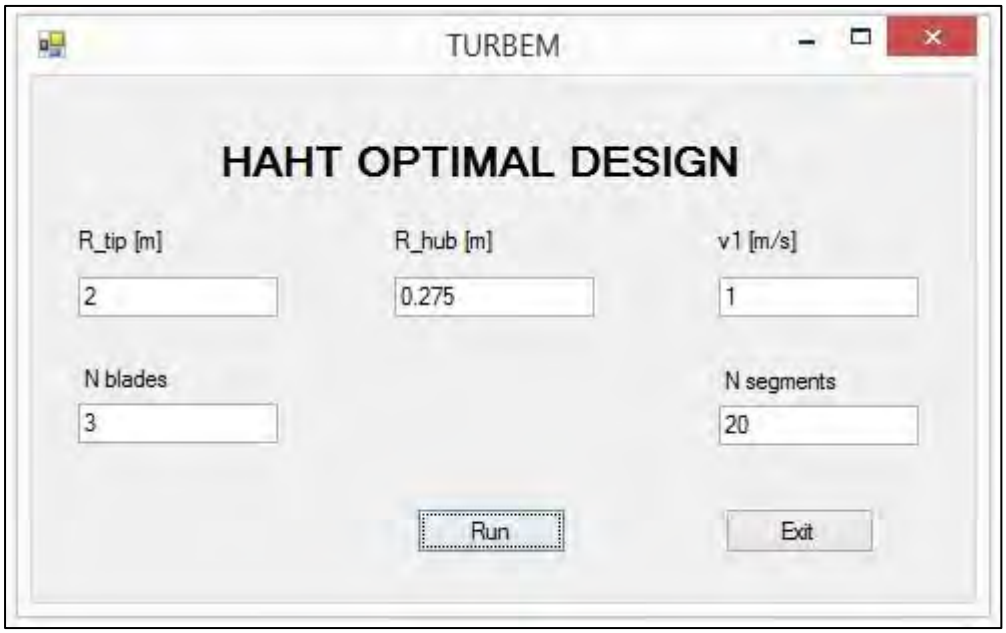

Figure 6-19: Input interface of Turbem software

The user inputs the tip radius (R_tip), the hub radius (R_hub), the current velocity (v_1), the number of blade (N blades) and the number of segments (N segments). Once all inputs are correctly set, the user clicks on run and the program generates two notepad documents with all the details of the turbine to be constructed. In this case it was set R_tip = 2 m, R_hub = 0.275 m, v1 = 1 m/s, N blade = 3 and N segments = 20. Results of Turbem are shown in the appendixes C. From the results we have designed a turbine and conducted strength analysis using Autodesk Inventor Professional and simulation CFD to see its performance.

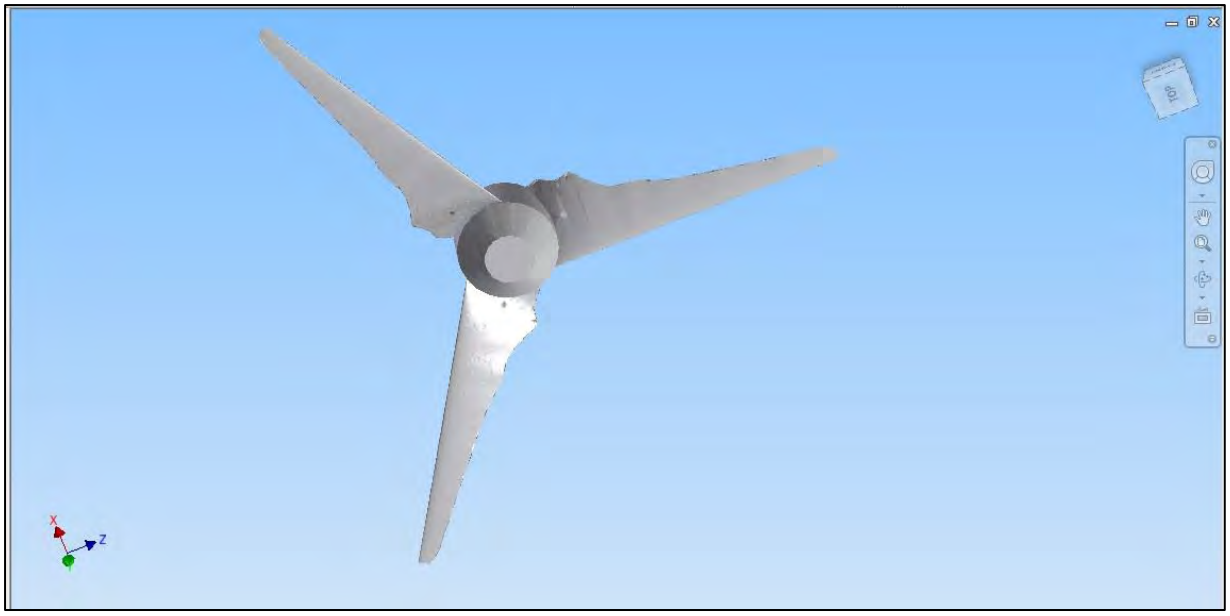

Figure 6-20: Design of a turbine rotor using data from Turbem software

The first page of the notepad file generated by Turbem shows the following results:

TURBINE OPTIMAL DESIGN

USER INPUT DATA

R_tip : 2.000

R_hub : 0.275

v1 : 1.000

N_segments : 20

N_blades : 3

Speed, lc, and teta OPTIMIZATION considering Fprandtl

Output 1: OPTIMIZATION WITH TIP SPEED FACTOR GLOBAL RESULTS

Tip Radius R_tip [m] : 2.000

Hub Radius R_hub [m] : 0.275

Free stream speed v1 [m/s] : 1.000

Number of Blades N_blades : 3

Number of segments N_segments : 20

RESULTS

Nominal omega [rad/s]	: 3.000
Power Raw [W]	: 12 566.371
Total power by Momentum Theory Ptcm [W]	: 2 839.156
Total Power by Blade Theory Ptld [W]	: 2 782.553
Total Torque by Momentum Theory Ttcm [Nm]	: 946.385
Total Torque by Blade Theory Ttld [Nm]	: 927.518
Total Axial Force by Momentum Theory Ftcm [N]	: 4 794.054
Total Axial Force by Blade Theory Ftld [N]	: 4 802.753
Power Factor Cp	: 0.226
Tip Factor Ctip	: 6.000

After this page, there are a lot of data and coordinates of the blades, all of which can be found in the appendixes.

Looking at the results section and noticing that the raw power of this turbine is twice the value expected from equation 4.10. This can easily be resolved by dividing the raw power value by two. The power, the torque and the axial force on the shaft of the turbine are expressed by two different values with one from momentum theory and the other one from blade theory. The power factor and the tip factor are also indicated on the same page. These values are smaller than those found during previous calculation in this research field but the reason of comparison of the two theories is because the authors Muñoz et al. (2014) have completed research using Turbem to construct a turbine and conducted experiments giving satisfactory results.

Chapter 7 : CONCLUSION AND RECOMMENDATION

Theory in this study is based on blade element momentum theory which is the main theory used in the design of horizontal axis turbines. This theory is used by manufacturers who adapt it to their needs and design different types of turbines. This study combined Betz, Schmitz and blade element momentum theory to design a turbine. The calculation results were used to build a prototype for simulation purposes using Autodesk Inventor Professional. Once the design was done, the turbine was analysed using Autodesk CFD and the results are satisfactory. The construction of an actual turbine rotor is recommended as a follow on research study.

The velocity profile of the Agulhas Current does not always provide a value equal to 1 m/s. That is why additional studies for the velocity range 0.4 m/s to 2 m/s was done. The sizes of the turbines are between 0.25 m to 5 m radius and the expected power output from the turbines are from 3.59 W for the smallest turbine working under very slow water velocity to 179 545.87 W for the bigger turbine of 5 m radius working at 2 m/s. Such turbines are going to be a great investment for the country and will contribute to its energy production. The number of sites on which the project can be constructed are known by Eskom engineers attached to ocean studies. In our case we can conclude by saying that this kind of turbine is a real solution for the country's energy production and is also a contribution to the renewable energy plan that South Africa wishes to reach for the sake of the next generation.

BIBLIOGRAPHY

Akimoto, H., Tanaka, K. and Uzawa, K. (2013). "A conceptual study of floating axis water current turbine for low-cost energy capturing from river, tide and ocean currents." *Renewable Energy*, 57(0), 283-288.

Anyi, M. and Kirke, B. (2011). "Hydrokinetic turbine blades: Design and local construction techniques for remote communities." *Energy for Sustainable Development*, 15(3), 223-230.

Asif, M. and Muneer, T. (2007). "Energy supply, its demand and security issues for developed and emerging economies." *Renewable and Sustainable Energy Reviews*, 11(7), 1388-1413.

Bahaj, A. S. (2011). "Generating electricity from the oceans." *Renewable and Sustainable Energy Reviews*, 15(7), 3399-3416.

Bahaj, A. S. and Myers, L. (2004). "Analytical estimates of the energy yield potential from the Alderney Race (Channel Islands) using marine current energy converters." *Renewable Energy*, 29(12), 1931-1945.

Bahaj, A. S. and Myers, L. E. (2003). "Fundamentals applicable to the utilisation of marine current turbines for energy production." *Renewable Energy*, 28(14), 2205-2211.

Bedard, R. (2008). "Prioritized research, development, deployment and demonstration (RDD&D) needs: marine and other hydrokinetic renewable energy." Palo Alto, CA: Electric Power Research Institute.

Chong, H.-Y., and Lam, W.-H. (2013). "Ocean renewable energy in Malaysia: The potential of the Straits of Malacca." *Renewable and Sustainable Energy Reviews*, 23, 169-178.

Christopher, A. L., Broeren, A. P. ., Giguère, P., Gopalarathnam, A. and Selig, M. S. (1997). *Summary of low-speeda airfoil data, Volume 3*, Virginia Beach, Virginia: SoarTech Publications.

Dabrowski, J. M., Ashton, P. J., Murray, K., Leaner, J. J. and Mason, R. P. (2008). "Anthropogenic mercury emissions in South Africa: Coal combustion in power plants." *Atmospheric Environment*, 42(27), 6620-6626.

Dictionary.com. (2016). *Collins English Dictionary - Complete & Unabridged 10th Edition*. City: Dictionary.com2016.

Électricité de France (EDF). (2012). "L'usine marémotrice de la France." Paris: EDF.

Eskom. (2013). "CO 0007". Generation Communication. Johannesburg: Eskom: South Africa, pp. 2.

Gale, J., Hendriks, C., Turkenberg, W., Beck, B., Surridge, T., Liebenberg, J., and Gilder, A. (2011). "10th International Conference on Greenhouse Gas Control TechnologiesThe current status of CCS development in South Africa." *Energy Procedia*, 4, 6157-6162.

Goundar, J. N. and Ahmed, M. R. (2013). "Design of a horizontal axis tidal current turbine." *Applied Energy*, 111(0), 161-174.

Goundar, J. N. and Ahmed, M. R. (2014). "Marine current energy resource assessment and design of a marine current turbine for Fiji." *Renewable Energy*, 65(0), 14-22.

Grabbe, M. (2008). "Marine current energy conversion." Licentiate thesis, Uppsala: Department of Engineering Sciences, Uppsala Universitet.

Grabbe, M., Lalander, E., Lundin, S. and Leijon, M. (2009). "A review of the tidal current energy resource in Norway." *Renewable and Sustainable Energy Reviews*, 13(8), 1898-1909.

Grogan, D. M., Leen, S. B., Kennedy, C. R. and Ó Brádaigh, C. M. (2013). "Design of composite tidal turbine blades." *Renewable Energy*, 57(0), 151-162.

Gundtoft, S. (2009). "Wind turbines." Tech. rep. University College of Aarhus.

Hammar, L., Ehnberg, J., Mavume, A., Francisco, F. and Molander, S. (2012). "Simplified site-screening method for micro tidal current turbines applied in Mozambique." *Renewable Energy*, 44(0), 414-422.

Hansen, A. C. and Butterfield, C. P. (1993). "Aerodynamics of Horizontal-Axis Wind Turbines." *Annual Review of Fluid Mechanics*, 25(1), 115-149.

Henderson, R. (2006). "Design, simulation, and testing of a novel hydraulic power take-off system for the Pelamis wave energy converter." *Renewable Energy*, 31(2), 271-283.

Ingram, G. (2005). "Wind turbine blade analysis using the blade element momentum method. Journal: School of Engineering, Durham University.

Jahromi, M. J., Maswood, A. I. and Tseng, K. J. (2013). "Design and evaluation of a tidal in-stream generator power port." *Systems Journal, IEEE*, PP(99), 1-1.

Korde, U. A. and Ertekin, R. C. (2014). "On wave energy focusing and conversion in open water." *Renewable Energy*, 62(0), 84-99.

Lasiecka, I. and Triggiani, R. (1990). "Exact controllability of the Euler-Bernoulli equation with boundary controls for displacement and moment." *Journal of Mathematical Analysis and Applications*, 146(1), 1-33.

Lee, J. H., Park, S., Kim, D. H., Rhee, S. H. and Kim, M.-C. (2012). "Computational methods for performance analysis of horizontal axis tidal stream turbines." *Applied Energy*, 98(0), 512-523.

Li, L., Li, Y. H., Liu, Q. K. and Lv, H. W. (2014). "A mathematical model for horizontal axis wind turbine blades." *Applied Mathematical Modelling*, 38(11-12), 2695-2715.

Li, Y. and Yu, Y.-H. (2012). "A synthesis of numerical methods for modeling wave energy converter-point absorbers." *Renewable and Sustainable Energy Reviews*, 16(6), 4352-4364.

Lutjeharms, J. R. E. (2006). "Three decades of research on the greater Agulhas Current." Ocean Science Discussions, European Geosciences Union, 3(4), 939-995.

Matona, T. (2014). *Damage to Majuba power station coal storage silo*. Johannesburg: Eskom.

Mbuseli, M. (2013). "Executive exchange on developing an ancillary service market for the Southern African Power Pool (SAPP)". Johannesburg: Southern African Energy Unit, Eskom.

Meisen, P. and Loiseau, A. (2009). "Ocean energy technologies for renewable energy generation." San Diego, CA: Global Energy Network Institute.

Menyah, K. and Wolde-Rufael, Y. (2010). "Energy consumption, pollutant emissions and economic growth in South Africa." *Energy Economics*, 32(6), 1374-1382.

Moreno, M., Sallent, R., Espi, A., Bao, D and, Teillet. Y. (2008). "Ocean current's energy: How to produce electrical energy thanks to the marine currents?" Report of the Renewable Energy Project. Gävle, Sweden: University of Gävle.

Muñoz, A. H., Chiang, L. E. and De la Jara, E. A. (2014). "A design tool and fabrication guidelines for small low cost horizontal axis hydrokinetic turbines." *Energy for Sustainable Development*, 22(0), 21-33.

Myers, L. E. and Bahaj, A. S. (2010). "Experimental analysis of the flow field around horizontal axis tidal turbines by use of scale mesh disk rotor simulators." *Ocean Engineering*, 37(2–3), 218-227.

Myers, L. E. and Bahaj, A. S. (2012). "An experimental investigation simulating flow effects in first generation marine current energy converter arrays." *Renewable Energy*, 37(1), 28-36.

Nicholls-Lee, R. F., Turnock, S. R. and Boyd, S. W. (2013). "Application of bend-twist coupled blades for horizontal axis tidal turbines." *Renewable Energy*, 50(0), 541-550.

Niiler, P. (2001). "The world ocean surface circulation." *International Geophysics*, 77, 193-204.

Nugraha . A. S. and Rijanto E. (2010). "Ocean current energy conversion system in Wallacea region using variable speed control approach." *Mechatronics, Electrical Power, and Vehicular Technology*, 01(1, 2010).

Rourke, F. O., Boyle, F. and Reynolds, A. (2010). "Marine current energy devices: Current status and possible future applications in Ireland." *Renewable and Sustainable Energy Reviews*, 14(3), 1026-1036.

Selig, M. S., Guglielmo, J. J., Broeren, A. P. and Giguère, P. (1995). *Summary of low speed airfoil data*: *Volume 1.* Virginia Beach, VA: SoarTech Publications.

Şen, Z. (2012). "Energy generation possibility from ocean currents: Bosphorus, Istanbul." *Ocean Engineering*, 50(0), 31-37.

Singh, R. K., Ahmed, M. R., Zullah, M. A. and Lee, Y.-H. (2012). "Design of a low Reynolds number airfoil for small horizontal axis wind turbines." *Renewable Energy*, 42(0), 66-76.

Statistics South Africa. (2011). "Mid-year population estimates 2011". Pretoria: Statistics South Africa

Steele, M., Schulz, N. Musana, F. and Baillie, M. (2012). *The Eskom factor: Power politics and the electricity sector in South Africa*. Johannesburg: Greenpeace Africa.

Tangler, J. L. (2004). "Wind turbine post-stall airfoil performance characteristics guidelines for blade-element momentum methods preprint." Golden, CO.: National Renewable Energy Laboratory.

Thumthae, C. and Chitsomboon, T. (2009). "Optimal angle of attack for untwisted blade wind turbine." *Renewable Energy*, 34(5), 1279-1284.

Twiddle, J. and Weir, T. (2006). "*Renewable energy resources."* Milton Park, UK: Taylor & Francis.

VanZwieten, J., Driscoll, F. R., Leonessa, A. and Deane, G. (2006a). "Design of a prototype ocean current turbine—Part I: mathematical modeling and dynamics simulation." *Ocean Engineering*, 33(11-12), 1485-1521.

VanZwieten, J., Driscoll, F. R., Leonessa, A. and Deane, G. (2006b). "Design of a prototype ocean current turbine—Part II: flight control system." *Ocean Engineering*, 33(11-12), 1522-1551.

Wang, S., Yuan, P., Li, D. and Jiao, Y. (2011). "An overview of ocean renewable energy in China." *Renewable and Sustainable Energy Reviews*, 15(1), 91-111.

Wimpie, v., Rooy. (2012). Agulhas Current ADCP and Temperature data. Eskom, South Africa.

Xiang, S., Cao, P., Erwin, R. and Kibbee, S. (2013). "OTEC Cold Water Pipe Global Dynamic Design for Ship-Shaped Vessels." *Presented at ASME 2013 32nd International Conference on Ocean, Offshore and Arctic Engineering*.

Yuen, K., Thomas, K., årten Grabbe, Deglaire, P., Bouquerel, M., Österberg, D. and Leijon, M. (2009). "Matching a permanent magnet synchronous generator to a fixed pitch vertical axis turbine for marine current energy conversion." *IEEE Journal of Oceanic Engineering,* 34(1), 8.

APPENDIXES A

STRENGTH ANALYSIS REPORT USING AUTODESK INVENTOR PROFESSIONAL

Analyzed File:	Turbine Betz.ipt
Autodesk Inventor Version:	2015 SP1 (Build 190203100, 203)
Creation Date:	2016-01-09, 08:38 PM
Simulation Author:	M.J. TSHIKAYA
Summary:	

A.1. PROJECT INFO (IPROPERTIES)

Summary

Author	Jimmy

Project

Part Number	Turbine Betz
Designer	Jimmy
Cost	R 0,00
Date Created	2015-01-26

Status

Design Status	WorkInProgress

Physical

Material	Steel AISI 8640 361 QT
Density	7,85 g/cm^3
Mass	504,558 kg
Area	2,70482 m^2
Volume	0,0642749 m^3
Center of Gravity	x=-0,1 m y=0,0735501 m z=0,155088 m

Note: Physical values could be different from Physical values used by FEA reported below.

A.2. SIMULATION AND RESULTS

GENERAL OBJECTIVE AND SETTINGS:

Design Objective	Single Point
Simulation Type	Static Analysis
Last Modification Date	2016-01-09, 08:33 PM
Detect and Eliminate Rigid Body Modes	No

MESH SETTINGS:

Avg. Element Size (fraction of model diameter)	0,1
Min. Element Size (fraction of avg. size)	0,2
Grading Factor	1,5
Max. Turn Angle	60 deg
Create Curved Mesh Elements	Yes

Material(S)

Name	Steel AISI 8640 361 QT	
General	Mass Density	7,85 g/cm^3
	Yield Strength	1306 MPa
	Ultimate Tensile Strength	1373 MPa
Stress	Young's Modulus	207 GPa
	Poisson's Ratio	0,33 ul
	Shear Modulus	77,8195 GPa
Part Name(s)	Turbine Betz.ipt	

OPERATING CONDITIONS

Force

Load Type	Force
Magnitude	100.000 N
Vector X	15.358 N
Vector Y	98.378 N
Vector Z	9.266 N

Selected Face(s)

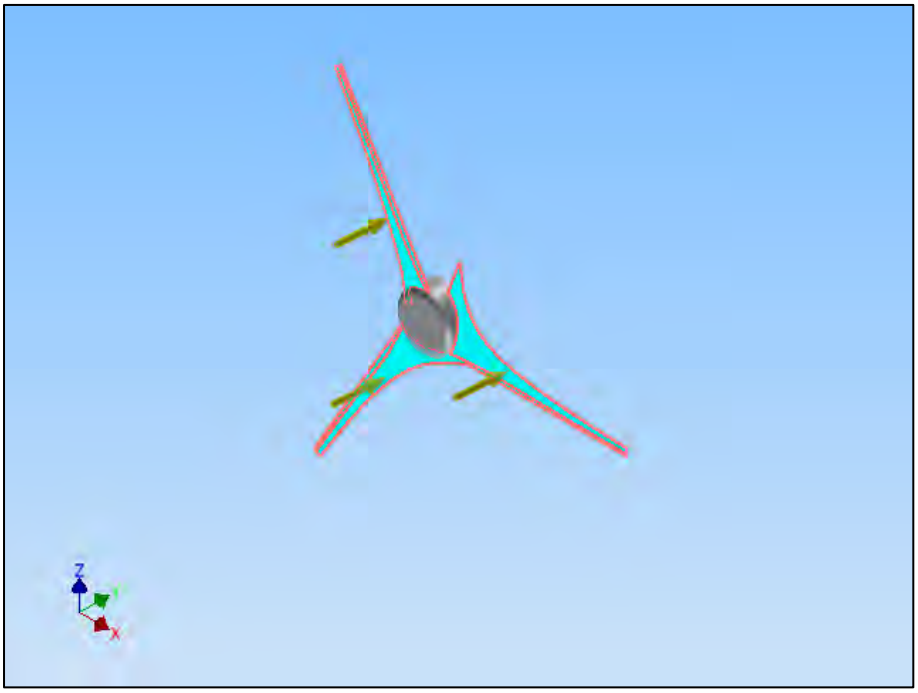

Results

A.3. Reaction Force and Moment on Constraints

Constraint Name	Reaction Force		Reaction Moment	
	Magnitude	Component (X,Y,Z)	Magnitude	Component (X,Y,Z)
Fixed Constraint:1	104,455 N	-36,3572 N	3,82583 N m	-0,359324 N m
		97,5016 N		-3,61694 N m
		-9,07579 N		1,194 N m
Pin Constraint:1	199,488 N	20,4559 N	6,86039 N m	2,44234 N m
		-198,437 N		3,26468 N m
		0 N		-5,51741 N m

A.4. Result Summary

Name	Minimum	Maximum

Volume	64273300 mm^3	
Mass	504,546 kg	
Von Mises Stress	0,000265919 MPa	11,6936 MPa
1st Principal Stress	-3,02251 MPa	9,07758 MPa
3rd Principal Stress	-11,1487 MPa	3,53068 MPa
Displacement	0 mm	3,89761 mm
Safety Factor	15 ul	15 ul
Stress XX	-9,22685 MPa	5,31335 MPa
Stress XY	-5,06021 MPa	4,79588 MPa
Stress XZ	-4,72321 MPa	3,92118 MPa
Stress YY	-5,58888 MPa	8,45981 MPa
Stress YZ	-3,44401 MPa	3,6002 MPa
Stress ZZ	-8,73662 MPa	6,74933 MPa
X Displacement	-0,247074 mm	0,260141 mm
Y Displacement	-0,000078675 mm	3,88747 mm
Z Displacement	-0,254145 mm	0,167424 mm
Equivalent Strain	0,00000000128644 ul	0,0000506983 ul
1st Principal Strain	-0,00000143483 ul	0,0000407222 ul
3rd Principal Strain	-0,0000554933 ul	0,00000035885 ul
Strain XX	-0,0000415515 ul	0,0000208174 ul
Strain XY	-0,0000325125 ul	0,0000308141 ul

Strain XZ	-0,0000303472 ul	0,000025194 ul
Strain YY	-0,000023196 ul	0,000028183 ul
Strain YZ	-0,0000221282 ul	0,0000231317 ul
Strain ZZ	-0,0000399952 ul	0,0000309208 ul

Figures

Von Mises Stress

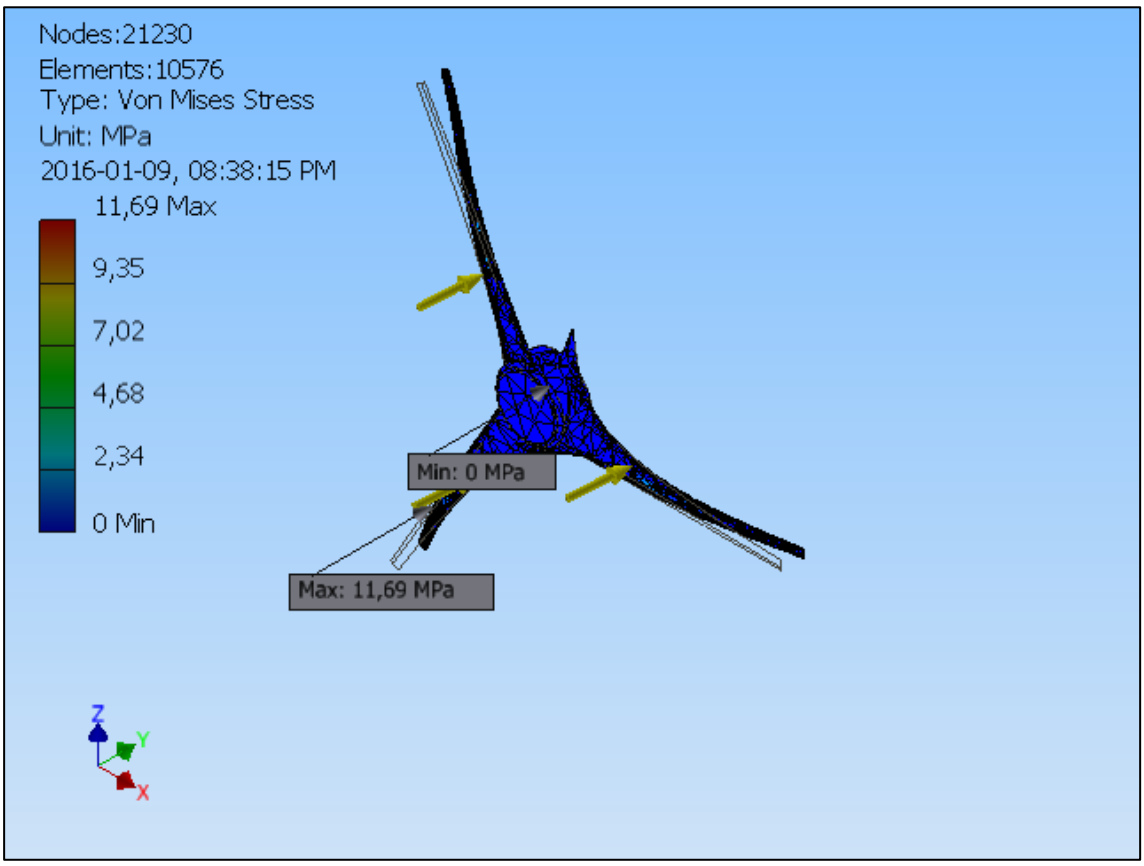

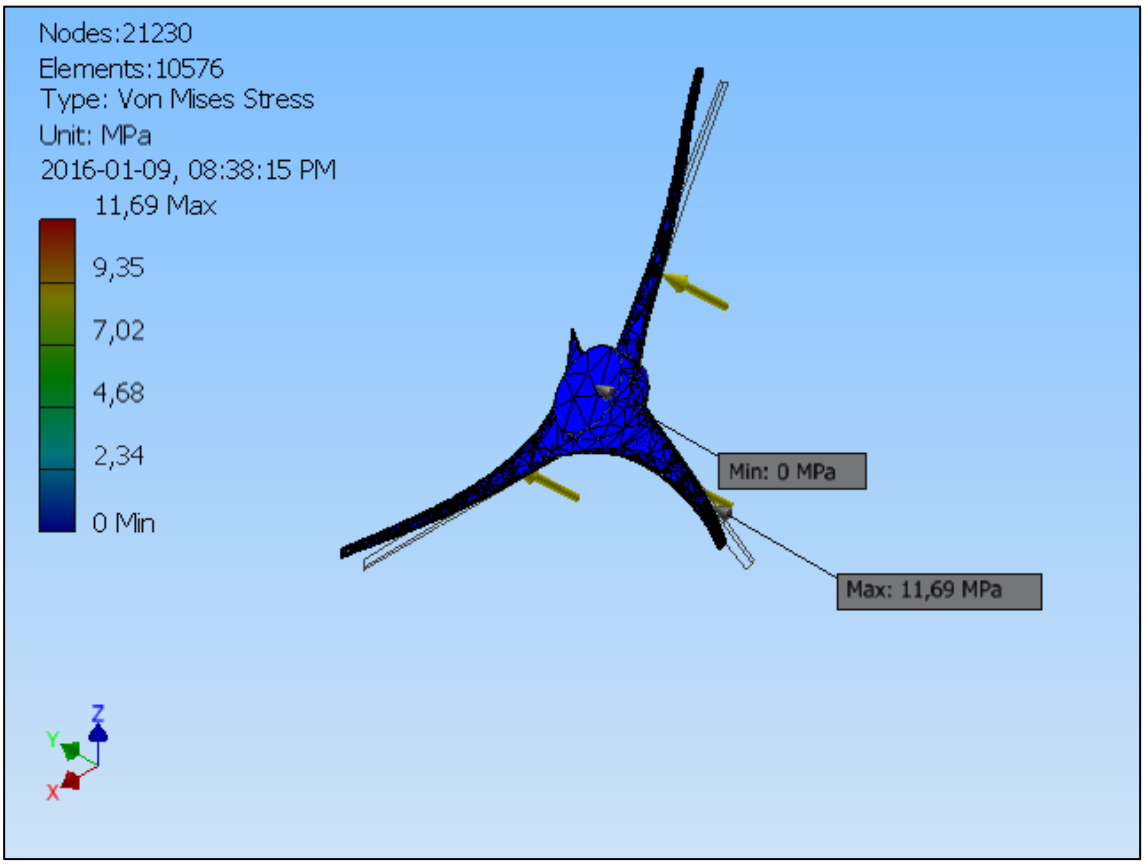

1st Principal Stress

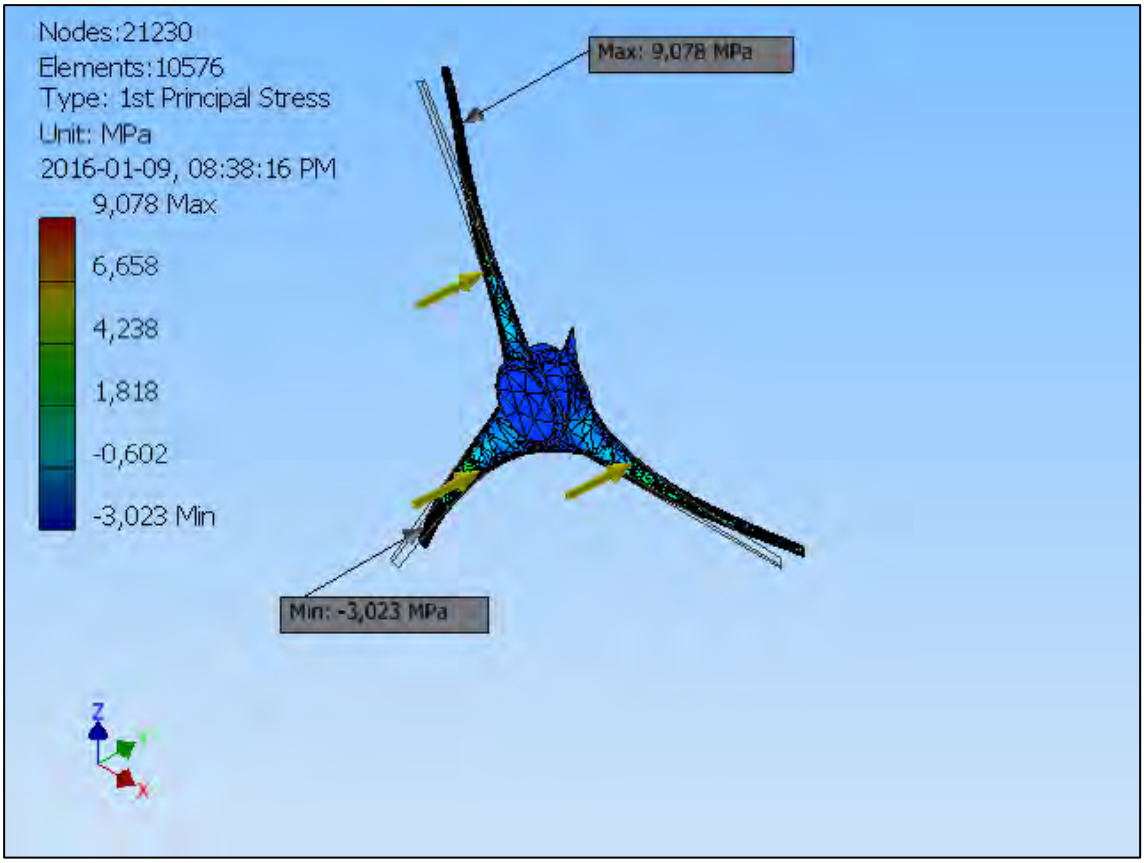

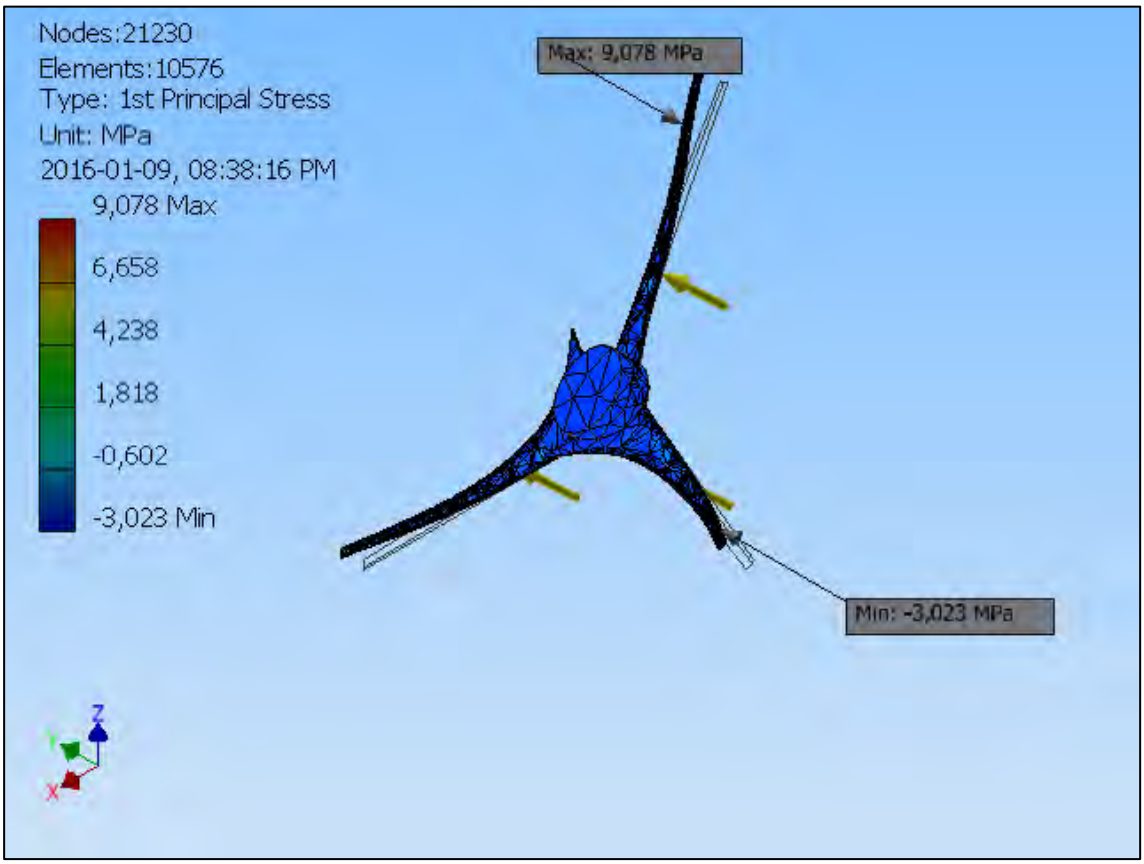

3rd Principal Stress

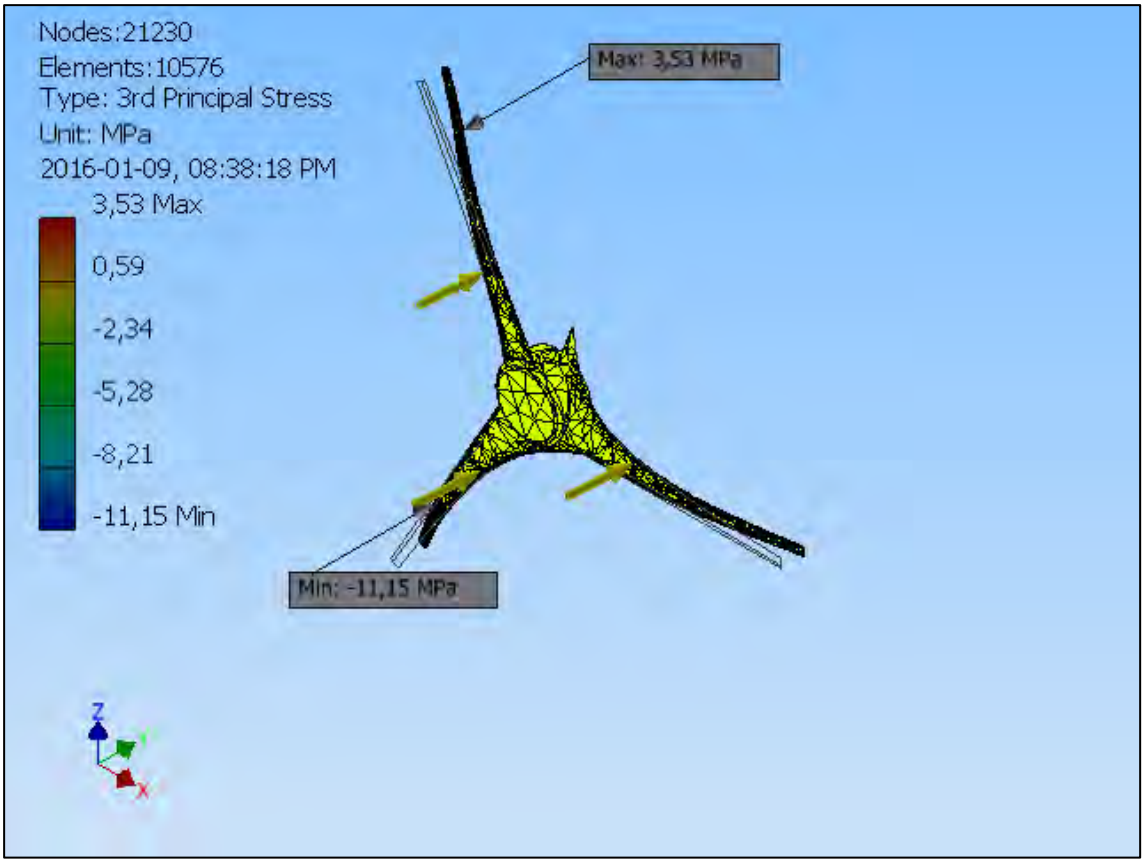

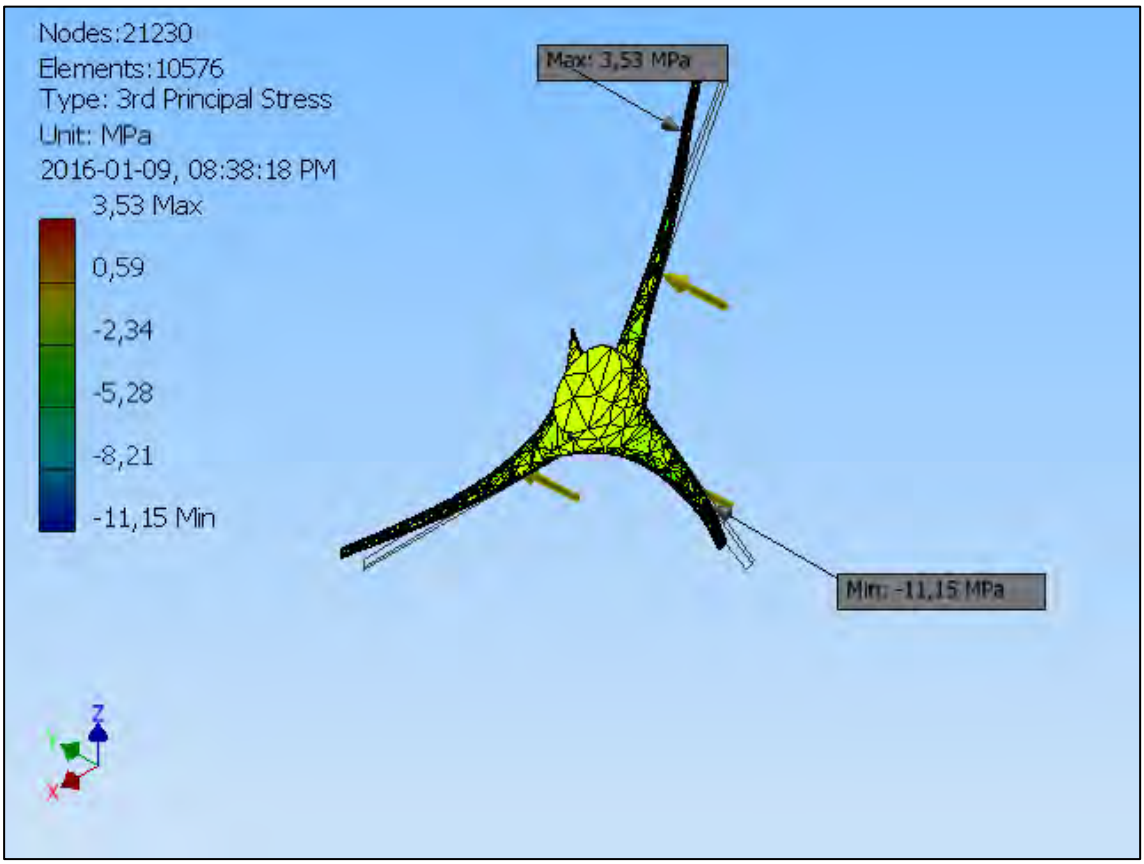

Displacement

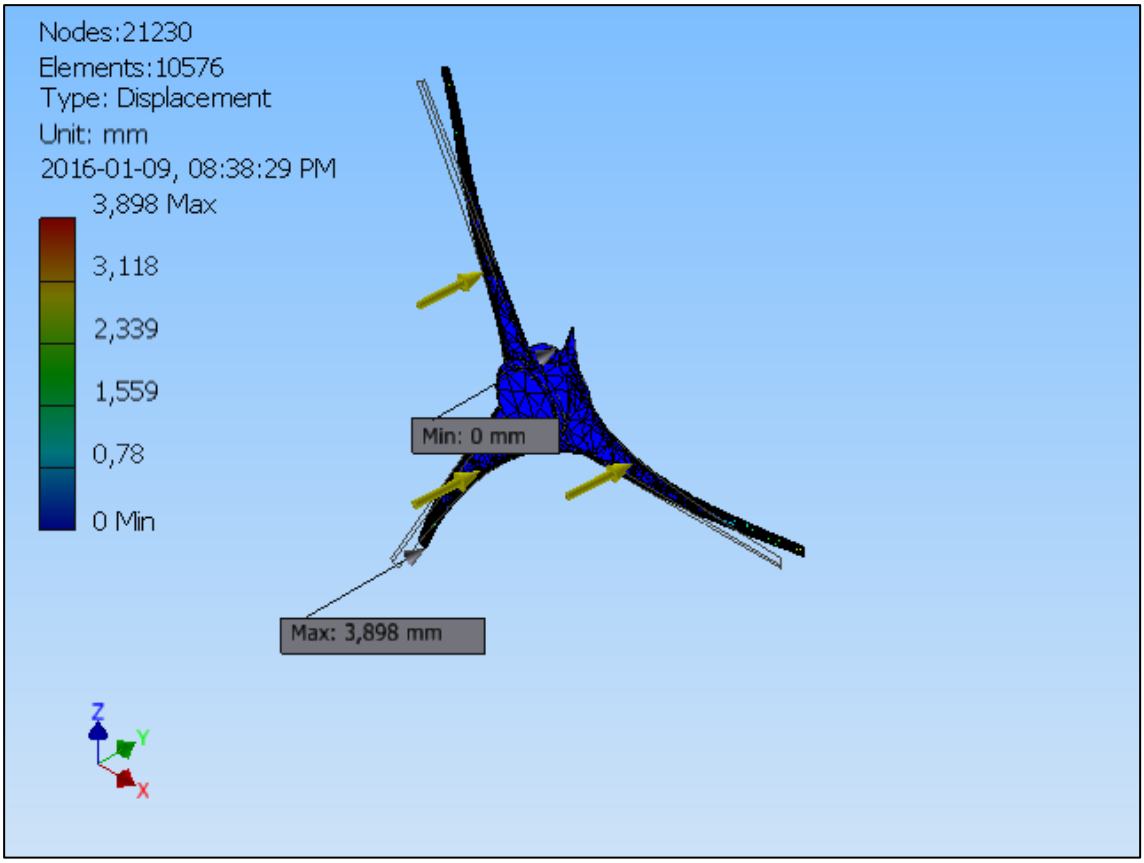

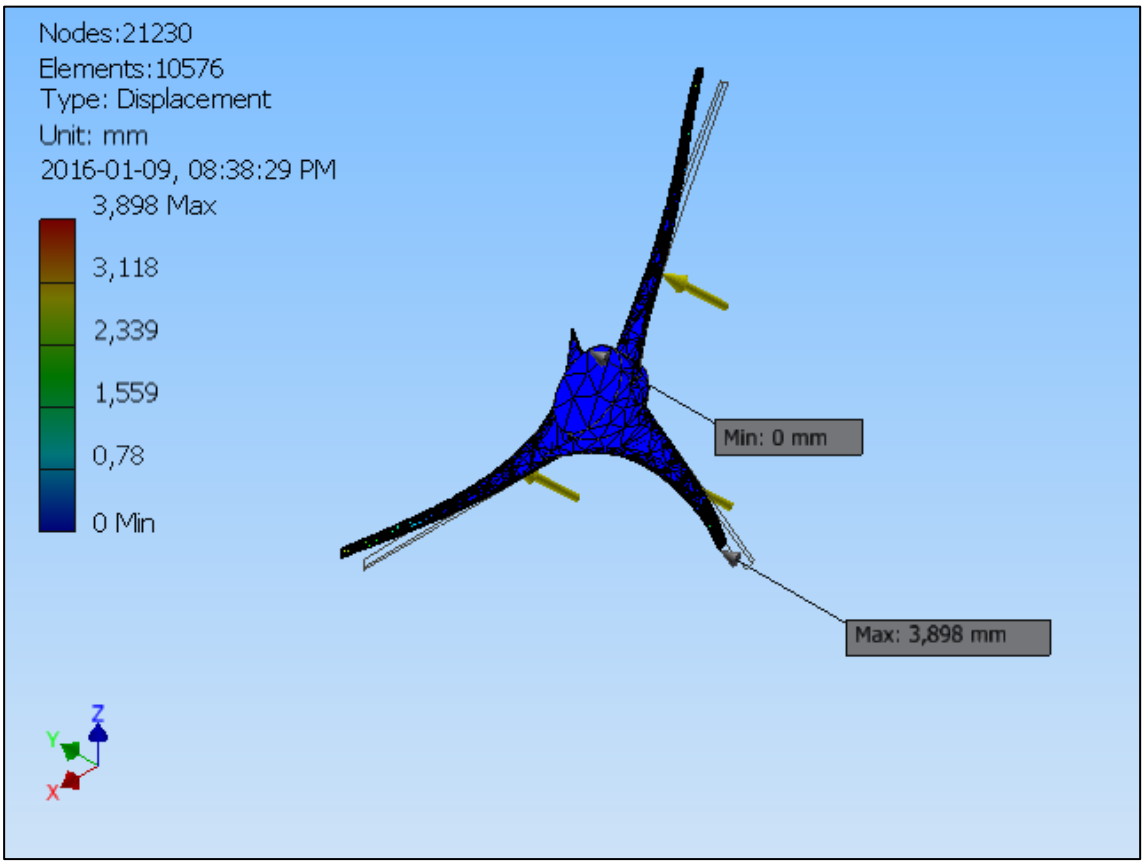

Safety Factor

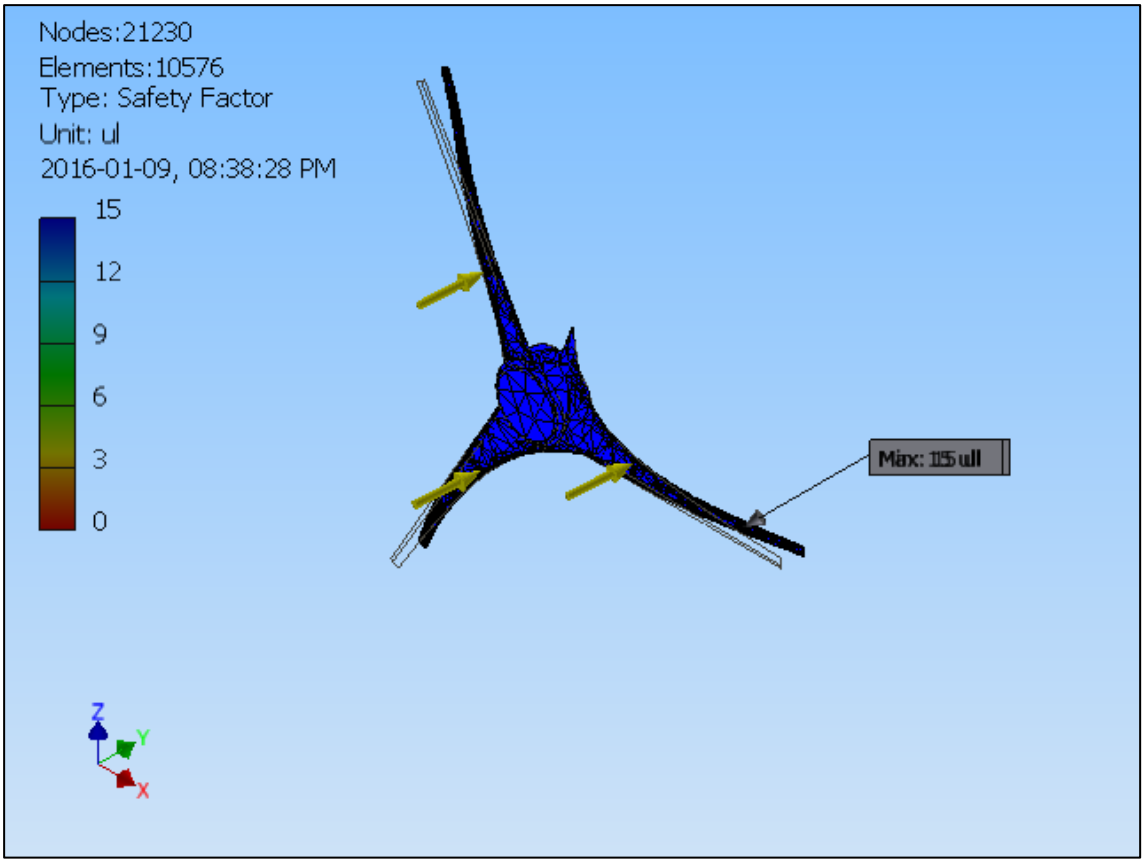

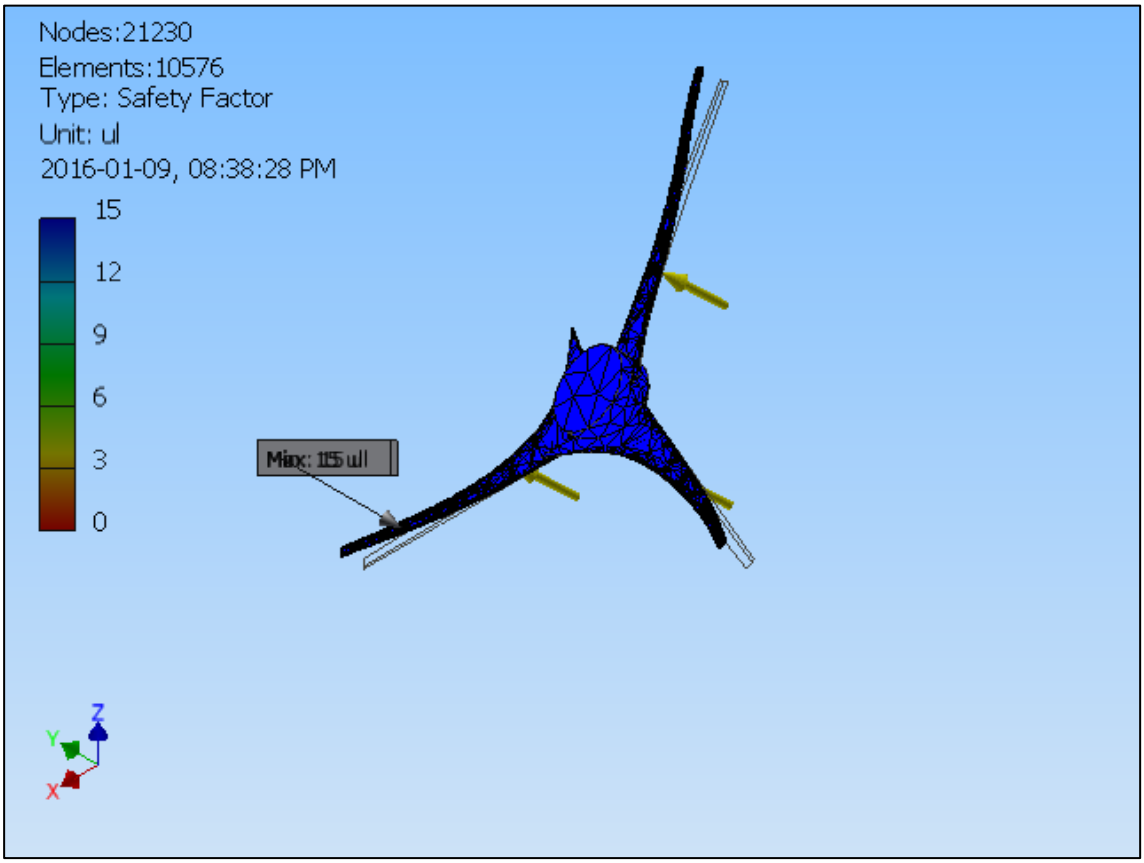

Equivalent Strain

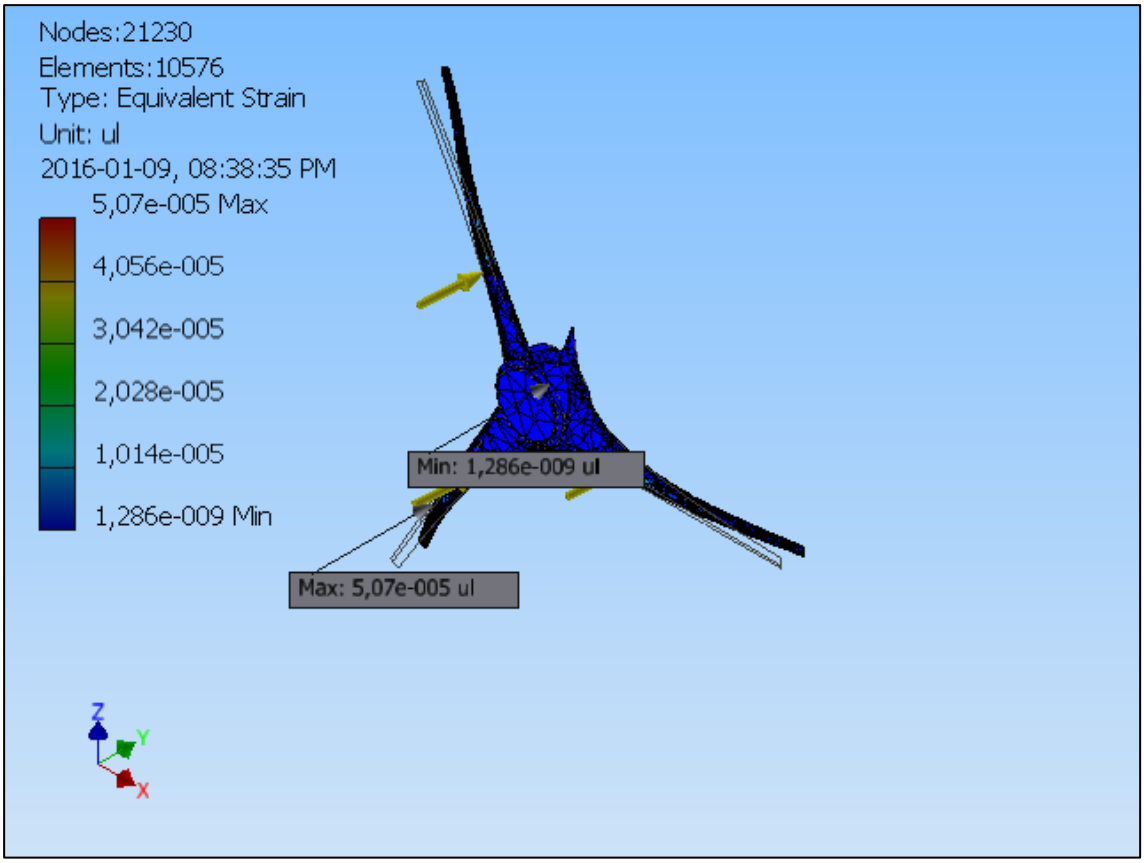

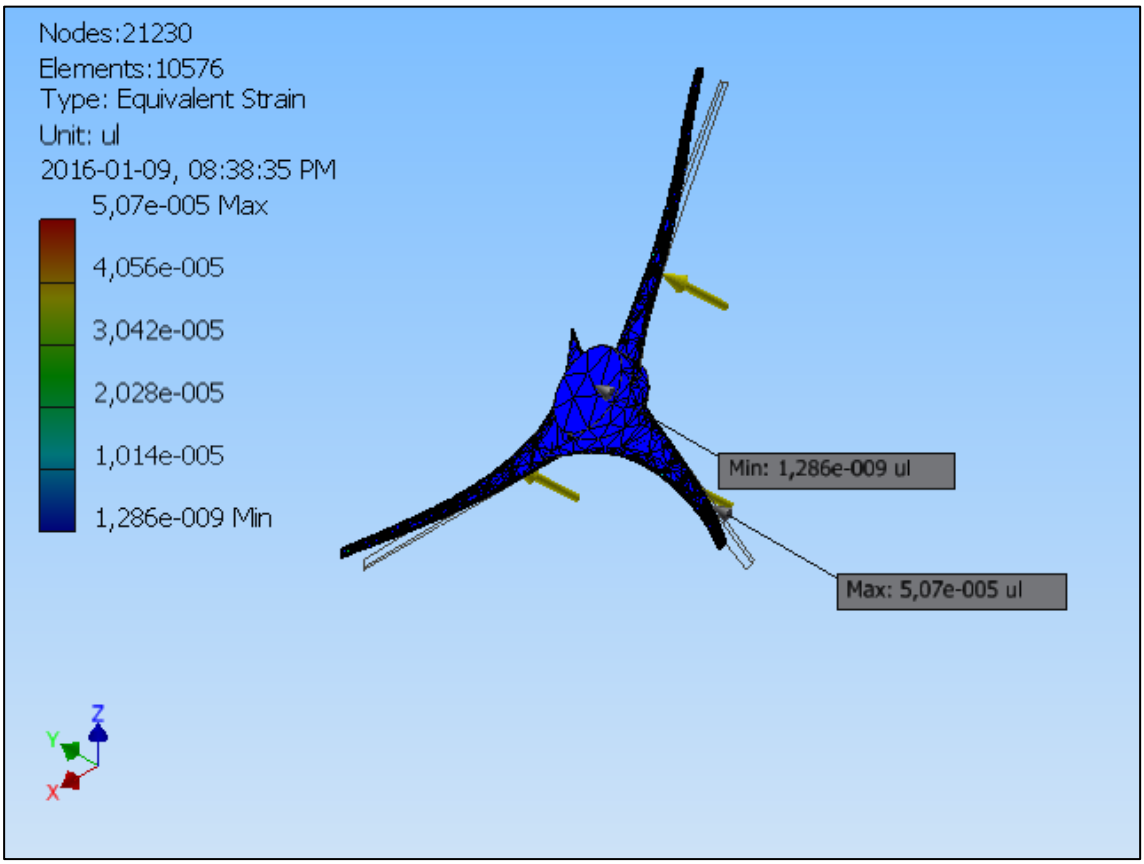

1st Principal Strain

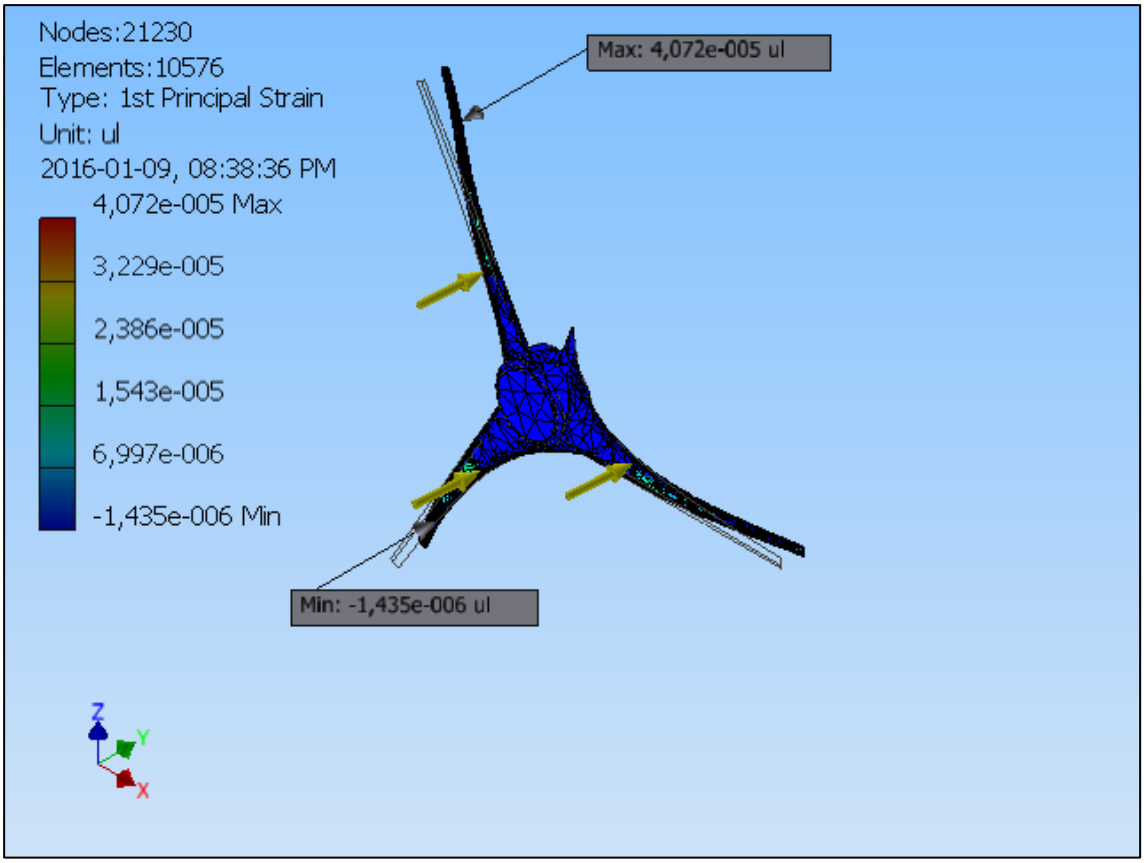

APPENDIXES B

SIMULATION USING AUDODESK CFD

B.1. Materials

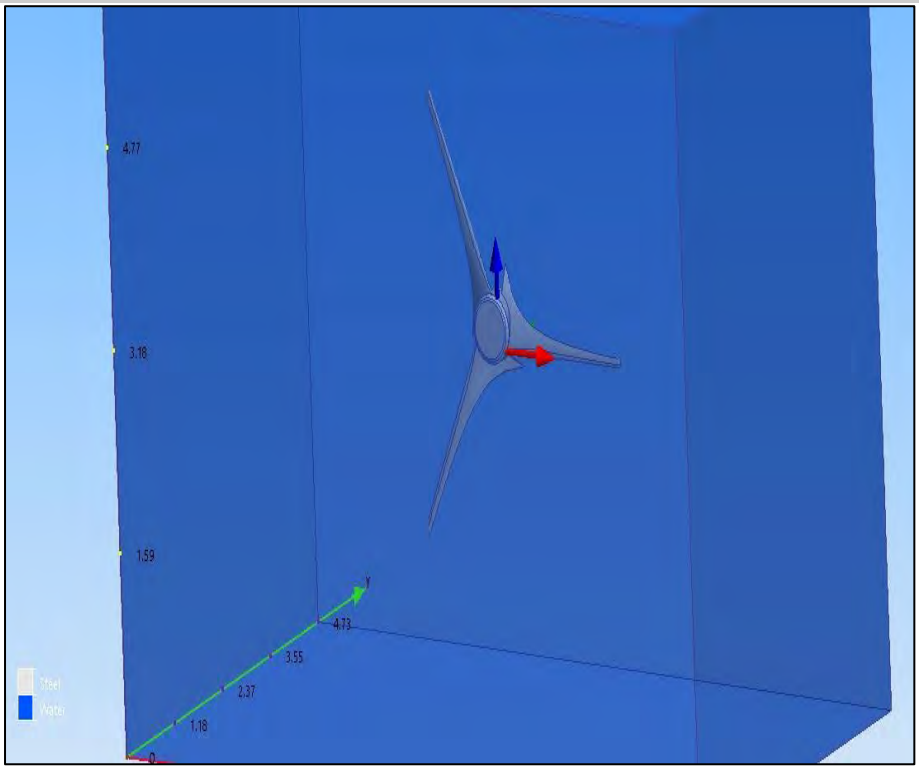

NAME	ASSIGNED TO	PROPERTIES	
Water	CFD Created Volume	Density	Piecewise Linear
		Viscosity	0.001003 Pa-s
		Conductivity	0.6 W/m-K
		Specific heat	4182.0 J/kg-K
		Compressibility	2185650000.0 Pa
		Emissivity	1.0
		Wall roughness	0.0 meter
		Phase	Linked Vapor Material
Steel	Turbine Betz	X-Direction	Piecewise Linear
		Y-Direction	Same as X-dir.
		Z-Direction	Same as X-dir.
		Density	7833.0 kg/m3
		Specific heat	465.0 J/kg-K
		Emissivity	0.3
		Transmissivity	0.0
		Electrical resistivity	1.7e-07 ohm-m
		Wall roughness	0.0 meter

B.2. Boundary conditions

TYPE	ASSIGNED TO
Velocity Normal(1 m/s)	Surface:16
Pressure(0 Pa Gage)	Surface:18

INITIAL CONDITIONS

TYPE	ASSIGNED TO

B.3. Mesh

Automatic Meshing Settings

Surface refinement	0
Gap refinement	0
Resolution factor	1.0
Edge growth rate	1.1
Minimum points on edge	2
Points on longest edge	10
Surface limiting aspect ratio	20

Mesh Enhancement Settings

Mesh enhancement	0
Enhancement blending	1
Number of layers	10
Layer factor	0.76
Layer gradation	1.05

Meshed Model

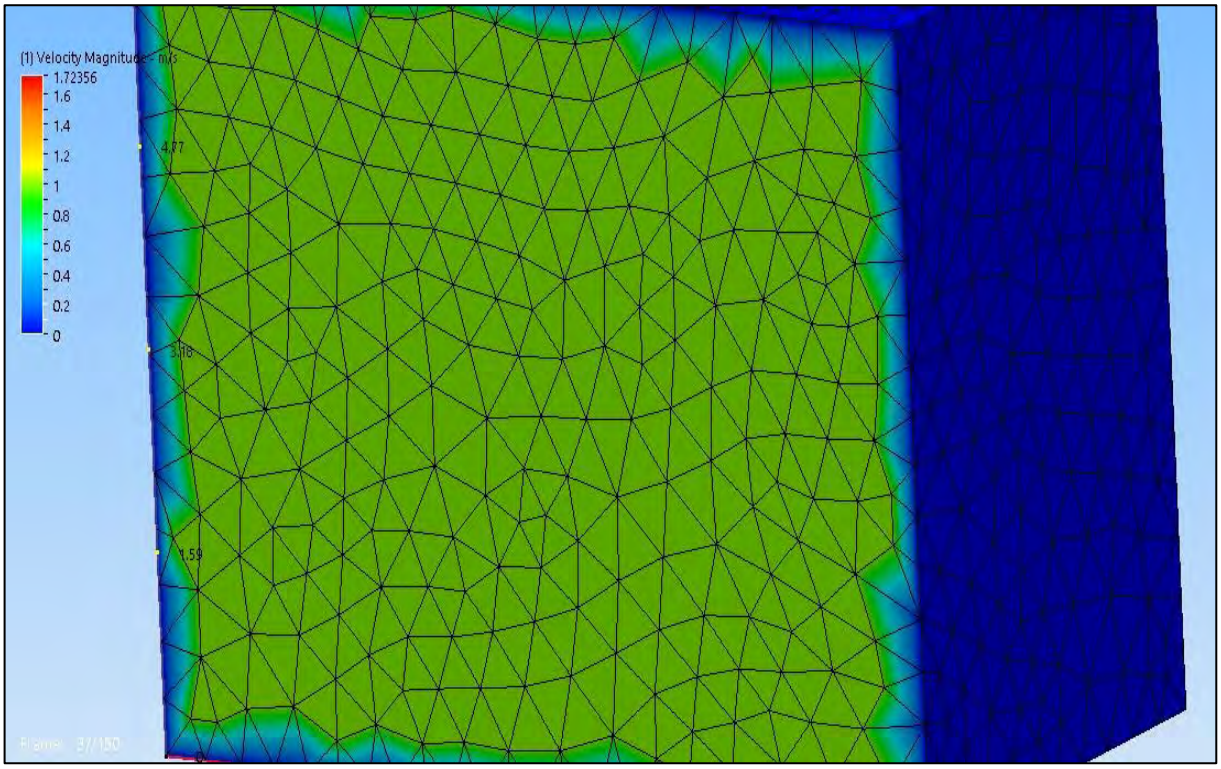

Figure 0-1: model meshed

Number of Nodes	10266
Number of Elements	53160

B.4. Physics

Flow	On
Compressibility	Incompressible
Heat Transfer	Off
Auto Forced Convection	Off
Gravity Components	0.0, 0.0, 0.0
Radiation	Off
Scalar	No scalar
Turbulence	On

B.5. Solver Settings

Solution mode	Transient
Solver computer	My Computer
Intelligent solution control	Off
Advection scheme	ADV 1
Turbulence model	k-epsilon

B.6. Convergence

Iterations run	300
Solve time	352 seconds
Solver version	15.2.20140731

1. *Energy Balance*

2. *Mass Balance*

	IN	OUT
Mass flow	50740.5 kg/s	-49879.1 kg/s
Volume flow	50.7464 m^3/s	-49.885 m^3/s

B.7. Results

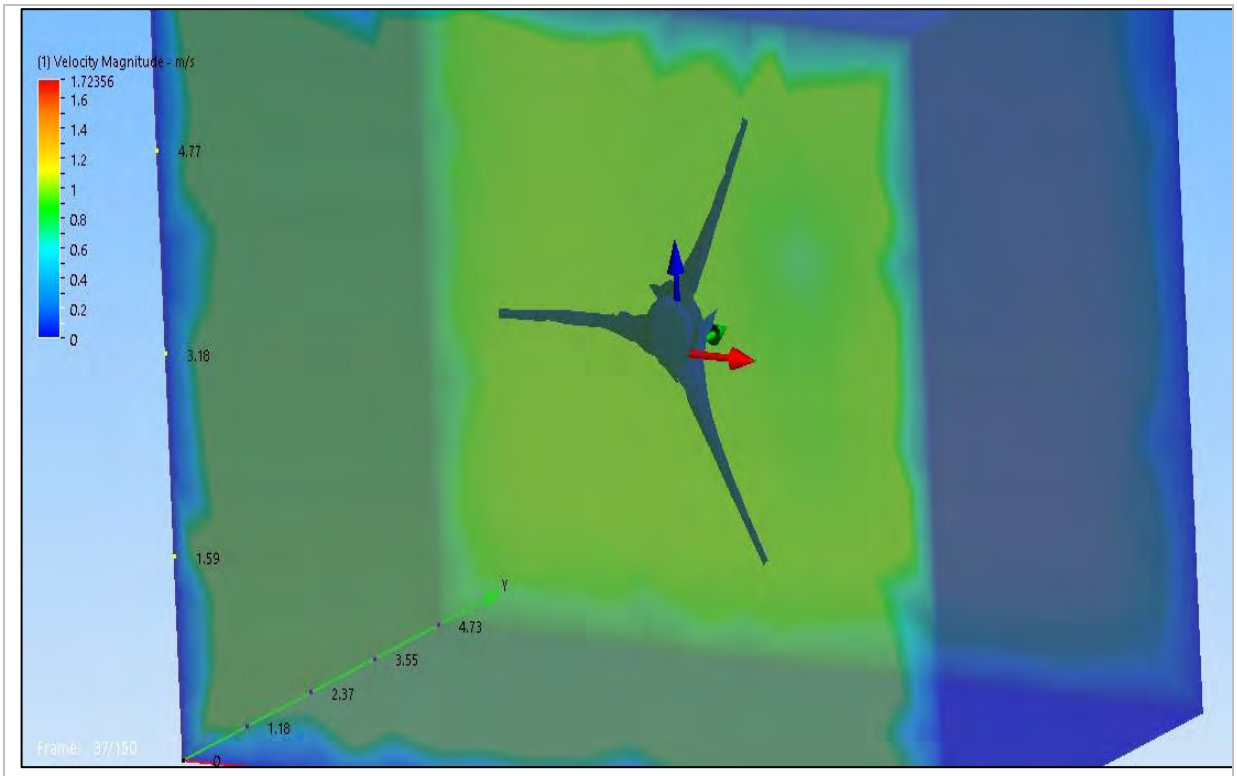

Figure 0-2: Turbine rotating following y axis

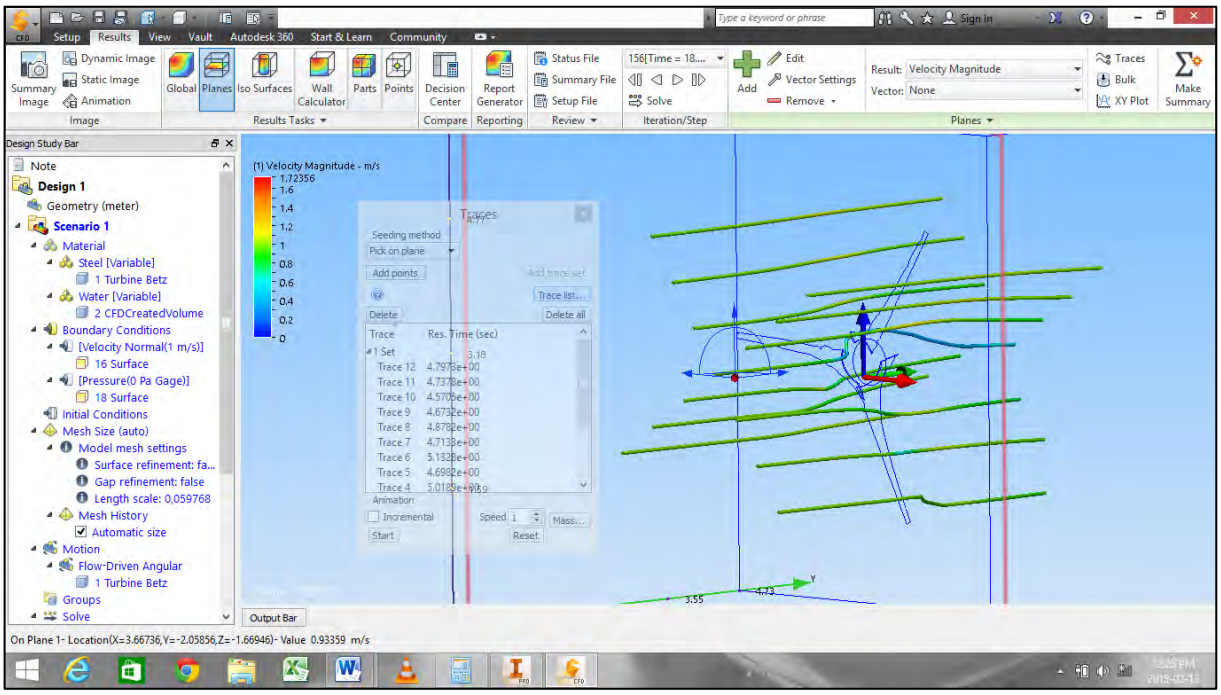

Figure 0-3: View of the result with traces

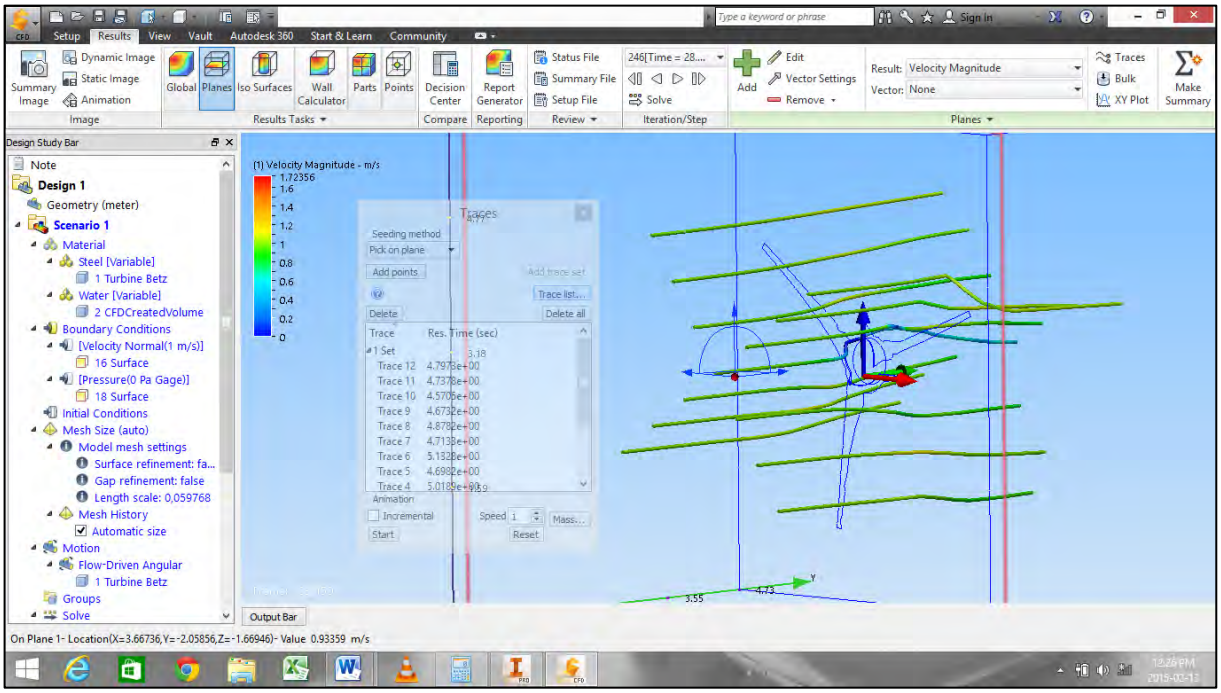

Figure 0-4: view of the result with traces

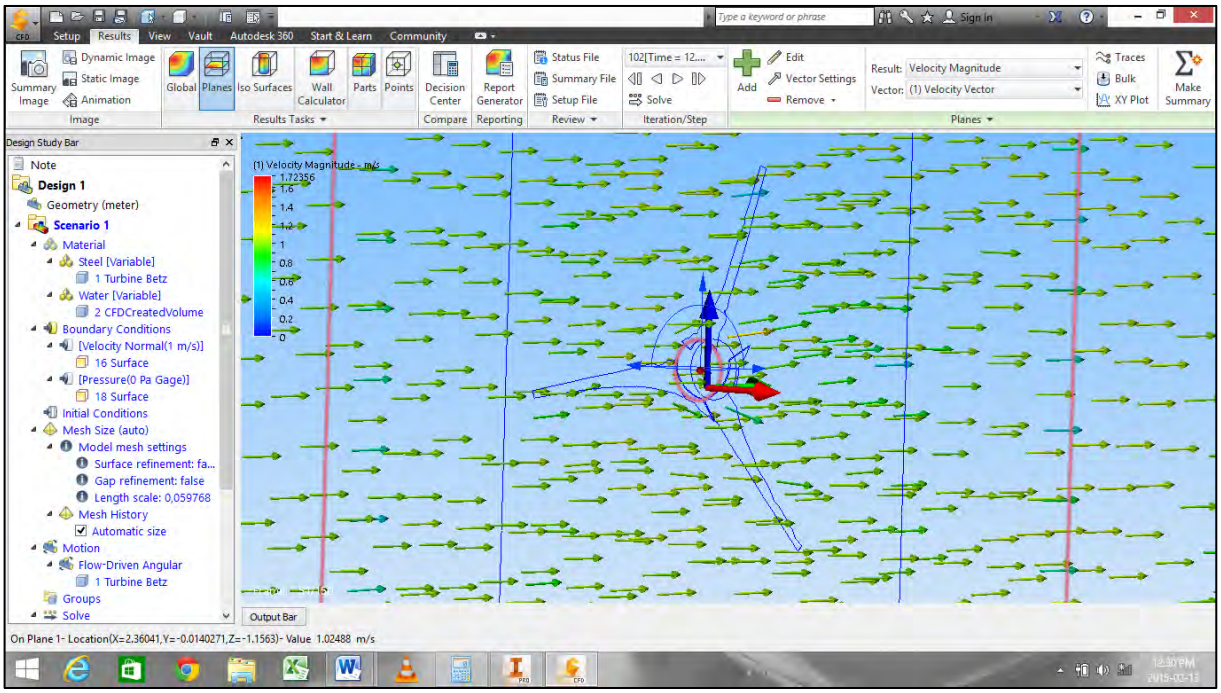

Figure 0-5: view of the results with arrows

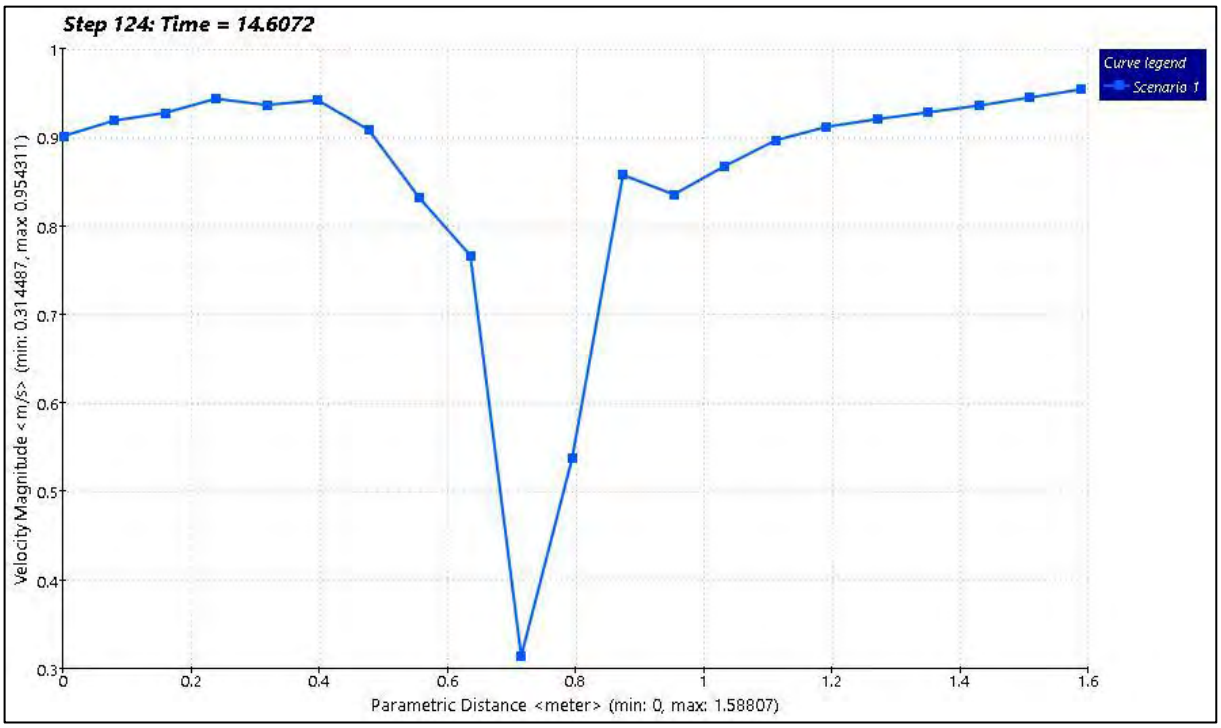

Figure 0-6: velocity profile near the hub

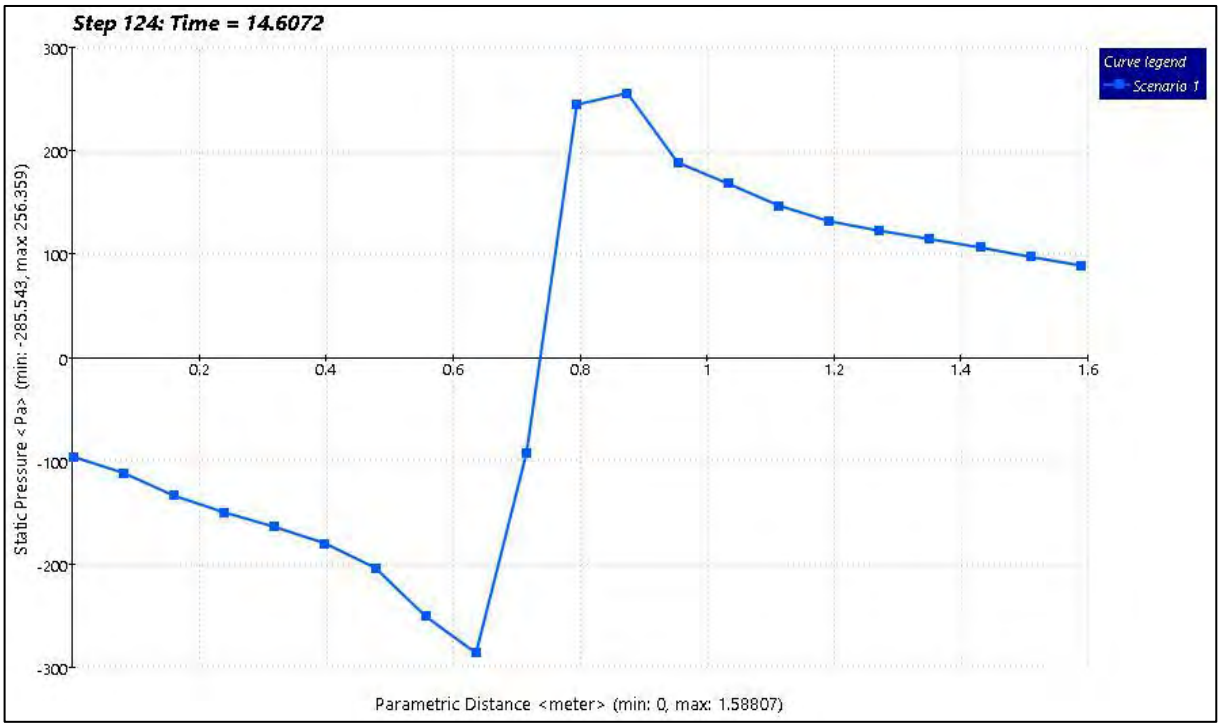

Figure 0-7: static pressure near the hub

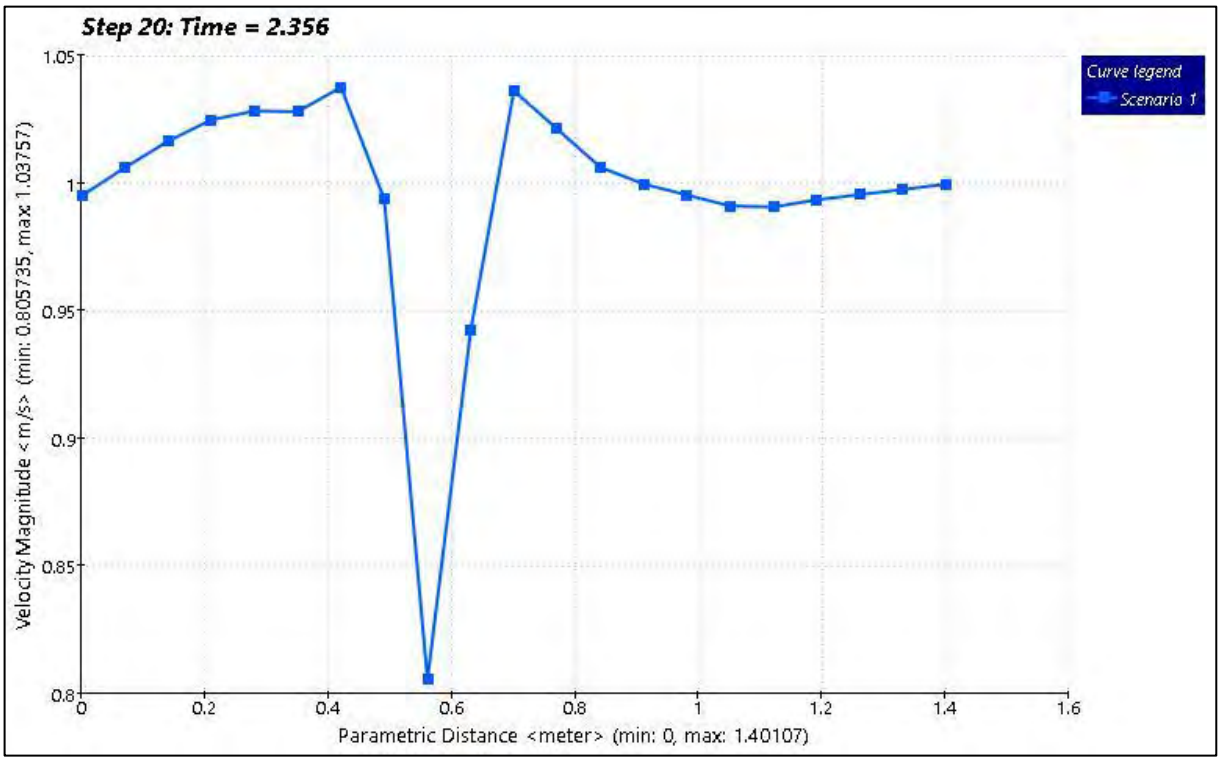

Figure 0-8: velocity profile half of the blade radius

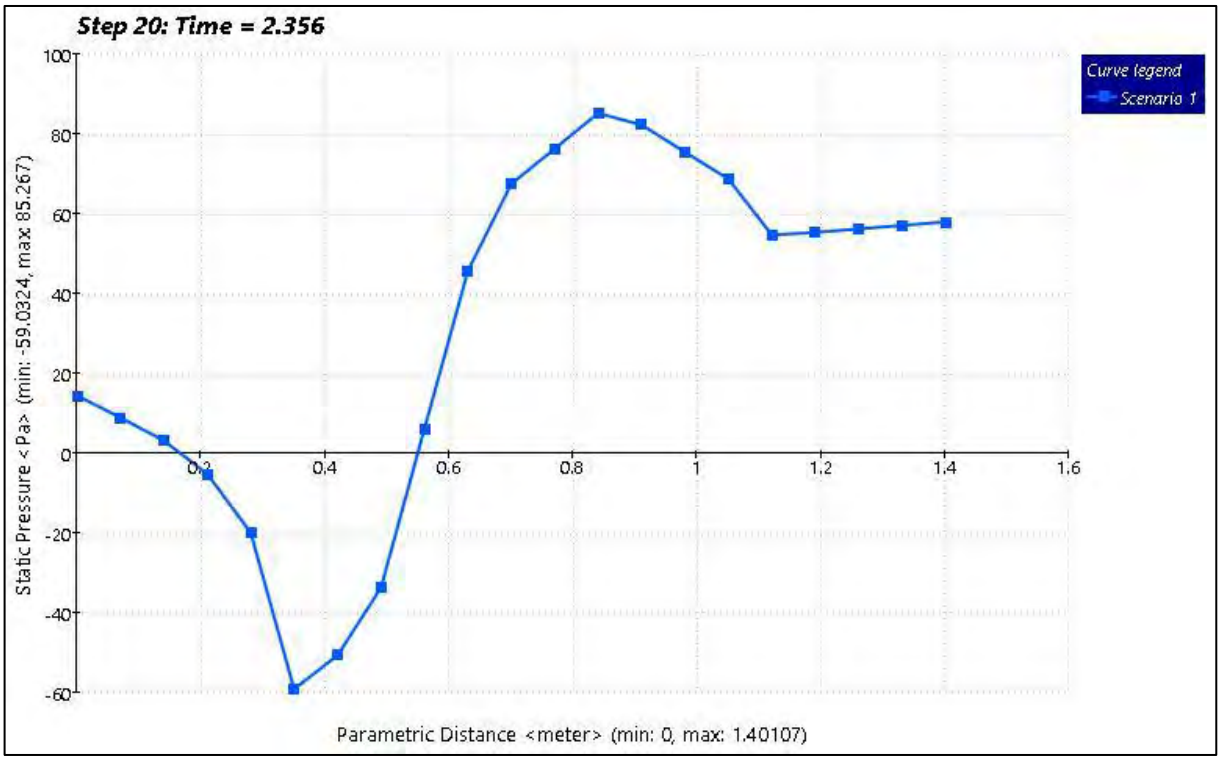

Figure 0-9: static pressure half of the blade radius

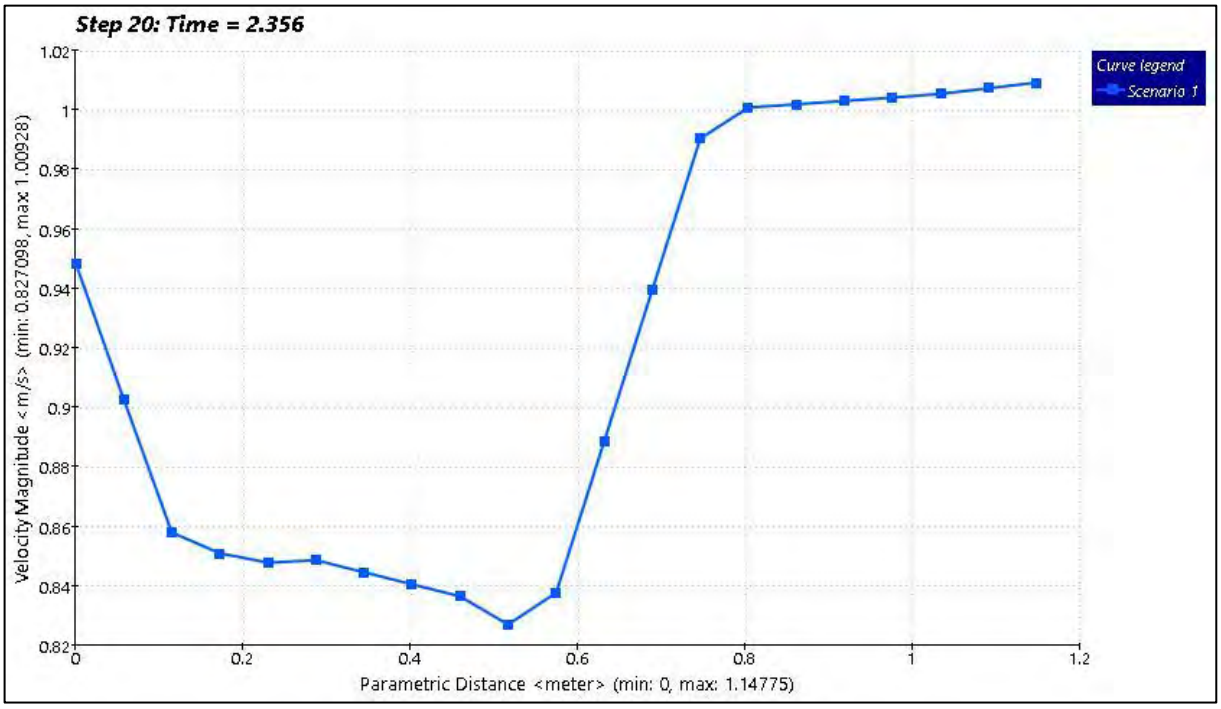

Figure 0-10: velocity profile near the tip

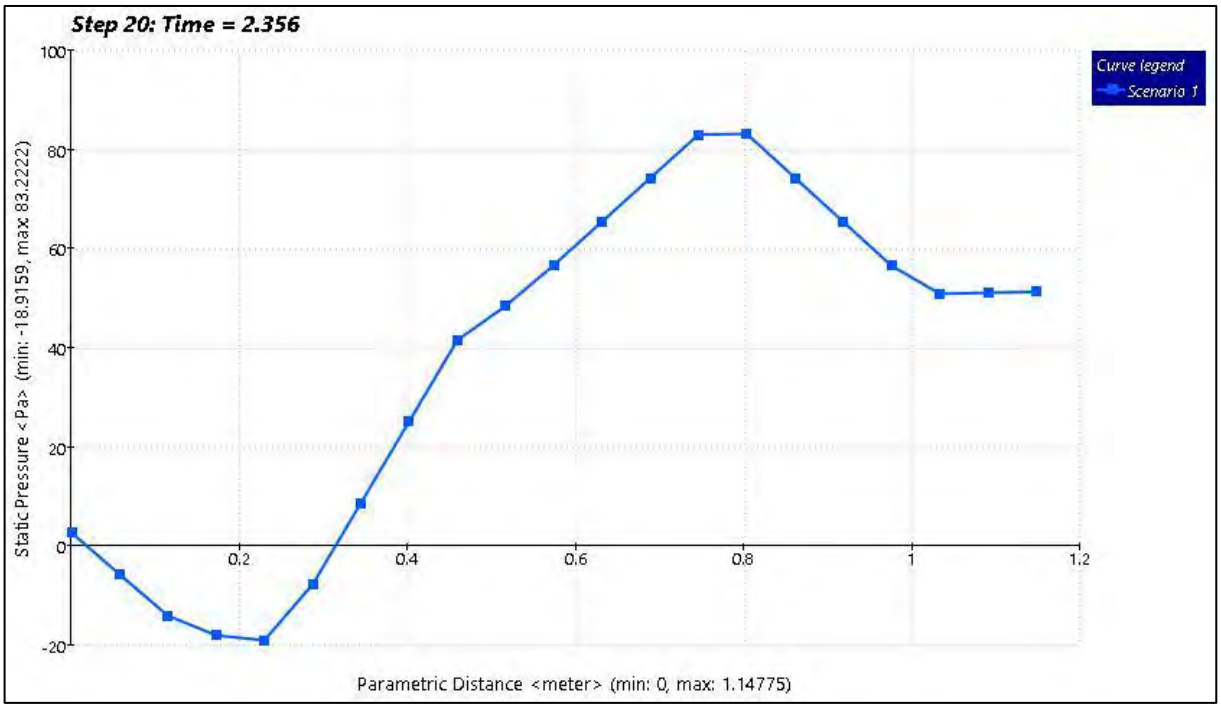

Figure 0-11: static pressure near the tip

3. *Inlets and Outlets*

inlet 1	inlet bulk pressure	36.545 N/m^2
	inlet bulk	0.0 C
	inlet mach number	6.60767e-08
	mass flow in	50740.5 kg/s
	minimum x,y,z of	0.0
	node near minimum	1299.0
	Reynolds number	6706410.0
	surface id	16.0
	total mass flow in	50740.5 kg/s
	total vol. flow in	50.7464 m^3/s
	volume flow in	50.7464 m^3/s
outlet 1	mass flow out	-49879.1 kg/s
	minimum x,y,z of	0.0
	node near minimum	1712.0
	outlet bulk pressure	-0.0 N/m^2
	outlet bulk	-0.0 C
	outlet mach number	6.6098e-08
	Reynolds number	6592560.0
	surface id	18.0
	total mass flow out	-49879.1 kg/s
	total vol. flow out	-49.885 m^3/s
	volume flow out	-49.885 m^3/s

4. *Field Variable Results*

VARIABLE	MAX	MIN
cond	54.9955 W/m-K	0.6 W/m-K
Dens	7833.0 kg/m^3	999.883 kg/m^3
econd	584093.0 W/m-K	0.0 W/m-K
emiss	1.0	0.0
evisc	139.675 kg/m-s	0.0 kg/m-s
gent	40.9857 1/s	0.0120809 1/s
press	1188.38 N/m^2	-451.686 N/m^2
ptotl	1608.81 N/m^2	-451.686 N/m^2

scal1	0.0	0.0
seebeck	0.0 V/K	0.0 V/K
spech	4182.0 J/kg-K	465.0 J/kg-K
temp	0.0 C	0.0 C
transmiss	0.0	0.0
turbd	0.247871 m^2/s^3	1.5082e-06 m^2/s^3
turbk	0.22568 m^2/s^2	0.0 m^2/s^2
visc	0.001003 kg/m-s	0.0 kg/m-s
vx vel	0.617327 m/s	-1.48614 m/s
vy vel	1.17248 m/s	-0.366379 m/s
vz vel	1.02362 m/s	-0.601454 m/s
wrough	0.0 m	0.0 m

5. *Component Thermal Summary*

PART	MINIMUM TEMPERATURE	MAXIMUM TEMPERATURE	VOLUME AVERAGED TEMPERATURE
Turbine Betz	0	0	-273,15
CFDCreatedVolume	0	0	-273,15

6. *Fluid Forces on Walls*

pressx	-1096.0 Newtons
pressy	0.0 Newtons
pressz	-275.29 Newtons
shearx	-0.065264 Newtons
sheary	485.66 Newtons

shearz	-0.040599 Newtons

Decision Centre

The material is water for the fluid because turbines are going to work under water and steel for the rotor because it is resistant and will allow as to get results0 since the purpose of this study is not to analyse the material but to analyse the behaviour of the turbine rotor under water. Using another tool like Autodesk CFD to measure the velocity profile and static pressure between two points.

APPENDIXES C

TURBINE OPTIMAL DESIGN USING TURBEM

C.1. USER INPUT DATA

R_tip : 2.000

R_hub : 0.200

v1 : 1.000

N_segments : 20

N_blades : 3

Speed, lc, and teta OPTIMIZATION considering Fprandtl

C.2. Output 1: OPTIMIZATION WITH TIP SPEED FACTOR GLOBAL

Tip Radius R_tip [m] 2.000

Hub Radius R_hub [m] 0.275

Free stream speed v1 [m/s] 1.000

Number of Blades N_blades 3

Number of segments N_segments 20

C.3. RESULTS

Nominal omega [rad/s] 3.000

Power Raw [W] 12,566.371

Total power by Momentum Theory Ptcm [W] 2,839.156

Total Power by Blade Theory Ptld [W] 2,782.553

Total Torque by Momentum Theory Ttcm [Nm] 946.385

Total Torque by Blade Theory Ttld [Nm] 927.518

Total Axial Force by Momentum Theory Ftcm [N] 4,794.054

Total Axial Force by Blade Theory Ftld [N] 4,802.753

Power Factor Cp [] 0.226

Tip Factor Ctip [] 6.000

****

RESULTS BY SECTION

r [m]	v1 [m/s]	omega [r/s]	teta[rad]	lc [m]	Pild [W/m]	Tild [Nm/m]	Fild [N/m]	Picm [W/m]	Ticm [Nm/m]	Ficm [N/m]	alfa [rad]	gamma [rad]	a	aprima	CL	CD	ga	gap	Fprandtl
0.245	1.000	3.000	0.631	0.495	308.922	102.974	493.209	304.985	101.662	489.554	0.095	0.726	0.198	0.229	0.598	0.012	-0.002	-0.002	1.000
0.335	1.000	3.000	0.461	0.495	501.617	167.206	814.576	496.132	165.377	804.846	0.107	0.568	0.258	0.157	0.676	0.012	-0.004	-0.002	1.000
0.425	1.000	3.000	0.351	0.455	677.183	225.728	1,107.542	676.274	225.425	1,100.013	0.114	0.465	0.290	0.110	0.718	0.013	-0.003	0.000	1.000
0.515	1.000	3.000	0.281	0.470	844.374	281.458	1,416.538	845.442	281.814	1,410.495	0.105	0.386	0.321	0.081	0.663	0.012	-0.002	0.000	1.000
0.605	1.000	3.000	0.221	0.385	1,005.238	335.079	1,671.002	1,008.271	336.090	1,667.521	0.116	0.337	0.325	0.060	0.734	0.013	-0.001	0.000	0.999
0.695	1.000	3.000	0.181	0.325	1,162.885	387.628	1,889.907	1,172.406	390.802	1,885.760	0.123	0.304	0.316	0.045	0.775	0.013	-0.001	0.000	0.999
0.785	1.000	3.000	0.141	0.310	1,314.888	438.296	2,221.489	1,325.248	441.749	2,216.377	0.122	0.263	0.342	0.037	0.770	0.013	-0.001	0.000	0.998
0.875	1.000	3.000	0.131	0.295	1,464.679	488.226	2,406.315	1,483.782	494.594	2,400.651	0.114	0.245	0.324	0.029	0.720	0.012	-0.001	0.000	0.997
0.965	1.000	3.000	0.101	0.260	1,609.917	536.639	2,680.721	1,626.900	542.300	2,676.770	0.121	0.222	0.332	0.024	0.760	0.013	-0.001	0.000	0.995
1.055	1.000	3.000	0.081	0.235	1,750.060	583.353	2,919.454	1,775.225	591.742	2,915.107	0.123	0.204	0.331	0.020	0.775	0.013	-0.001	0.000	0.992
1.145	1.000	3.000	0.071	0.220	1,883.154	627.718	3,117.227	1,924.091	641.364	3,111.397	0.120	0.191	0.324	0.017	0.757	0.013	-0.001	0.000	0.987
1.235	1.000	3.000	0.051	0.205	2,006.489	668.830	3,423.865	2,045.012	681.671	3,419.481	0.123	0.174	0.340	0.015	0.773	0.013	-0.001	0.000	0.982
1.325	1.000	3.000	0.041	0.190	2,120.975	706.992	3,619.802	2,191.084	730.361	3,613.830	0.122	0.163	0.336	0.013	0.771	0.013	-0.001	0.000	0.972
1.415	1.000	3.000	0.031	0.175	2,214.129	738.043	3,791.294	2,215.605	738.535	3,791.012	0.123	0.154	0.335	0.011	0.773	0.013	0.000	0.000	0.957

1.505	1.000	3.000	0.021	0.160	2,286.416	762.139	3,939.530	2,376.486	792.162	3,932.669	0.124	0.145	0.334	0.010	0.779	0.013	-0.001	0.000	0.935
1.595	1.000	3.000	0.011	0.145	2,316.220	772.073	4,037.064	2,408.528	802.843	4,030.824	0.126	0.137	0.336	0.009	0.787	0.014	-0.001	0.000	0.901
1.685	1.000	3.000	0.001	0.135	2,287.563	762.521	4,157.698	2,383.447	794.482	4,151.551	0.125	0.126	0.356	0.008	0.783	0.014	-0.001	0.000	0.855
1.775	1.000	3.000	0.001	0.115	2,159.490	719.830	3,842.860	2,262.510	754.170	3,836.936	0.122	0.123	0.338	0.007	0.767	0.014	-0.001	0.000	0.769
1.865	1.000	3.000	0.001	0.105	1,849.866	616.622	3,526.529	1,880.924	626.975	3,524.706	0.111	0.112	0.365	0.006	0.701	0.013	0.000	0.000	0.649
1.955	1.000	3.000	0.001	0.065	1,153.195	384.398	2,287.301	1,143.826	381.275	2,287.766	0.106	0.107	0.364	0.005	0.669	0.015	0.000	0.000	0.402

C.4. Output 2 : Section *Geometry*

Section 0

0.3997 -0.2920 0.2450	0.1469 -0.0967 0.2450	0.0189 -0.0058 0.2450
0.3822 -0.2783 0.2450	0.1366 -0.0889 0.2450	0.0153 -0.0036 0.2450
0.3652 -0.2649 0.2450	0.1266 -0.0815 0.2450	0.0120 -0.0017 0.2450
0.3486 -0.2518 0.2450	0.1171 -0.0744 0.2450	0.0091 -0.0001 0.2450
0.3324 -0.2392 0.2450	0.1079 -0.0677 0.2450	0.0066 0.0012 0.2450
0.3166 -0.2268 0.2450	0.0991 -0.0612 0.2450	0.0044 0.0023 0.2450
0.3013 -0.2148 0.2450	0.0906 -0.0551 0.2450	0.0025 0.0031 0.2450
0.2863 -0.2032 0.2450	0.0826 -0.0493 0.2450	0.0010 0.0036 0.2450
0.2717 -0.1919 0.2450	0.0749 -0.0438 0.2450	-0.0002 0.0039 0.2450
0.2574 -0.1809 0.2450	0.0677 -0.0386 0.2450	-0.0010 0.0039 0.2450
0.2436 -0.1702 0.2450	0.0607 -0.0338 0.2450	-0.0015 0.0036 0.2450
0.2302 -0.1599 0.2450	0.0542 -0.0292 0.2450	-0.0016 0.0031 0.2450
0.2171 -0.1499 0.2450	0.0481 -0.0250 0.2450	-0.0014 0.0023 0.2450
0.2045 -0.1402 0.2450	0.0423 -0.0210 0.2450	-0.0009 0.0013 0.2450
0.1922 -0.1308 0.2450	0.0369 -0.0174 0.2450	0.0000 0.0000 0.2450
0.1803 -0.1218 0.2450	0.0318 -0.0141 0.2450	0.0000 0.0000 0.2450
0.1688 -0.1131 0.2450	0.0271 -0.0110 0.2450	0.0012 -0.0015 0.2450
0.1577 -0.1047 0.2450	0.0228 -0.0083 0.2450	0.0027 -0.0033 0.2450

Output : Blade Stresses by Beam Theory

Section Structural Properties

r	xca	yca	xcp	ycp	lca	Area	Icc	Inn	Jpp	lc	teta
[m]	[m]	[m]	[m]	[m]	[m]	[m2]	[m4]	[m4]	[m4]	[m]	[deg]
0.2450	0.0711	0.0520	0.0999	0.0730	0.1779	3.7548E-003	6.4809E-007	3.5499E-005	3.6147E-005	0.4950	0.6310
0.3350	0.0789	0.0392	0.1108	0.0550	0.1779	3.7548E-003	6.4809E-007	3.5499E-005	3.6147E-005	0.4950	0.4610
0.4250	0.0760	0.0278	0.1068	0.0391	0.1779	3.1725E-003	4.6266E-007	2.5342E-005	2.5805E-005	0.4550	0.3510
0.5150	0.0803	0.0232	0.1129	0.0326	0.1779	3.3851E-003	5.2675E-007	2.8853E-005	2.9379E-005	0.4700	0.2810
0.6050	0.0668	0.0150	0.0939	0.0211	0.1779	2.2714E-003	2.3717E-007	1.2991E-005	1.3228E-005	0.3850	0.2210
0.6950	0.0569	0.0104	0.0799	0.0146	0.1779	1.6186E-003	1.2043E-007	6.5967E-006	6.7171E-006	0.3250	0.1810
0.7850	0.0546	0.0078	0.0767	0.0109	0.1779	1.4727E-003	9.9693E-008	5.4606E-006	5.5603E-006	0.3100	0.1410
0.8750	0.0520	0.0069	0.0731	0.0096	0.1779	1.3336E-003	8.1753E-008	4.4780E-006	4.5597E-006	0.2950	0.1310
0.9650	0.0460	0.0047	0.0647	0.0066	0.1779	1.0359E-003	4.9330E-008	2.7020E-006	2.7513E-006	0.2600	0.1010
1.0550	0.0417	0.0034	0.0586	0.0048	0.1779	8.4628E-004	3.2922E-008	1.8033E-006	1.8362E-006	0.2350	0.0810
1.1450	0.0390	0.0028	0.0549	0.0039	0.1779	7.4170E-004	2.5288E-008	1.3851E-006	1.4104E-006	0.2200	0.0710

1.2350 0.0364 0.0019 0.0512 0.0026 0.1779 6.4400E-004 1.9065E-008 1.0443E-006 1.0633E-006 0.2050 0.0510

1.3250 0.0338 0.0014 0.0475 0.0019 0.1779 5.5321E-004 1.4068E-008 7.7056E-007 7.8463E-007 0.1900 0.0410

1.4150 0.0311 0.0010 0.0437 0.0014 0.1779 4.6931E-004 1.0124E-008 5.5456E-007 5.6468E-007 0.1750 0.0310

1.5050 0.0285 0.0006 0.0400 0.0008 0.1779 3.9230E-004 7.0745E-009 3.8750E-007 3.9458E-007 0.1600 0.0210

1.5950 0.0258 0.0003 0.0362 0.0004 0.1779 3.2219E-004 4.7719E-009 2.6138E-007 2.6615E-007 0.1450 0.0110

1.6850 0.0240 0.0000 0.0337 0.0000 0.1779 2.7929E-004 3.5855E-009 1.9639E-007 1.9998E-007 0.1350 0.0010

1.7750 0.0205 0.0000 0.0287 0.0000 0.1779 2.0266E-004 1.8880E-009 1.0342E-007 1.0530E-007 0.1150 0.0010

1.8650 0.0187 0.0000 0.0262 0.0000 0.1779 1.6895E-004 1.3121E-009 7.1870E-008 7.3183E-008 0.1050 0.0010

1.9550 0.0116 0.0000 0.0162 0.0000 0.1779 6.4745E-005 1.9269E-010 1.0555E-008 1.0747E-008 0.0650 0.0010

Output : Forces by Momentum Theory per unit span length

r Ficm Ficm_t Ficm_c Ficm_n Ficm_acum Ficm_t_acum Micm_acum Micm_t_acum Micm_cc_acum Micm_nn_acum Micm_pp_acum

[m] [N] [N] [N] [N] [N] [N] [Nm] [Nm] [Nm] [Nm] [Nm]

0.2450 489.55 414.95 623.86 150.49 53,267.26 9,997.46 8,066.02 55,489.52 49,562.91 614.78 -1,411.85

0.3350 804.85 493.66 800.16 501.22 52,777.71 9,582.51 7,203.59 50,739.53 48,647.21 2,188.87 -1,732.75

0.4250 1,100.01 530.41 876.30 850.57 51,972.86 9,088.85 6,385.59 46,061.97 45,449.15 2,871.18 -1,520.96

0.5150 1,410.50 547.21 916.90 1,203.42 50,872.85 8,558.44 5,615.34 41,483.42 41,413.60 3,021.70 -1,752.27

0.6050 1,667.52 555.52 907.54 1,505.19 49,462.36 8,011.22 4,894.32 37,031.80 37,204.01 3,019.19 -1,067.16

0.6950 1,885.76 562.30 892.58 1,753.73 47,794.84 7,455.70 4,223.31 32,730.27 32,955.84 2,812.19 -602.94

0.7850 2,216.38 562.74 868.63 2,115.30 45,909.08 6,893.40 3,602.91 28,598.45 28,820.97 2,598.40 -531.15

0.8750 2,400.65 565.25 873.99 2,306.25 43,692.70 6,330.66 3,033.15 24,666.11 24,850.97 2,180.21 -465.33

0.9650 2,676.77 561.97 829.00 2,606.47 41,292.05 5,765.41 2,514.26 20,949.82 21,096.57 1,920.13 -255.39

1.0550 2,915.11 560.89 794.92 2,860.17 38,615.28 5,203.44 2,045.95 17,474.45 17,582.70 1,618.22 -130.78

1.1450 3,111.40 560.14 779.46 3,063.82 35,700.17 4,642.55 1,628.12 14,261.43 14,341.00 1,294.67 -83.92

1.2350 3,419.48 551.96 725.56 3,386.90 32,588.77 4,082.40 1,260.70 11,328.44 11,377.98 1,050.95 -45.76

1.3250 3,613.83 551.22 698.88 3,588.20 29,169.29 3,530.44 942.96 8,703.21 8,734.54 797.46 -16.57

1.4150 3,791.01 521.93 639.18 3,773.01 25,555.46 2,979.23 674.83 6,403.22 6,421.06 582.17 4.53

1.5050 3,932.67 526.35 608.82 3,920.75 21,764.45 2,457.30 453.68 4,444.42 4,452.96 401.98 17.84

1.5950 4,030.82 503.35 547.66 4,025.04 17,831.78 1,930.94 279.89 2,839.55 2,842.46 258.64 23.76

1.6850 4,151.55 471.50 475.65 4,151.08 13,800.96 1,427.59 151.41 1,597.47 1,597.62 149.98 8.26

1.7750 3,836.94 424.88 428.72 3,836.51 9,649.41 956.09 65.36 729.02 729.09 64.40 10.78

1.8650 3,524.71 336.18 339.70 3,524.37 5,812.47 531.21 17.55 205.90 205.92 17.02 -5.56

1.9550 2,287.77 195.03 197.31 2,287.57 2,287.77 195.03 0.00 0.00 0.00 -0.20 0.00

Output : Forces by Blade Theory per unit span length

r	Fild	Fild_t	Fild_c	Fild_n	Fild_acum	Fild_t_acum	Mild_acum	Mild_t_acum	Mild_cc_acum	Mild_nn_acum	Mild_pp_acum
[m]	[N]	[N]	[N]	[N]	[N]	[N]	[Nm]	[Nm]	[Nm]	[Nm]	[Nm]
0.2450	493.21	420.30	630.34	150.28	53,363.92	9,854.75	7,891.34	55,489.52	49,459.86	557.93	-1,404.59
0.3350	814.58	499.12	809.38	507.51	52,870.71	9,434.45	7,042.24	50,739.53	48,575.43	2,110.23	-1,728.51
0.4250	1,107.54	531.12	879.56	857.39	52,056.14	8,935.33	6,238.06	46,061.97	45,398.42	2,785.42	-1,518.46
0.5150	1,416.54	546.52	917.91	1,209.42	50,948.59	8,404.20	5,481.68	41,483.42	41,376.54	2,936.06	-1,751.01
0.6050	1,671.00	553.85	906.67	1,508.95	49,532.06	7,857.68	4,774.49	37,031.80	37,177.74	2,935.92	-1,066.29
0.6950	1,889.91	557.74	888.84	1,758.63	47,861.05	7,303.83	4,117.14	32,730.27	32,936.73	2,735.10	-602.19
0.7850	2,221.49	558.34	864.99	2,120.98	45,971.15	6,746.10	3,510.00	28,598.45	28,807.91	2,527.11	-530.75
0.8750	2,406.31	557.97	867.52	2,312.81	43,749.66	6,187.76	2,953.10	24,666.11	24,840.51	2,119.52	-465.02
0.9650	2,680.72	556.10	823.56	2,610.99	41,343.34	5,629.78	2,446.42	20,949.82	21,089.73	1,866.31	-255.13
1.0550	2,919.45	552.94	787.35	2,865.14	38,662.62	5,073.68	1,989.79	17,474.45	17,578.15	1,572.74	-130.54
1.1450	3,117.23	548.23	767.98	3,070.48	35,743.17	4,520.74	1,582.92	14,261.43	14,337.80	1,258.23	-83.72

1.2350 3,423.87 541.56 715.40 3,391.81 32,625.94 3,972.51 1,225.39 11,328.44 11,376.18 1,021.29 -45.62

1.3250 3,619.80 533.58 681.50 3,594.89 29,202.08 3,430.95 916.61 8,703.21 8,733.46 775.21 -16.46

1.4150 3,791.29 521.59 638.85 3,773.31 25,582.28 2,897.37 655.84 6,403.22 6,420.47 565.73 4.67

1.5050 3,939.53 506.40 589.02 3,928.03 21,790.98 2,375.79 442.02 4,444.42 4,452.72 392.04 17.96

1.5950 4,037.06 484.06 528.44 4,031.50 17,851.45 1,869.38 273.78 2,839.55 2,842.39 253.20 23.84

1.6850 4,157.70 452.53 456.69 4,157.24 13,814.39 1,385.32 149.10 1,597.47 1,597.62 147.71 8.29

1.7750 3,842.86 405.54 409.38 3,842.45 9,656.69 932.79 65.15 729.02 729.09 64.22 10.79

1.8650 3,526.53 330.63 334.15 3,526.20 5,813.83 527.25 17.70 205.90 205.92 17.17 -5.56

1.9550 2,287.30 196.62 198.91 2,287.10 2,287.30 196.62 0.00 0.00 0.00 -0.20 0.00

Output : Stresses

r sigmaf_icm_cc sigmaf_icm_nn Tau_icm_pp sigmaf_icm_cc sigmaf_icm_nn Tau_icm_pp

[m] MPa MPa MPa MPa MPa MPa

0.2450 68.14 0.16 -0.03 68.00 0.16 -0.03

0.3350 66.88 0.59 -0.04 66.78 0.59 -0.04

0.4250 80.45 0.94 -0.05 80.36 0.94 -0.05

0.5150 66.51 0.92 -0.05 66.45 0.92 -0.05

0.6050 108.71 1.44 -0.06 108.63 1.44 -0.06

0.6950 160.08 1.88 -0.05 159.99 1.88 -0.05

0.8750 161.41 1.71 -0.05 161.34 1.71 -0.05

0.9650 200.15 1.75 -0.04 200.08 1.75 -0.04

1.0550 225.91 1.54 -0.03 225.85 1.54 -0.03

1.1450 224.58 1.18 -0.02 224.53 1.18 -0.02

1.2350 220.22 0.82 -0.02 220.19 0.82 -0.02

1.3250 212.34 0.38 -0.01 212.32 0.38 -0.01

1.4150 199.78 -0.09 0.00 199.76 -0.09 0.00

1.5050 181.28 -0.56 0.01 181.27 -0.56
0.01

1.5950 155.47 -0.98 0.02 155.47 -0.98
0.02

1.6850 108.27 -0.98 0.01 108.27 -0.98
0.01

1.7750 79.94 -1.18 0.02 79.94 -1.18 0.02

1.8650 29.66 -0.52 -0.01 29.66 -0.52 -0.01

1.9550 0.00 0.06 0.00 0.00 0.06 0.00

Output 2 : Torque vs Omega Curves

Raw Power [W]	v1 [m/s]	omega [r/s]	Ptcm [W]	Ptld [W]	Ttcm [Nm]	Ttld [Nm]	Ftcm [N]	Ftld [N]	Full Positive Torque
196.350	0.250	0.600	0.521	0.519	0.868	0.865	9.138	9.157	False
196.350	0.250	0.900	27.709	27.436	30.788	30.485	201.820	201.901	False
196.350	0.250	1.200	15.838	15.913	13.198	13.261	171.115	171.110	False
196.350	0.250	1.500	6.052	5.981	4.035	3.987	133.177	133.191	False
1,570.796	0.500	0.600	12.669	12.740	21.114	21.234	196.072	195.976	False
1,570.796	0.500	0.900	10.399	10.350	11.555	11.500	86.973	87.360	False
1,570.796	0.500	1.200	4.952	4.980	4.127	4.150	56.912	56.828	False
1,570.796	0.500	1.500	329.176	327.049	219.450	218.032	1,131.210	1,132.176	False
1,570.796	0.500	1.800	274.196	274.546	152.331	152.525	1,011.398	1,011.021	False
1,570.796	0.500	2.100	228.290	229.747	108.710	109.403	889.619	889.641	False
1,570.796	0.500	2.400	175.036	176.163	72.932	73.401	796.707	796.712	False
1,570.796	0.500	2.700	146.998	146.320	54.444	54.193	894.659	894.665	False
1,570.796	0.500	3.000	45.031	46.385	15.010	15.462	240.731	240.664	False
1,570.796	0.500	3.300	16.469	15.867	4.990	4.808	152.950	152.972	False

APPENDIXES D

13th International Conference on Sustainable Energy technologies (SET2014)

25-28th August, 2014
Geneva
Paper ID: SET2014-E20035

Deep sea (ocean current) power energy technology

Mutombo Jimmy Tshikaya*, Freddie Inambao

Department of Mechanical Engineering, University of KwaZulu – Natal, Mazisi Kunene Road, Glenwood,
Durban, KwaZulu – Natal, South – Africa.

**tshikaya.mutombo@gmail.com*

APPENDIX D

DEEP SEA (OCEAN CURRENT) POWER ENERGY TECHNOLOGY

13TH INTERNATIONAL CONFERENCE ON SUSTAINABLE ENERGY TECHNOLOGIES (SET2014)

25-28TH AUGUST, 2014

GENEVA

13th International Conference on Sustainable Energy technologies (SET2014)
25-28th August, 2014
Geneva
Paper ID: SET2014-E20035

Deep sea (ocean current) power energy technology

Mutombo Jimmy Tshikaya*, Freddie Inambao

Department of Mechanical Engineering, University of KwaZulu – Natal, Mazisi Kunene Road, Glenwood, Durban, KwaZulu – Natal, South – Africa.

*tshikaya.mutombo@gmail.com

ABSTRACT

There is a growing demand of electrical energy in South African due to the increasing use in domestic, commercial and industrial sector. The country produces most of its electricity from the use of coal while the environmental issues are debated by researchers, journalists, industrialists and politicians all over the world in order to fight against the global warming and climate change. The study focuses on the design of a system generating electricity from Agulhas Current in Indian Ocean along South-Africa coastline by a sustainable and reliable energy supply. To achieve this objective, the design and construction of a hydrokinetic horizontal axis turbine are demonstrated and explained in this paper. Knowing the average velocity of the water current, the depth and other properties of different sites, the power generated is estimated using standard formula. In this paper we will assume the blade length for a turbine diameter selected for low Reynolds's number (low velocity) to design a proper turbine running for the sites where the speed has been measured and considered as possible sites for implantation of a system generating electricity. With the blade length according to Betz or Schmitz approaches, we determine the blade profiles which are the twist angles and chord lengths at different selected sections along the blade. We compare different air foils running under low wind velocity and adapt their profiles to evaluate the power output under deep ocean current condition. Making reasonable assumption for the efficiency of the turbine, generator and transmission, the power output has been estimated.

KEYWORDS: *ocean current, Agulhas current, chord length, pitch angle, Betz, Schmitz.*

1. INTRODUCTION

Water covers a huge surface of the planet where we are living [1] and as researchers, taking advantage of this reality can be a great advantage to humanity. Nobody ignores the importance of electricity for development of civilization which makes energy the most important thing in the word to run everything. So we turn our focus into the huge quantity of water available and try to generate electricity by harnessing the energy from it.

This paper focuses on the use of the ocean energy from Agulhas current in Indian Ocean along South – Africa [2] and we convert the energy from the current into electricity by using a horizontal axis marine turbine. This conversion can be possible only if turbines are able to extract energy from the source and convert it in another form which is electricity in this one. This technology has been studied already but only for water current with a velocity higher than the one we are interested in. However, our focus will be on the study of a system which can harvest energy from very slow velocity water current. Many different characteristics are taken into consideration like the current velocity, the water depth, the aquatic activity, the distance offshore, the sea bed, etc. [3].

A total of 51 deployments made from September 2005 to September 2010 give characteristics of the site where data collection using the Acoustic Doppler Current Profiler (ADCP). Sites where deployments were made are: Cape Morgan, East London, Fish River and Port Edward [4]. Unfortunately these data are not published to public but some of the deployment can be found on Eskom Ltd website.

This study is based on the horizontal axis marine turbine which can be used for Agulhas Current along South Africa coastline. Many studies on wind turbine were done and helped for design of different type of horizontal axis turbine [5]. We will analyze some of them and adapt their profiles to experiment them in marine current conditions. To achieve this objective it's important to understand the technology used in harvesting energy from the power of ocean current [6].

2. POWER IN THE OCEAN CURRENT

Kinetic energy in the ocean current is converted into another source of energy when the water current moves the rotor of the turbine. The pressure change and velocity can be explained using Bernoulli's equation. To make good assumption and analyze the condition, we sketch a velocity profile and evaluate the velocity and pressure upstream the rotor, when the interaction happens and downstream the rotor. Figure 1.

The speed of the water current downstream the rotor of the turbine is v_1 because it is moving in a free movement without any disturbance. Once it interacts with the rotor and during the passage through this, the speed will reduce to v_3. The pressure downstream the rotor is p_1. When it interacts with the rotor, the pressure rises to $p+$ and

falls suddenly to p- after passing the rotor. The pressure downstream the rotor will rise to a pressure p_3 which is equal to p_1. The change in pressure Δp is equal to "$p+ - p-$". Let's analyze the power in the rotor.

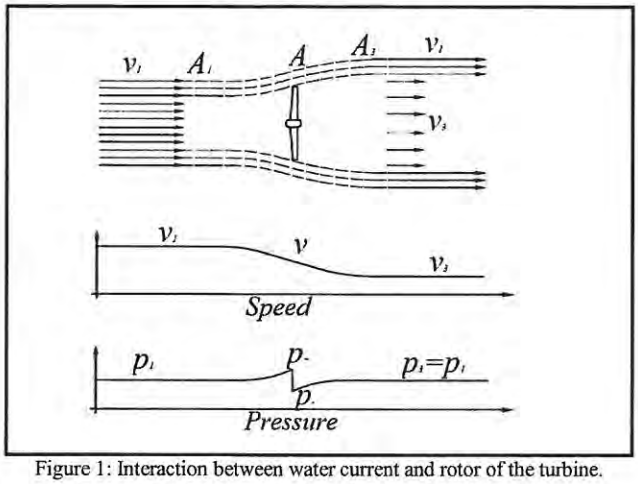

Figure 1: Interaction between water current and rotor of the turbine.

Using Bernoulli's equation, the total pressure is constant [7]. This equation states that the relationship between the speed and the pressure is such that if the speed of the flow goes up, the pressure goes down and vice versa (Eq. 1). It is assumed that the flow is frictionless and the density of the fluid is to remain constant.

$$\frac{1}{2}\rho v^2 + p = p_{tot} \quad \text{[Pa]} \quad (1)$$

From Figure 1 we apply Bernoulli's equation and we get

$$p_1 + \frac{1}{2}\rho v_1^2 = p_+ + \frac{1}{2}\rho v^2 \quad \text{[Pa]} \quad (2)$$

$$p_+ - \Delta p + \frac{1}{2}\rho v^2 = p_1 + \frac{1}{2}\rho v_2^2 \quad \text{[Pa]} \quad (3)$$

Subtracting Eq. (3) from Eq. (2) we get

$$p_+ + p_1 - \Delta p + \frac{1}{2}\rho v^2 + \frac{1}{2}\rho v_1^2 = p_1 + p_+ + \frac{1}{2}\rho v_2^2 + \frac{1}{2}\rho v^2$$

$$\Delta p = \frac{1}{2}\rho(v_1^2 - v_2^2) \quad \text{[Pa]} \quad (4)$$

These formulas can also be expressed in change of momentum basis. Our assumptions are based on a square meter on a rotor plane where the mass flow is clearly equal to "ρ multiplied by v". Knowing that momentum is the result of mass times velocity and that pressure is equal to force per surface, we come to a result expressing the differential pressure as:

$$\Delta p = \rho v(v_1 - v_2) \quad \text{[Pa]} \quad (5)$$

Comparing Eq. (4) and Eq. (5), we noticed that they both have expression v_1 and v_3. Figure 1 shows v as the velocity of the fluid when it interacts with the rotor. We can then extract it from the two equations above.

$$\frac{1}{2}\rho(v_1^2 - v_2^2) = \rho v(v_1 - v_2)$$

$$\frac{1}{2}\rho(v_1 + v_2)(v_1 - v_2) = \rho v(v_1 - v_2)$$

$$\frac{1}{2}(v_1 + v_2) = v \quad \text{[m/s]} \quad (6)$$

Eq. (6) clearly indicates that the speed of the fluid in the rotor is the mean value of the speed upstream and downstream the rotor.

From formula above, we deduct the power in the turbine which is the change in kinetic energy in the fluid.

$$P = \frac{1}{2}\rho v(v_1^2 - v_2^2)A \quad \text{[W]} \quad (7)$$

Were A is the surface area swept by the rotor.

The axial force on the rotor known as the thrust can be calculated as

$$T = \Delta p A \quad [\text{N}] \quad (8)$$

In this study, data has been collected from different sites and the authors are trying to create a system running in existing conditions [8]. Thus velocity v_1 of the fluid known from site data collection is used in formulas above. The axial interference factor "a" which is a number between 0 and 1 is defined to avoid the use of the velocity "v" in the rotor and velocity "v_3" after the rotor in our next formula. We assume:

$$v = (1-a)v_1 \quad [\text{m/s}] \quad (9)$$

Using Eq. (9) and Eq. (6), Eq. (7) and Eq. (8) we get

$$\frac{1}{2}(v_1 + v_3) = (1-a)v_1$$
$$v_3 = v_1(1-2a)$$
$$P = 2\rho a(1-a)^2 v_1^3 A \quad [\text{W}] \quad (10)$$
$$T = 2\rho a(1-a)v_1^2 A \quad [\text{N}] \quad (11)$$

From Eq.(10) and (11) of P and T, we define two coefficients, "C_P" for the power production and "C_T" for the axial forces as:

$$C_p = 4a(1-a)^2 \quad [\text{-}] \quad (12)$$
$$C_T = 4a(1-a) \quad [\text{-}] \quad (13)$$

Eq.(10) and Eq.(11) can be written as

$$P = \frac{1}{2}\rho v_1^3 A C_p \quad [\text{W}] \quad (14)$$
$$T = \frac{1}{2}\rho v_1^2 A C_T \quad [\text{N}] \quad (15)$$

Curves of the two coefficient C_P and C_T as a function of "a" is shown in Fig. 2.

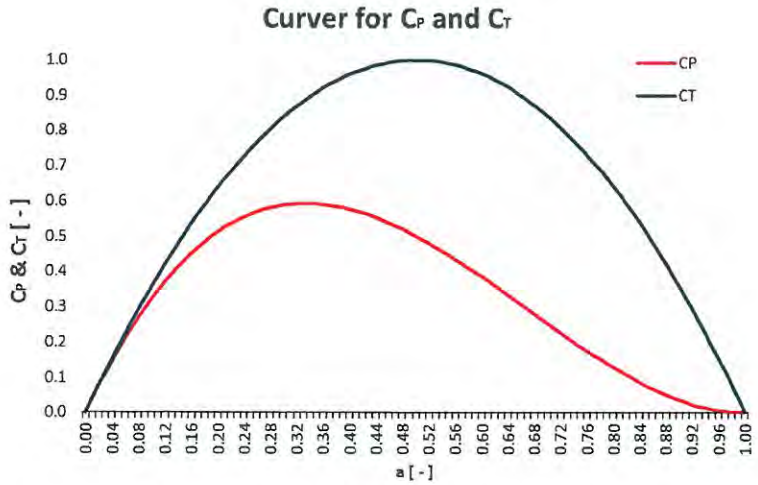

Fig. 2 Coefficient of power C_P and coefficient of axial force C_T for idealized wind or marine current turbine.

We can find the optimum and minimum value of the coefficient C_P on the curve from Fig. 2 or by a simple calculation using the derivative of the function C_P and equalizing it to zero. Values of "a" which gives "C_P =0" are maximum and minimum of the function C_P.

$$C_p = 4a(1-a)^2$$
$$C_p' = 4(1-a)(1-3a)$$
$$C_p' = 0 \Rightarrow (1-a) = 0 \text{ or } (1-3a) = 0$$
$$For\ a = 1 \Rightarrow C_p = 4 * 1(1-1)^2 = 0$$
$$For\ a = \frac{1}{3} \Rightarrow C_p = 4 * \frac{1}{3}\left(1 - \frac{1}{3}\right)^2 = \frac{16}{27} = 0.5926$$

C_P as a minimum value $C_P=0$ when a=1 and an optimum value $C_P=16/27 \approx 0.5926$ for $a=1/3 \approx 0.33333$
Doing the same for C_T we can find the optimum value $C_T=1$ for a=1/2.
The above values brings us to the formula of the power according to Betz

$$P_{Betz} = C_{P,Betz} \frac{1}{2} \rho v_1^3 A \quad [W] \quad (16)$$

With $C_{P,Betz} = 16/27$

3. VELOCITY AND POWER

The Acoustic Doppler Current Profile (ADCP) data collected from September 2005 to December 2010 with 51 deployments on the east coast of South Africa give details of the velocity variation of the Agulhas current [8]. Data are in a tables containing many fields and values which can be arranged using excel and put in a graph as shown in figure 3. Each deployment was done for a period of 3 to 5 months. The data is given in bins that divide the water column in horizontal sections. In this folder we found the depth of the center of the bin, the range or distance from the ADCPs transducer to the center of that bin, the direction at which the current flow at that specific time and the current velocity.

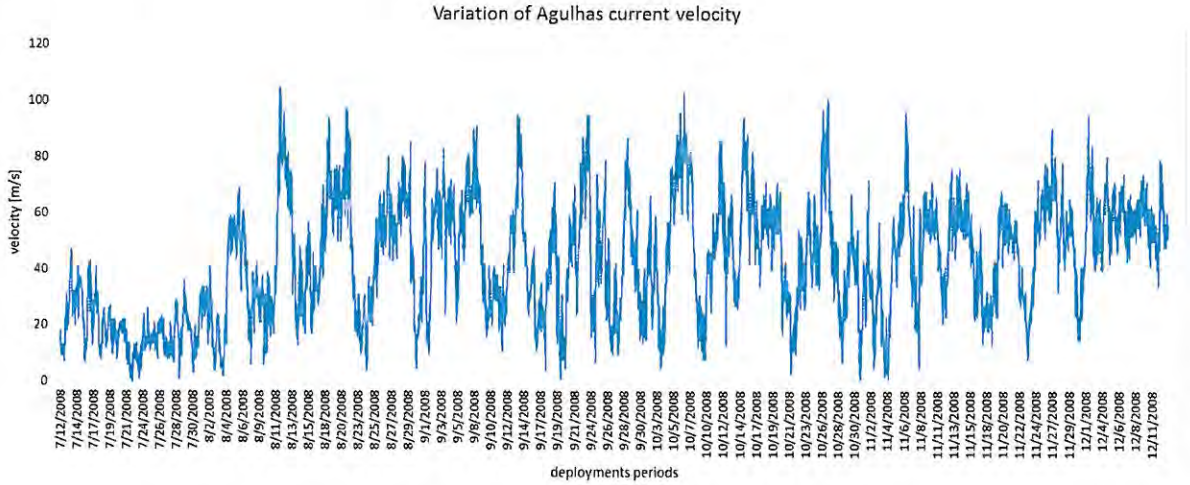

Figure 3: Variation of velocity of Agulhas current from July 12, 2008 to December 13, 2008 (CM301_BIN1)

The velocity of Agulhas current at each site is not constant. The graph in Fig. 3 is a representative curve of the variation of the velocity from Cape Morgon which is one of the 51 deployments. This deployment is called CM301 and was measured from July 2008 to December 2008. We use the formulas of the power according to Betz and estimate the power available on the rotor for an ideal marine current turbine. Results of our calculations are shown in Fig. 4.

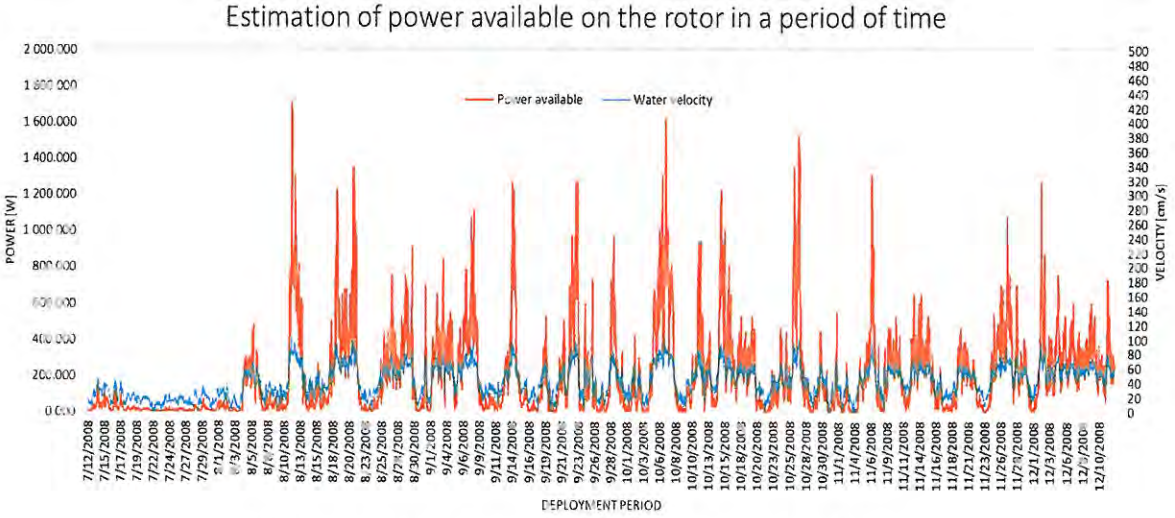

Fig. 4: estimation of power available on the rotor from deployment CM301.

Due to the weakness of the velocity, the power available is also weak and difficult to harvest with a small scale turbine. It's imperative to design an appropriate turbine which can run for this range of velocity and generate a maximum power [5]. The Reynolds number for a small turbine is a parameter to take into consideration for the design of the profile in order to harvest the maximum power possible from the power available on the rotor. The Reynolds number is a dimensionless value that measures the ration of inertial forces to viscous forces and describes the degree of laminar or turbulent flow. Systems that operate at the same Reynolds number will have the same flow characteristics even if the fluid, speed and characteristics lengths vary. In our case the characteristic length used in Reynolds number formula is the mean value of the chord length.

$$R_e = \frac{\rho v l}{\mu} = \frac{v l}{\upsilon} \qquad [-] \qquad (17)$$

With

v: Velocity of the fluid
l: The characteristics length, the chord of the foil
ρ: The density of the fluid
μ: The dynamic viscosity of the fluid
ν: The kinematic viscosity of the fluid

The mean value of the velocity of the deployment CM301 from Fig. 3 was found using an excel table equal to 42.83m/s and the kinematic viscosity. For this calculation we assume $1.004 \times 10^6\, m^2/_s$ at 20°C. The length chord is a characteristic depending on the radius of the rotor. Betz and Schmitz give us different approaches on the calculation of the chord length, c, and the pitch angle, β.
After Betz we have the following formulas based on Fig. 5 showing a blade element:

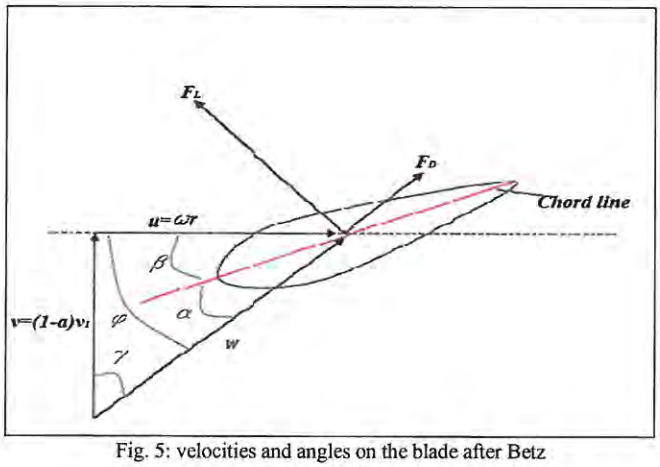

Fig. 5: velocities and angles on the blade after Betz

$$\lambda = \frac{v_{tip}}{v_1} = \frac{\omega R}{v_1} \qquad [-] \qquad (18)$$

$$\gamma_{(r)} = arctan\,\frac{3r\lambda}{2R} \qquad [rad] \qquad (19)$$

$$\varphi_{(r)} = arctan\,\frac{2R}{3r\lambda} \qquad [rad] \qquad (20)$$

$$\beta_{(r)Betz} = arctan\,\frac{2R}{3r\lambda} - \alpha_D \qquad [rad] \qquad (21)$$

$$c_{(r)Betz} = \frac{16\pi R}{9BC_{L,D}\lambda\sqrt{\lambda^2(\frac{r}{R})^2+\frac{4}{9}}} \qquad [m] \qquad (22)$$

With:

$\Upsilon_{(r)}$: angle of relative fluid to rotor axis
$\phi_{(r)}$: angle of relative fluid to rotor plane
$\beta_{(r)Betz}$: pitch angle of the blade
R: blade radius [m]
r: radius of local blade element [m]
λ: tip speed ratio
α_D: angle of attack giving the maximum glide ratio
B: number of blades
$C_{L,D}$: coefficient of lift at the chosen angle of attack

Schmitz has developed a more detailed model of analysis for the flow in the rotor plane. Unfortunately we can only give the formulas without all demonstration as this paper is limited in page numbers. According to Schmitz we have the following formulas:

$$\beta_{(r)Schmitz} = \frac{2}{3}\arctan\frac{R}{r\lambda} - \alpha_D \quad [\text{rad}] \quad (23)$$

$$\varphi_1 = \arctan\frac{v_1}{\omega r} = \arctan\frac{R}{r\lambda} \quad [\text{rad}] \quad (24)$$

$$\varphi_{max} = \frac{2}{3}\varphi_1 \quad [\text{rad}] \quad (25)$$

$$c_{(r)Schmitz} = \frac{1}{B}\frac{16\pi r}{C_L}\sin^2\left(\frac{1}{3}\arctan\left(\frac{R}{\lambda r}\right)\right) \quad [\text{m}] \quad (26)$$

$$C_{P,Schmitz} = \frac{P_{Schmitz}}{\frac{1}{2}\rho v_1^3 A} \quad [\text{-}] \quad (27)$$

$$P_{schmitz} = \frac{1}{2}\rho\pi R^2 v_1^3 \int_0^1 4\lambda\left(\frac{r}{R}\right)^2 \frac{\sin^3\left(\frac{2}{3}\varphi_1\right)}{\sin^2(\varphi_1)} d\left(\frac{r}{R}\right) \quad [\text{W}] \quad (28)$$

4. ROTOR PROFILE AND EVALUATION OF THE POWER

The design of the rotor depends on the condition in which the turbine is going to operate. The power that a turbine can harness from the ocean current also depends on the rotor design. The characteristics of the flow are the most important value in order to choose the profile of the rotor. We refer to a similar study which is based on wind turbine and analyze their systems in marine current energy approaches. Many airfoil profile have been analyzed at different Reynolds numbers [9]. In this study, we adapt a low – speed airfoil profile and analyze the result while using it for ocean current. The blade of the rotor is hit in an angle of attack "α" by the water current, creating a force which can be divided in two components that we can describe as the lift force "F_L" which is perpendicular to the water direction and the drag force "F_D"[10].

The lift force as shown in Fig. 6 is calculated as

$$F_L = C_L\frac{1}{2}\rho\omega^2(bc) \quad [\text{N}] \quad (29)$$

With:

C_L: coefficient of lift depending on the angle of attack

ρ: density of the fluid

ω: relative fluid speed

b: wide of the blade

c: length of the chord line.

The drag force also shown in figure 6 is calculated as

$$F_D = C_D\frac{1}{2}\rho\omega^2(bc) \quad [\text{N}] \quad (30)$$

With: C_D: coefficient of drag depending on the angle of attack

Most of the blade are designed with an angle of attack less than 15° to avoid the phenomenon called "stall" [11]. The different angles in the design of the blade are well described in Fig. 5, taking as reference the chord line of the blade [12]. In addition to the angle of attack, we also have the angle relative to the rotor axis "Υ(R), the angle of relative wind to the rotor plane "ϕ(R), and the pitch angle of the blade "β(R) All these angles depend on the given radius [10]. We also take into consideration the glide ratio ($GR=C_L/C_D$) for marine turbine which must be as high as possible and can even reach a value of 100 or more. Angles of attack between 5° and 10° are the ones that give a maximum value of the glide ratio.

The wind turbine profile we adapt for our experimentation is the "Gottingen 417a (M. Fox)" usually called Goe 417a [9]. We have chosen this particular profile because the value of the glide ratio is high for the range of Reynolds number we obtain for a small horizontal axis turbine running in a low – speed water current. Its properties are compared with the "BW-3" designed by Bergey Windpower for use on their small wind turbine systems. The Goe 417a has a wedge-shaped drag polar and a $C_{L,max}$ of 1.4 and offer a better performance than the BW-3 according the maximum L/D. Hence the Goe 417a is suited for low velocity wind turbine or in another way for small Reynolds Number. The main reason we used it in our research is because the Agulhas Current in which we are going to build our system has a velocity less than 1.3m/s in most of the time. Fig. 7 shows the drag polar for different Reynolds Number of Goe 417a. This curves allow us to find the better value of the glide ratio and to choose a better value for the angle of attack for the design of the blades.

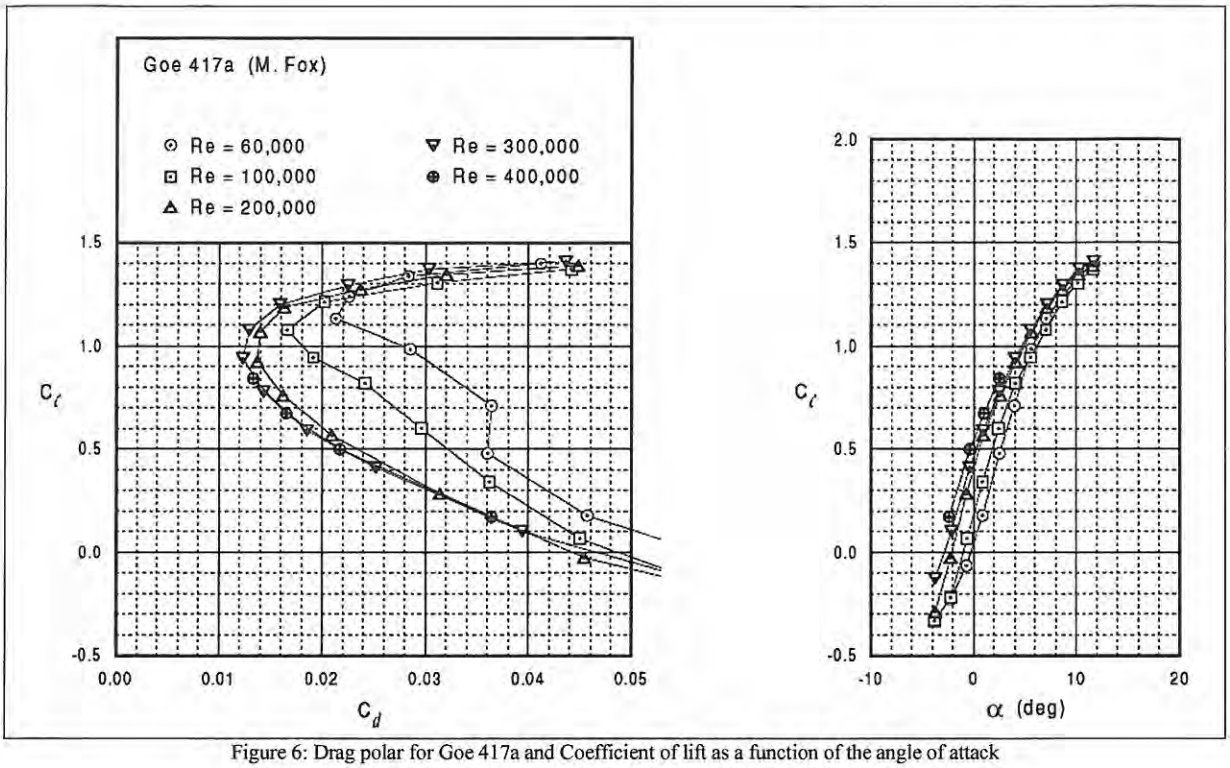

Figure 6: Drag polar for Goe 417a and Coefficient of lift as a function of the angle of attack

From Fig. 6, we calculate the highest value of the glide ratio C_L/C_D and found the optimum for C_L=1.23. This value gives us an angle of attack of 8.5°. We also chose a tip speed ratio of 5 to avoid cavitation [13]. The number of blade we choose is 3 and we assume a blade radius of 1m [14]. We can now evaluate the parameters of the blade after Betz (Table 1) and Schmitz (Table 2) and find the chord length which is important to evaluate the Reynolds number and design the blades.

Table 1: Values of different angles and chord length after Betz

Pitch angle, β, and chordlength, c, after Betz

Blade number	Tip speed ratio λ	Angle of attack, α (deg)	Angle of attack, α (rad)	Lift coefficient C_L	Rotor radius, R (meter)	Station no. (1 root, 10 tip)	Blade element, r (meter)	Blade twist, β (rad)	Blade twist, β (deg)	Relative velocity angle, θ (rad)	Relative velocity angle, θ (deg)	Chord length after Betz c (meter)
3	5	8.5	0.148353	1.23	1	10	1	-0.0158	-0.90536	0.13255153	7.594643	0.060011501
3	5	8.5	0.148353	1.23	1	9	0.9	-0.00127	-0.07303	0.14707836	8.426969	0.066543262
3	5	8.5	0.148353	1.23	1	8	0.8	0.016796	0.962322	0.16514868	9.462322	0.074648549
3	5	8.5	0.148353	1.23	1	7	0.7	0.039869	2.284298	0.18822151	10.7843	0.084961882
3	5	8.5	0.148353	1.23	1	6	0.6	0.070316	4.028808	0.21866895	12.52881	0.098501483
3	5	8.5	0.148353	1.23	1	5	0.5	0.112249	6.431417	0.26060239	14.93142	0.116996725
3	5	8.5	0.148353	1.23	1	4	0.4	0.173398	9.934949	0.32175055	18.43495	0.143589352
3	5	8.5	0.148353	1.23	1	3	0.3	0.269871	15.46249	0.41822433	23.96249	0.184415049
3	5	8.5	0.148353	1.23	1	2	0.2	0.43965	25.19007	0.5880026	33.69007	0.251872385
3	5	8.5	0.148353	1.23	1	1	0.1	0.778942	44.6301	0.92729522	53.1301	0.363255519

Table 2: Values of different angles and chord length
Pitch angle, β, and chordlength, c, after Schmitz

Blade number	Tip speed ratio λ	Angle of attack, α (deg)	Angle of attack, α (rad)	Lift coefficient C_L	Rotor radius, R (meter)	Station no. (1 root, 10 tip)	Blade element, r (meter)	Blade twist, β (rad)	Blade twist, β (deg)	Relative velocity angle, θ (rad)	Relative velocity angle, θ (deg)	Chord length after Schmitz c (meter)
3	5	8.5	0.148353	1.23	1	10	1	-0.01676	-0.96005	0.13159704	7.539955	0.058890996
3	5	8.5	0.148353	1.23	1	9	0.9	-0.00257	-0.14746	0.1457793	8.352538	0.065020223
3	5	8.5	0.148353	1.23	1	8	0.8	0.014966	0.857496	0.16331911	9.357496	0.072507334
3	5	8.5	0.148353	1.23	1	7	0.7	0.03718	2.130264	0.18553311	10.63026	0.081823531
3	5	8.5	0.148353	1.23	1	6	0.6	0.066147	3.789966	0.21450037	12.28997	0.093653719
3	5	8.5	0.148353	1.23	1	5	0.5	0.105318	6.034273	0.25367092	14.53427	0.108984503
3	5	8.5	0.148353	1.23	1	4	0.4	0.160745	9.210034	0.30909841	17.71003	0.129114937
3	5	8.5	0.148353	1.23	1	3	0.3	0.243649	13.96005	0.39200174	22.46005	0.154993062
3	5	8.5	0.148353	1.23	1	2	0.2	0.375246	21.5	0.52359878	30	0.182501293
3	5	8.5	0.148353	1.23	1	1	0.1	0.589746	33.78997	0.73809915	42.28997	0.177258059

Following the two different approaches, we can visualize the curves on Fig. 7 to compare the optimal chord length. It's clearly shown that the two approaches have the same chord length at the tip but different at the root.

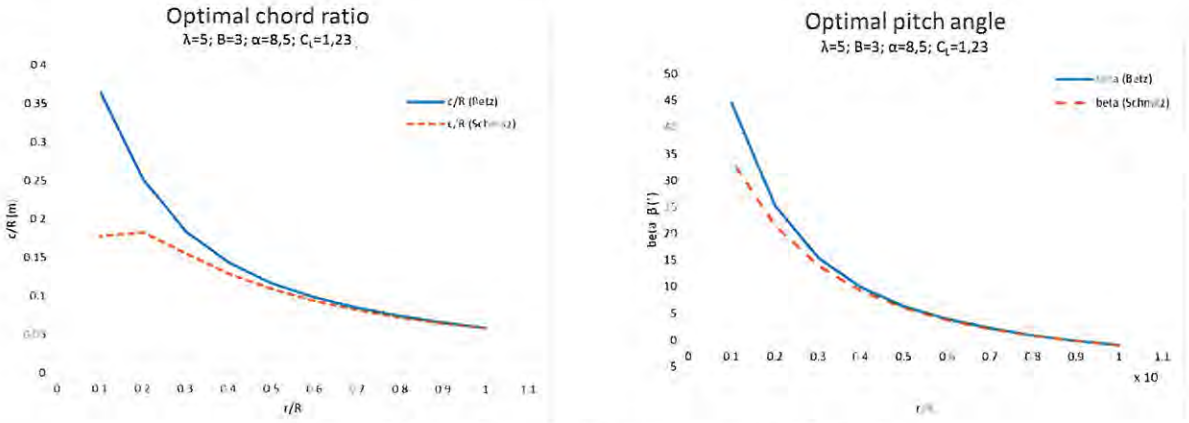

Figure 7: Optimal chord ratio and pitch angle of a blade.

5. POWER AVAILABLE AND POWER OUTPUT FROM THE SYSTEM

After finding the rotor and the different characteristics, we evaluate the power output from the turbine. We apply formulas to estimate the power available to the grid after lost in the gear box, generator and converter. The simplest design is the one with the rotor followed by the gear box, then come the generator, the convertor and finally the grid. Typical values for the efficiencies of those elements at nominal power are:
0.95 to 0.98 for the gear box
0.95 to 0.97 for the generator
0.96 to 0.98 for the converter.
The total efficiency of the turbine can is:

$$\eta_{total,turbine} = \frac{P_{grid}}{P_{max}} = \eta_{rotor}\eta_{gearbox}\eta_{gen}\eta_{conv} \quad [-] \quad (31)$$

$$\eta_{rotor} = \eta_{wake}\eta_{tip}\eta_{profile} \quad [-] \quad (32)$$

$$\eta_{wake} = \frac{C_{P\_Schmitz}}{C_{P\_Betz}} \quad [-] \quad (33)$$

$$\eta_{tip} = \left(1 - \frac{0.92}{B\sqrt{\lambda^2+4/9}}\right)^2 \quad [-] \quad (34)$$

$$\eta_{profile} = 1 - \frac{\lambda}{GR} \quad [-] \quad (35)$$

Using all formulas above and data from the site we can use an excel table to evaluate the power generated from the power available on the rotor of a specific turbine (Fig. 8). The velocity of Agulhas current at Cape Morgan from July 2008 to December 2008 as shown in Fig. 3 has a mean value of 0.43m/s with a maximum of about 1.05m/s.

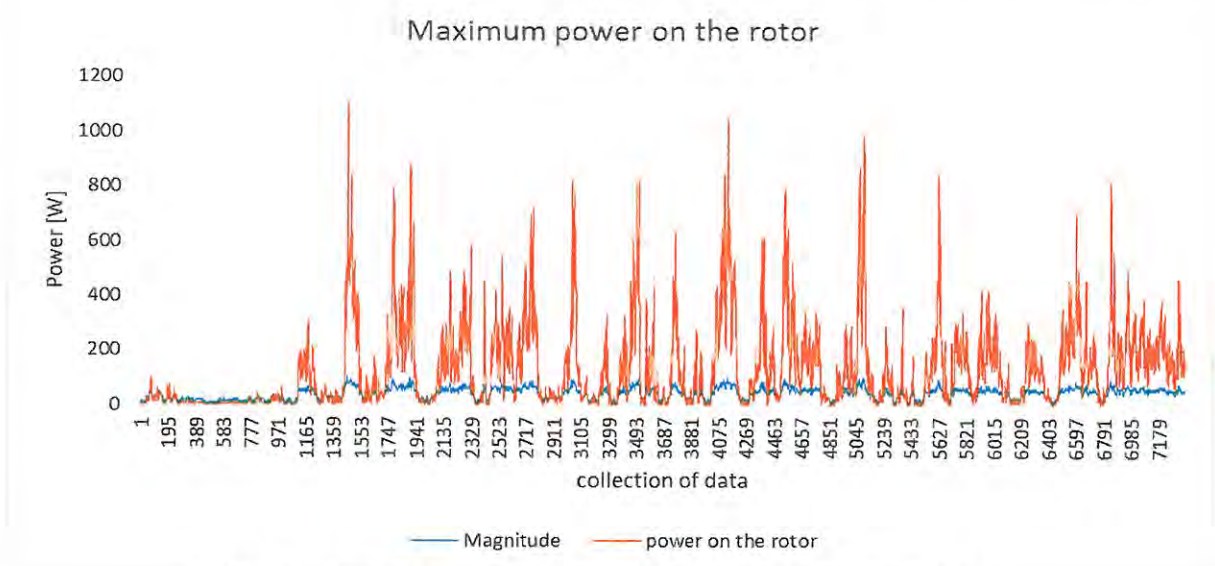

Figure 8: Evaluation of maximum power produced using equation 16 on deployment CM301.

Assuming a small turbine with a rotor of 1m radius, we will have the following results:

$$R_e = \frac{0.42 * 0.144}{1.004 * 10^{-6}} = 61673.3$$

With this range of Reynolds number we decided to accommodate the Goe 417a profile for use in water because it gives us a good glide ratio. At that value of the maximum glide ratio, we found a lift coefficient of 1.23 and an angle of attack of 8.5°. All this brings us to a system which can produce a maximum power as shown in formula 0.14. Results of the maximum power produced during the period of the deployment CM301 are shown in Fig. 8.
Assuming different turbine with different radius and different water velocity,
Table 3 shows different value of maximum power that can be available on the rotor of the turbine. These value are results found using a excel table and the appropriated formula (Eq. 16).

Table 3: Maximum power available on the rotor at different velocity and blade radius after Betz.

velocity [m/s]	Maximum power [W], at R=1m	Maximum power[W], at R=2m	Maximum power [W], at R=3m	Maximum power [W], at R=4m	Maximum power [W], at R=5m
0.1	0.96	3.84	8.63	15.34	23.97
0.2	7.67	30.68	69.03	122.72	191.75
0.3	25.89	103.55	232.98	414.19	647.17
0.4	61.36	245.45	552.25	981.78	1 534.03
0.5	119.85	479.38	1 078.62	1 917.54	2 996.16
0.6	207.09	828.38	1 863.85	3 313.51	5 177.36
0.7	328.86	1 315.43	2 959.72	5 261.73	8 221.45
0.8	490.89	1 963.56	4 418.01	7 854.24	12 272.25
0.9	698.94	2 795.77	6 290.49	11 183.09	17 473.58
1	958.77	3 835.08	8 628.93	15 340.32	23 969.24
1.1	1 276.12	5 104.49	11 485.10	20 417.96	31 903.06
1.2	1 656.75	6 627.02	14 910.79	26 508.07	41 418.85
1.3	2 106.42	8 425.67	18 957.75	33 702.68	52 660.43
1.4	2 630.86	10 523.46	23 677.78	42 093.83	65 771.61
1.5	3 235.85	12 943.39	29 122.63	51 773.57	80 896.20

Evaluation of the power to the grid is an application of the total efficiency to the maximum power obtained already.
For λ=5 and r=R, we get

$$\varphi_{max} = \frac{2}{3} arctan \frac{1}{5} = 0.132 rad = 7.54°$$

$$\varphi_1 = arctan \frac{1}{5} = 0.197 rad = 11.31°$$

Using Eq. 28, we can calculate the values of the maximum power available on the rotor after Schmitz and from there we will evaluate the efficiency and the power output.

Table 4: Maximum power available on the rotor at different velocity and blade radius after Schmitz

velocity [m/s]	Maximum power [W], at R=1m	Maximum power[W], at R=2m	Maximum power [W], at R=3m	Maximum power [W], at R=4m	Maximum power [W], at R=5m
0.1	0.63	2.53	5.70	10.13	15.83
0.2	5.07	20.26	45.59	81.04	126.63
0.3	17.09	68.38	153.85	273.51	427.36
0.4	40.52	162.08	364.68	648.32	1 013.00
0.5	79.14	316.56	712.27	1 266.25	1 978.52
0.6	136.76	547.02	1 230.80	2 188.09	3 418.89
0.7	217.16	868.65	1 954.46	3 474.60	5 429.07
0.8	324.16	1 296.64	2 917.45	5 186.58	8 104.03
0.9	461.55	1 846.20	4 153.95	7 384.80	11 538.75
1	633.13	2 532.51	5 698.15	10 130.04	15 828.19
1.1	842.69	3 370.77	7 584.23	13 483.08	21 067.32
1.2	1 094.04	4 376.18	9 846.40	17 504.71	27 351.11
1.3	1 390.98	5 563.92	12 518.83	22 255.70	34 774.52
1.4	1 737.30	6 949.21	15 635.72	27 796.83	43 432.54
1.5	2 136.81	8 547.22	19 231.25	34 188.88	53 420.13

With a turbine of 1m radius at a velocity of 0.6m/s and, assuming the efficiency of the gearbox at 0.95, the efficiency of the generator at 0.95 and the efficiency of the converter at 0.96 we get the following results:

$P_{max,Betz} = 207.09W$

$P_{max,Schmitz} = 136.76W$

$C_{P,Schmitz} = \frac{P_{Schmitz}}{\frac{1}{2}\rho v_1^3 A} = \frac{136.76}{207.09} = 0.66$

$\eta_{wake} = \frac{C_{P,Schmitz}}{C_{P,Betz}} = \frac{136.76*27}{207.09*16} = 1.11$

$\eta_{tip} = (1 - \frac{0.92}{B\sqrt{\lambda^2+4/9}})^2 = (1 - \frac{0.92}{3\sqrt{5^2+4/9}})^2 = 0.88$

$\eta_{profile} = 1 - \frac{\lambda}{GR} = 1 - \frac{5}{51} = 0.90$

$\eta_{total} = \eta_{Gearbox}\eta_{Gen}\eta_{conv}\eta_{wake}\eta_{tip}\eta_{profile} = 0.95 * 0.95 * 0.96 * 1.1 * 0.88 * 0.90 = 0.75$

$P_{Grid} = P_{max,Betz} * \eta_{total} = 207.09 * 0.75 = 155.32W$

Table 5 gives us values of the power at the grid for different water velocity and different radius

Table 5: Power output available at the grid

velocity [m/s]	Maximum power [W], at R=1m	Maximum power[W], at R=2m	Maximum power [W], at R=3m	Maximum power [W], at R=4m	Maximum power [W], at R=5m
0.1	0.72	2.88	6.47	11.51	17.98
0.2	5.75	23.01	51.77	92.04	143.82
0.3	19.42	77.66	174.74	310.64	485.38
0.4	46.02	184.08	414.19	736.34	1 150.52
0.5	89.88	359.54	808.96	1 438.15	2 247.12
0.6	155.32	621.28	1 397.89	2 485.13	3 883.02
0.7	246.64	986.57	2 219.79	3 946.30	6 166.09
0.8	368.17	1 472.67	3 313.51	5 890.68	9 204.19
0.9	524.21	2 096.83	4 717.87	8 387.32	13 105.18
1	719.08	2 876.31	6 471.70	11 505.24	17 976.93
1.1	957.09	3 828.37	8 613.83	15 313.47	23 927.30
1.2	1 242.57	4 970.26	11 183.09	19 881.05	31 064.14
1.3	1 579.81	6 319.25	14 218.32	25 277.01	39 495.32
1.4	1 973.15	7 892.59	17 758.33	31 570.37	49 328.71
1.5	2 426.89	9 707.54	21 841.97	38 830.18	60 672.15

6. DISCUSSION AND SUGGESTIONS

The horizontal axis marine turbine in this study is based on theory and will be constructed for experimental studies in a laboratory at University of KwaZulu – Natal. The calculations done in this paper are based on one of the 51 deployments done. This is just to give an idea of the power that can be harvested from the turbine designed. From Fig. 3 it's visible that there are many periods of time when the velocity of the current is over 40cm/s. For this value of the water current velocity, the turbine can generate sufficient power according to the rotor design. In this study a technology which can harvest enough energy form the Agulhas current even when the current velocity is low is developed. This was carried out because most of the turbines already designed don't fit the conditions of the Agulhas. The improvement on the rotor and the blades are going to be studied deeply and the final design will be the one which can run and produce a great quantity of energy for a low water current

velocity. For that we used a rotor turbine similar to the ones for low velocity wind turbine. Our system shows that it is possible to produce energy but further in the study we will evaluate the cost in case the system must be constructed on a commercial scale. We suggest the center of innovation project to encourage and promote studies on the marine current energy technology because it has many advantages.

7. CONCLUSION

The use of a horizontal axis turbine in the Agulhas current at Cape Morgan shows that it's possible to harvest energy from the low velocity ocean current. The technology needs to be adapted to the property of the current and the design according to the variations of the velocity. The maximum power according to Betz has a great value when the velocity and the blade radius are bigger. The efficiency of the system is greater than 0.75 and the power output has a value which satisfies us for a velocity higher than 0.6m/s. For a mean value water velocity higher than 1.5m/s, the turbine profile must be designed in another way taking into consideration the Reynolds number in order to make a turbine that can harvest a maximum power from the power available on the rotor. More effort must be undertaken for the project to be realized and built to solve a pollution problem and to increase the power production in South Africa.

REFERENCES

[1] N. Maximenko, R. Lumpkin and L. Centurioni, Chapter 12 - Ocean Surface Circulation, in S. M. G. J. G. Gerold Siedler and A. C. John eds., International Geophysics, Academic Press, 2013, pp. 283-304.
[2] L. M. BeaL and H. L. Bryden, Observations of an Agulhas Undercurrent, Deep Sea Research Part I: Oceanographic Research Papers, 44 (1997), pp. 1715-1724.
[3] M. Krug, J. Tournadre and F. Dufois, Interactions between the Agulhas Current and the eastern margin of the Agulhas Bank, Continental Shelf Research, 81 (2014), pp. 67-79.
[4] E. Marais, S. Chowdhury and S. P. Chowdhury, Theoretical resource assessment of marine current energy in the Agulhas Current along South Africa's East coast, Power and Energy Society General Meeting, 2011 IEEE, 2011, pp. 1-8.
[5] R. K. Singh, M. R. Ahmed, M. A. Zullah and Y.-H. Lee, Design of a low Reynolds number airfoil for small horizontal axis wind turbines, Renewable Energy, 42 (2012), pp. 66-76.
[6] C. J. Bai, F. B. Hsiao, M. H. Li, G. Y. Huang and Y. J. Chen, Design of 10 kW Horizontal-Axis Wind Turbine (HAWT) Blade and Aerodynamic Investigation Using Numerical Simulation, Procedia Engineering, 67 (2013), pp. 279-287.
[7] I. Lasiecka and R. Triggiani, Exact controllability of the Euler-Bernoulli equation with boundary controls for displacement and moment, Journal of Mathematical Analysis and Applications, 146 (1990), pp. 1-33.
[8] V. Wimpie, Rooy. Ocean current data, 2012.
[9] A. L. Christopher, P. B. Andy, P. Giguère, A. Gopalarathnam and M. S. Selig, Summary of Low - Speed Airfoil Data, Soar Tech Publications, Virginaia Beach, Virginia 23451, USA, 1997.
[10] D. M. Grogan, S. B. Leen, C. R. Kennedy and C. M. Ó Brádaigh, Design of composite tidal turbine blades, Renewable Energy, 57 (2013), pp. 151-162.
[11] C. Thumthae and T. Chitsomboon, Optimal angle of attack for untwisted blade wind turbine, Renewable Energy, 34 (2009), pp. 1279-1284.
[12] M. Anyi and B. Kirke, Hydrokinetic turbine blades: Design and local construction techniques for remote communities, Energy for Sustainable Development, 15 (2011), pp. 223-230.
[13] L. E. Myers and A. S. Bahaj, Experimental analysis of the flow field around horizontal axis tidal turbines by use of scale mesh disk rotor simulators, Ocean Engineering, 37 (2010), pp. 218-227.
[14] J. N. Goundar and M. R. Ahmed, Marine current energy resource assessment and design of a marine current turbine for Fiji, Renewable Energy, 65 (2014), pp. 14-22.